Effects of Polymer Architecture on Gecko-inspired Dry Adhesives

L. Callens

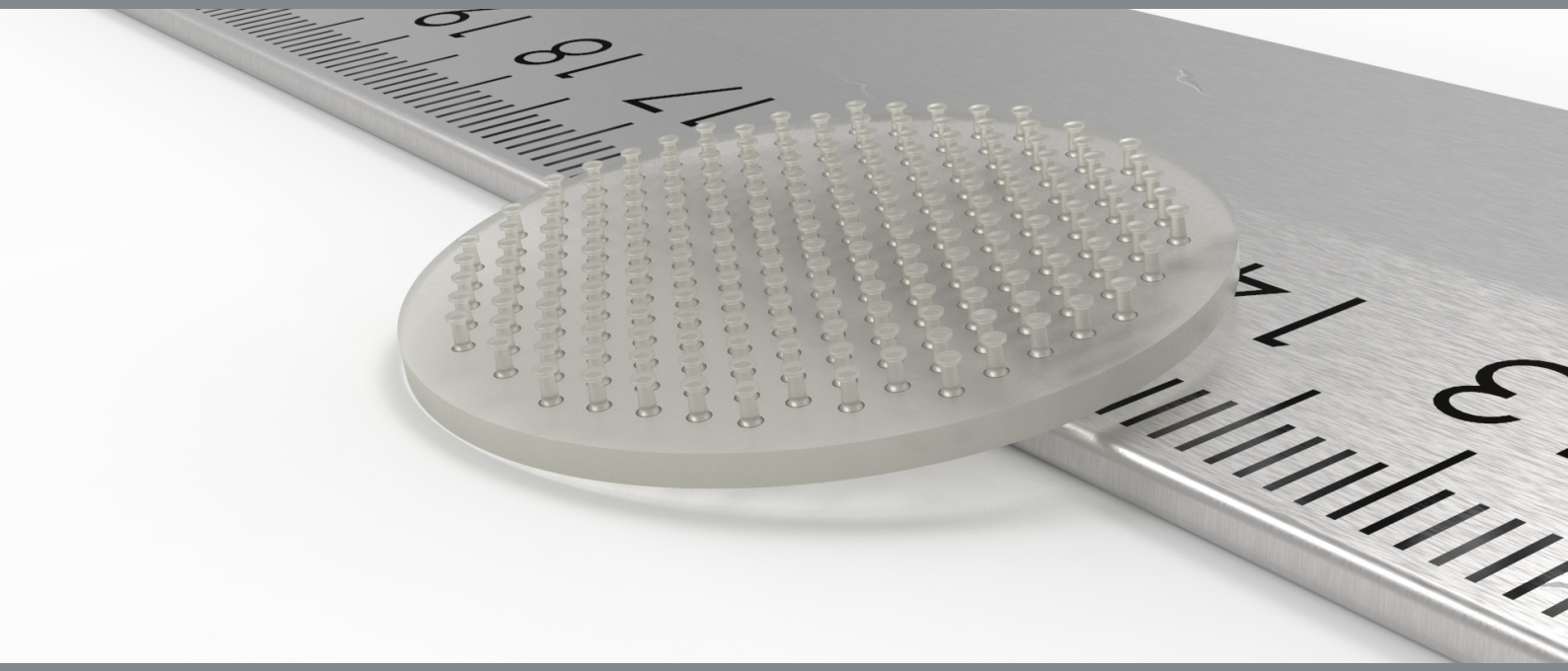

TU Delft

Novel Aerospace Materials Group
Aerospace Structures and Materials Department
Faculty of Aerospace Engineering
Delft University of Technology

Author: Lander Callens
Supervisor: Dr. Santiago J. Garcia Espallargas

GRADUATION COMMITEE

Chair Holder:	Prof. Dr. Ir. Sybrand van der Zwaag
Committee members:	Dr. Santiago J. Garcia Espallargas
	Prof. Clemens A. Dransfeld
	PhD candidate Vincenzo Montano

Delft, December 2020

Acknowledgment

This report is the result of research conducted at the Novel Aerospace Materials (NovAM) group at the Delft University of Technology. It marks the end of my MSc studies in Aerospace Structures & Materials at the Aerospace Faculty of the Delft University of Technology. This would have been impossible without the help and contribution of a great many people.

First of all, I would like to thank my supervisor, Santiago Garcia Espallargas, for his invaluable input and feedback during the entire thesis project. Special thanks go to Vincenzo Montano, for his patience and helping me with his knowledge on thermoplastic polyurethanes. I would also like to thank Sybrand van der Zwaag, for his critical and decisive feedback and steering me in the right direction when needed.

Next to that, I would like to express my gratitude to the entire NovAM group, each of you has helped me in some way. Here, Shanta Visser deserves special thanks for not only keeping things running smoothly, but also helping make NovAM the amazing group that it is. I would also like to thank Yasir Khan, for the entertaining discussions during the endless coffee breaks.

Special thanks also goes to the personnel of the Delft Aerospace Materials and Structures Laboratory. in particular to Fred Bosch, for his guidance and invaluable help during the manufacturing process, to Marlies Nijemeisland, for her assistance with the experimental setup and to Johan Bijleveld for sharing his extensive knowledge on chemistry.

I would also like to express my thanks to the Leibniz Institute for New Materials Saarbrucken for lending us their moulds, which where the basis of our manufacturing process.

Finally, this would not have been possible without the unconditional support of my family. Thanks to my godfather, Pieter Vinken for his guidance and support. I would also like to thank my parents for motivating me when things got hard, celebrating with me when things went right, and in general supporting me in every possible way.

Lander Callens
Delft, 2020

Abstract

Unlike traditional wet-adhesives, dry adhesives are bioinspired solid polymers that owe their adhesion to hierarchical structures. Gecko's are the most recognizable living creatures relying on this concept to climb walls. A close look at the gecko's fingers reveals a hierarchical system of micro-and nanoscale filaments. These ensure excellent adaptability and contact to (rough) surfaces and the formation of a large amount of close-range van der Waals surface interactions. The reversible nature of these bonds allows for reversible and repeatable adhesion. This hierarchical system has been identified as the main reason for dry adhesion and has been object of intense research to manufacture man-made solid adhesives. Despite the many efforts, there are some unclear aspects resulting from contradictory scientific reports and a strong focus on a particular polymer chemistry used to make the hierarchical structures. This has left the effects of the material choice on dry adhesion largely neglected. In this research project, we aimed to shed some light on the role of different polymer architecture features on dry adhesion.

Most available research has focused on the use of commercial siloxane elastomers that offer almost no control on the polymer synthesis. Instead, we opted to use thermoplastic polyurethane chemistry due to the large versatility this chemistry offers in terms of modification of relevant polymer architecture features. In the absence of available works on thermoplastics a new manufacturing process of such hierarchical structures had to be developed relying on heating, pressure and vacuum to respectively melt the polymer, overcome the high viscosity and impede oxidation. We studied the effects of the polymer architecture and properties on adhesion using a single micropillar architecture and varying the chemical composition (polyol length, aromatic content, hard/soft block ratio), the testing temperature and the pull-off speed.

As to the polymer architecture, the best results were found with a short polyol and the lowest hard block fraction that still guaranteed structural integrity. Next to that, it was found that having aromatic rings in the hard segments was crucial, likely due to its beneficial effect on nanophase separation. With those compositions, values exceeding those of state-of-the-art dry adhesives were found, with a maximum of 440 kPa at the Tg and high retraction speeds. Furthermore, we show that while existing models are valid for thermoplastic polyurethanes well below their Tg, once they exhibit viscoelastic behaviour, the loss factor is a much more reliable indicator of performance than the reported stiffness. The effect of the surface energy was also evident but minimal compared to the mechanical properties of the polymers.

Contents

1 Introduction

1.1 How do Geckos Adhere?

Many different kinds of animals can stick to vertical surfaces. Amongst these species, the gecko is one of the most interesting. It does not secrete a sticky fluid, yet adheres with ease to all kinds of surface, rough or smooth, wet or dry. Autumn et al. [4] showed that this excellent adhesion results from the micro- and nanostructure of the gecko feet. This structure uses contact splitting to not only inhibit crack growth, but more importantly greatly increase the adaptability of the gecko skin.

Adaptability is thé key to dry adhesion, because of the energy balance that is struck upon two solid materials making contact. When two elastic objects are pressed together, two things happen[16]. Firstly, parts of their respective surfaces are close enough together to form close-range surface interactions (see section 1.1.2). These bonds work to adhere both objects to each other and have to be broken for detachment to occur. Secondly, the applied load causes both objects to deform elastically. This deformation leads to elastic energy being created and stored in both objects. Elastic energy depends on both the deformation and the stiffness of the material, and is given by eq. (1.1), where k is the stiffness constant of the material and Δx is the deflection. Releasing this energy requires the object to return to its original, undeformed state.

$$U_E = \frac{1}{2} k \Delta x^2 \tag{1.1}$$

When the load that forced the objects together is removed, the stored elastic energy will force the objects to detach, while the surface interactions try to hold them together. For most solid objects consisting of conventional materials, the elastic energy is large enough to break surface interactions, and the objects will detach. However, if this elastic energy is lower than the energy required to break all the bonds, the objects cannot detach and they adhere to each other. In such a case, external energy has to be applied to break the surface interactions and detach the objects. This external energy is applied in the form of a mechanical load. Therefore, the larger the difference between the strength of the interface and the stored elastic energy, the higher the force required to detach the objects.

This is where the adaptability of the gecko skin comes into play. The ingenious micro- and nanostructure is optimised to keep the elastic energy storage to a minimum. Furthermore, as it is so easy for the skin to deform, a large part of its surface can form close-range surface interactions with the target surface. As a result, the force required to separate a gecko toe from its target surface is several orders of magnitude larger than it would be if the skin were to be smooth like it is for other animals, and $100mm^2$ of gecko toe skin can require up to $10N$ to detach[4], even though the skin consists of β-keratin, which shows no inherent adhesive properties.

1.1.1 Microstructure

This excellent adaptability is a result of the hierarchical micro- and nanostructure of the gecko toe, shown in fig. 1.1. The toe consists of increasingly smaller elements, each of which helps it adapt to roughness on a specific scale, ranging from centimeters to nanometers. Starting on the centimetre scale, each gecko foot and toe adapts to the curvature of branches, the shape of rocks etc. A level lower, the skin of each toe has ridges, which help adapting to millimetre-scale roughness such as found in the the bark on trees. Each of those wrinkles is in turn covered in thousands microscopic hairs, setae. These setae adapt to microscale roughness in the target surface. Lastly, the end of each setae is covered in hundreds of spatulae, even smaller hairs that overcome nanoscale roughness. This system of splitting up a contact surface into multiple smaller surfaces is called contact splitting. While contact splitting decreases the total surface area, it can greatly improve adhesion. This is thanks to the three benefits of contact splitting[17]: firstly,

it increases the strength of the interface, secondly, it greatly reduces the stored elastic energy and lastly, it slows down crack growth.

As to the first benefit, the structure allows for as much spatulae as possible to come within a nanometer or less from the desired surface, without having to apply enormous deformation loads. At this range, the close-range surface interactions that are responsible for the adhesive force, are formed. Since such a large percentage of the gecko toe skin can form these interactions, the total amount of surface interactions per unit area is several order of magnitude larger than it is for its unstructured skin (eg. the back of its paws), despite having the same chemical compositions. This means that all else being equal, the interface between a gecko toe and its target surface is much stronger than that of its unstructured counterparts, therefore requiring a higher load to detach.

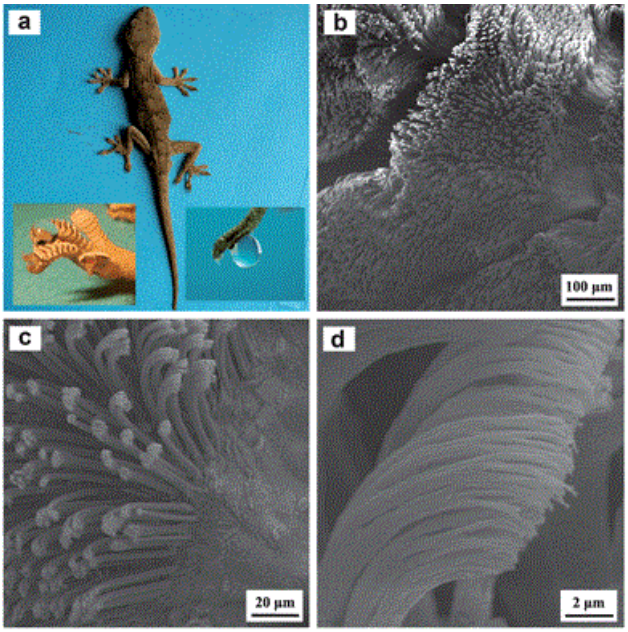

Figure 1.1: The hierarchical microstructure of the gecko toe. Figure **a** shows the gecko, its toe and the superhypdrophobic effect of its skin. Figure **b** shows one of the ridges that covers the gecko toe, which is in turn covered by thousands of setae. These setae are shown more closely on Figure **c**, where it can be seen how each tip is covered in spatulae. Figure **d** shows a close-up of the seta tip, where the hundreds of spatulae can clearly be seen. Image taken from Liu et al.[22].

Secondly, the adaptability of the gecko toe helps in keeping the elastic energy to a minimum. This is where hairs are superior to smooth skin. First of all, a hair is essentially a very slender pillar, which can buckle and bend easily under compression. The total force required to deflect all the hairs covering a patch of skin is much lower than the force required to cause the same deflection in the skin itself. Secondly, each hair deflects individually. As opposed to skin, where adapting to roughness not only requires deflection but also causes complex internal strains, the deflection of an individual hair does not affect the strain in its neighbours. This lower strain also means a lower internal elastic energy. As a result of this higher adaptability, there is less internal strain energy available to revert the system to its original, detached state. The lower internal elastic energy translates to a larger required external energy, meaning that a stronger force is needed for detachment.

Thirdly, on top of increased adaptability, this intricate hierarchical system also helps with crack containment. In a single continuous surface, a crack can grow unobstructed until the entire surface is detached. With contact splitting however, each individual surface has to form a crack before it can detach. Once a crack has formed and grown until the surface detaches, an entirely new crack has to be formed in the next surface before it can start detaching. This means that premature cracks formed by imperfections, damage or contamination only affect small parts of the system and do not greatly reduce the adhesion. Furthermore, the energy required to form a new crack is much higher than that required to grow an exist-

ing crack. As a result, the total energy needed to detach the entire surface is much larger, leading to better adhesion.

Although it is the structure of the setae and spatulae that is responsible for the adhesive strength of the gecko toe, the entire multi-scale hierarchical system is what enables the gecko to make such effective use of this adhesion. This cannot be underestimated when creating dry adhesives for commercial applications. As of now, synthetic setae (often single or double level systems) can attain and even surpass the adhesive strength of the gecko on smooth surfaces such as glass, however when it comes to rougher surfaces, let alone real-world objects with shapes and irregularities and roughness, the adhesive performance of the gecko is still unmatched.

1.1.2 Surface Interactions

Even though it is well understood how the microstructure enables the formation of extraordinary amounts surface interactions, the nature of these bonds is still under discussion. Autumn et al.[5] first posed that the adhesion is caused almost purely by van der Waals bonds. Testing both hydrophobic and hydrophilic surfaces, they found that adhesion was different for both, which would suggest that capillary forces play a role. However, further testing showed that it was not the polarity but polarizability that was correlated with adhesion. They therefore found the dielectric constant to be a much more relevant indication of adhesion than water contact angle. Additionally, they argued that the hydrophobic nature of the gecko skin lends itself to removing all water between the skin and a surface, ensuring even closer contact. This would further suggest that capillary forces are irrelevant in gecko adhesion.

A later study by Huber et al. [14] disagrees with this conclusion, as they found that the presence of water significantly affects adhesion. When testing adhesion of a single spatula on hydrophilic and hydrophobic substrates in similar temperature and humidity as Autumn et al. they found adhesion on the hydrophilic substrate to be roughly twice as strong as on the hydrophobic substrate. No mention of surface energy or polarizability is made, so this difference might be caused by other factors than the hydrophilicity, therefore not necessarily disproving Autumn et al. However, when varying the humidity between 1.5% and 60% they discovered a linear correlation between environmental humidity and adhesion, for both the hydrophilic and hydrophobic substrates. On the other hand, fully submerged adhesion tests showed a clear decrease in adhesion, which would suggest that capillary forces are at the very least not the sole responsible for adhesion.

From these results, Huber et al. concluded that water monolayer adsorption affects the adhesion of a gecko spatula and therefore capillary effects do play a role. However, due to the complexity of humidity dependant adhesion, the measured results cannot be fully described by theory. This study does not account for the significant effect of humidity on the viscoelastic properties of β-keratin[7][8], despite the interrelation between bulk material properties and adhesion. For this reason, they have not proven without a doubt that the correlation between humidity and adhesion is caused by capillary forces.

Puthoff et al. expanded on this study by accounting for changes in the mechanical behaviour of β-keratin. When testing the adhesion of setae on hydrophilic and -phobic substrates in varying humidity, their results were similar to those of Huber et al. However, additionally, they measured the effect of humidity on the mechanical behaviour of the β-keratin, as shown in fig. 1.2. They found that at room temperature, β-keratin gradually becomes softer and more compliant, behaviour that has been shown to benefit performance in synthetic dry adhesives[29][10]. This suggests that the effect of humidity on adhesion is a result of mechanical changes, casting further doubt on the contribution of capillary forces, while highlighting that material properties can greatly affect adhesion.

In conclusion, while a consensus has not been reached, it is likely that the surface interactions in dry adhesives and its biological inspirations mainly rely on van der Waals forces. Additional benefits of capillarity or even polarity might occur, yet they are not likely to make up the bulk of the interfacial bonds.

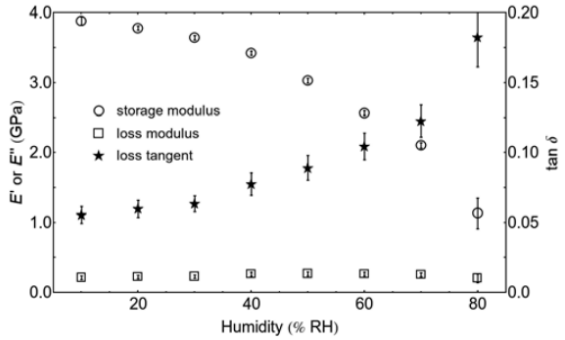

Figure 1.2: Changes in the mechanical behaviour of β-keratin as a function of humidity[27], showing amongst others, a large reduction in stiffness.

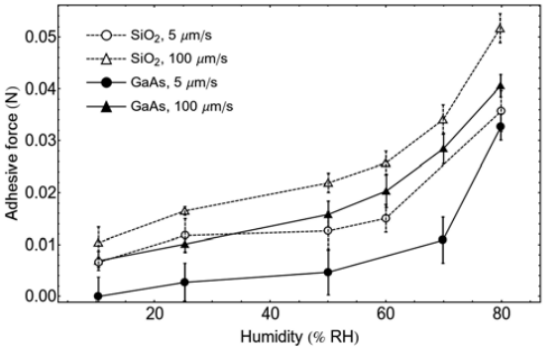

Figure 1.3: Adhesion of Gecko setae on hydrophilic (SiO_2) and hydrophobic ($GaAs$) surfaces at varying humidity and velocities.

1.2 Synthetic Dry Adhesion

Not long after discovering the effect of microstructure on adhesion, materials mimicking the hierarchical structure of the gecko setae were developed. The first published concept, by Sitti and Fearing[30] set the direction for future research in two ways. Firstly, Sitti and Fearing created nanopillars with different geometries, made from silicone rubber, polyester resin and polyimide. As silicone rubber is naturally tacky, they used two non-adherent materials as a reference. Their results showed that the natural adhesion of the material had an almost negligible effect on final adhesion, as long as the material was stiff enough to keep the nanohairs from buckling. Secondly, experiments with smaller, longer and more dense nanofibres showed the importance of geometry. The longer and more slender nanohairs suffered from fibre condensation, meaning that they were too soft to resist their mutual attraction and bunched together, greatly reducing the adhesion performance. Combined with the importance of contact splitting, this lead most dry adhesive studies to focus heavily on the microstructure, and neglect the bulk material properties.

Since this initial publication, a wide variety of dry adhesive research has been done. Ranging from underwater adhesion to reversibility controlled by infrared light, the fields of study in dry adhesion are too numerous to discuss in detail. For that reason, section 1.2.1 gives a short summary of these fields and explains why this research projects focused on the relation between polymer architecture and adhesive strength. Next, section 1.2.2 discusses the state of the art in polymer design for dry adhesion and where additional research is needed.

1.2.1 State-of-the-art Dry Adhesives

Figure 1.4 shows a simplified view of dry adhesive research. While this is not complete and does not contain all fields of study, it does show the most well-developed of these fields. Whereas adhesion on rough surfaces and reversibility focus on improving the applicability of dry adhesives, the other fields aim to improve the maximum adhesive strength.

As mentioned earlier, a large part of dry adhesive studies aim to improve the geometry of the microstructure. These studies can be divided into two fields: the first of which aims to design the optimal micropillar shape, while the second aims to optimise existing micropillars by tweaking their geometry. In the first field, research seems to converge on a pillar shape that optimally combines performance and manufacturability, the mushroom-shaped micropillar, variations on which are shown in fig. 1.5. The second field has lead to a thorough understanding of how tuning the geometry of this micropillar can lead to the strongest adhesion.

However, this focus on microstructure has two important effects. First of all, the state-of-the-art micropillars are well-designed, meaning that further optimisation is likely to result in only small improvements in performance. Secondly, in order to study the microstructure, most research projects opted to use a single material and eliminate the effects of material choice on dry adhesion. This lead to these effects

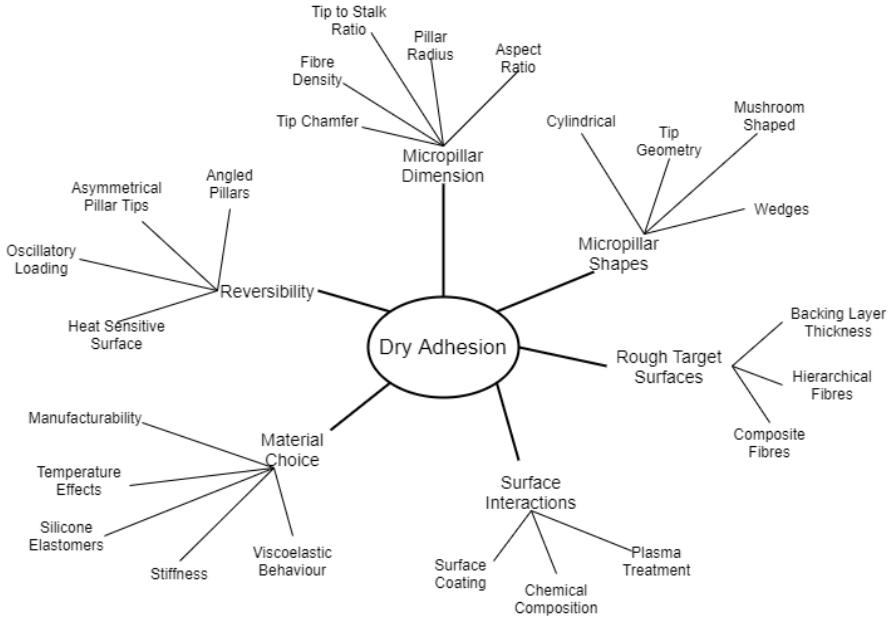

Figure 1.4: Several of the most prominent fields of study in dry adhesion. The subdivision shows the subjects of some of the research projects inside of these fields.

being neglected and underrepresented in research.

Recently, this has started to change, as the thorough understanding of microstructure left reseachers free to study other fields. While some studies focus on optimising the polymer for the manufacturing process[34] and others aim to find which existing polymer performs best[29], most studies help understand how the polymer should be designed to improve adhesive performance. These studies have shown that the material choice should not be neglected and shows great promise for further improvements in dry adhesive performance. Combined with the fact that several important questions in this field remain unanswered, understanding the effects of material choice on dry adhesion is an excellent research objective.

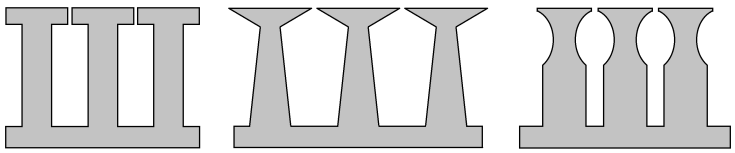

Figure 1.5: Profile view of two possible mushroom-shaped micropillars. The left profile is similar to that used by Sitti and Kim[19], while the middle profile represents the pillars proposed by Aksak et al.[3]. The last profile shows the concept used by Gorb et al.[13].

1.2.2 Polymer Design for Dry Adhesion based on Mathematical Models

The current understanding of how polymer design affects dry adhesion is best reflected in the existing models used to predict adhesive performance. Therefore, this section discusses the state-of the art in these models. For brevity's sake, only two models are discussed here: the Kendall-Maugis model and the Dugdale-Barenblatt model. These models are widely used and represent two kinds of models.

The model developed by Kendall, predicts the adherence of a flat punch, based on thermodynamics. Although it is one of the few models accounting for polymer properties, the simplistic geometry used in this model makes it less accurate when it comes to the microstructures of modern dry adhesives.

The Dugdale-Barenblatt (DB) model is based on fracture mechanics and is also often used. This method is more complex and focuses mostly flaw sensitivity. The DB model is very useful when it comes to geom-

etry design and predicting how shape changes can affect performance. A good example of this use is by Aksak et al.[3], who used it to determine the optimal shape of a mushroom-like micropillar.

When the focus is on material properties instead of geometry, Kendall's model is preferred. It can be used to directly calculate the adhesive strength of a micropillar with only the radius of the pillar and the stiffness and surface free energy of the polymer. One could see the Kendall model as having three parts: the geometric ($\sqrt{8\pi a^3}$), the elastic ($\sqrt{E^*}$) and the surface free energy part ($\sqrt{\gamma}$). Although the geometric part is highly simplified, the other two parts have been shown to fit nicely to experimental results[29]. Since this study focuses on the effect of bulk material properties, the Kendall model is more applicable.

The Kendall-Maugis Model

This method was first used by Kendall[18] in 1971. However in the 1999 book by Maugis[23], this method is explained more deeply and in a slightly different form. As this form is the most widely used in dry adhesive research, it is often called the Kendall-Maugis method. In this report, the derivation and explanation given by Maugis was used.

The Kendall-Maugis model relies on the energy balance at detachment. They pose that in order for the interface to fail, the energy released (G) due to a change in the area of interface should be equal to the energy required (w) to create that same area change in the interface. If G is lower than w, the energy released by a crack is lower than the energy required to create that crack, meaning that a crack cannot form. Therefore, one can say that the interface fails once

$$G = w \tag{1.2}$$

Using thermodynamics, the energy release rate (G) can be calculated. Given by eq. (1.3), this is the amount of stored energy in the system that is released due to a change in interface area. U_E and U_P denote, respectively, elastic and potential energy.

$$G = \left(\frac{\partial U_E}{\partial A} + \frac{\partial U_P}{\partial A} \right)_P \tag{1.3}$$

The energy of adhesion (w) is given by eq. (1.4). In this equation, γ_P denotes the energy required to create a solid-air interface for the pillar, while γ_S denotes the same for the substrate. The energy required to create a solid-solid interface between the pillar and the substrate is given by γ_I. Therefore, w is the energy used to create a unit area of pillar-substrate interface.

$$w = (\gamma_P + \gamma_S) - \gamma_I \tag{1.4}$$

Solving eq. (1.2) requires G to be defined in measurable parameters. The potential energy is given by eq. (1.5), whileeq. (1.6) describes the elastic energy.

$$U_P = -P\delta \tag{1.5}$$

$$U_E = \int P(\delta)\, d\delta \tag{1.6}$$

Assuming that the pillar is cylindrical and fully rigid, while the substrate is an infinite halfspace and purely elastic, the deflection is given by eq. (1.7)[31]. In this equation, δ is the deflection, or the vertical displacement of the pillar.

$$\delta = \frac{2P}{3aE^*} \tag{1.7}$$

Using this definition for the deflection gives eq. (1.8). Combining this with eq. (1.2) results in the critical pull-off force at which total rupture occurs (P_c), given by eq. (1.9).

$$G = \frac{P_c^2}{6\pi a^3 E^*} \tag{1.8}$$

$$P_c = \sqrt{6\pi a^3 E^* \gamma} \tag{1.9}$$

This equation can be split up into a geometric part K_g, which depends solely on pillar geometry and two material property parts, $\sqrt{E^*}$ and $\sqrt{\gamma}$.

$$K_g = \sqrt{8\pi a^3} \tag{1.10}$$

Application to Dry Adhesives

Despite its widespread use, there is an important inaccuracy when applying eq. (1.9) to micropillar adhesion. The model was created for a rigid pillar and an elastic substrate. Performance of dry adhesives is tested on glass, steel or silicone wafer substrates, which are several orders of magnitude stiffer than the micropillars. As a result the deflection on which eq. (1.9) is based does not accurately represent the geometry and deflection of dry adhesives. Assuming the pillar to behave as a linear elastic cylinder, eq. (1.11) represents the deflection more accurately. This results in eq. (1.12), which is similar to the existing formula, but has an updated geometric part.

$$\delta = \frac{Ph}{\pi a^2 E^*} \tag{1.11}$$

$$P_c = \sqrt{\frac{2\pi^2 a^4}{h} \gamma E^*} \tag{1.12}$$

While this study did not investigate the effects of geometry, meaning K_g was of little importance, it was necessary to show that altering the deflection model did not affect the manner in which the polymer properties were incorporated in eq. (1.9). With the updated deflection model, this resulted in eq. (1.12). In this equation, K_g has indeed changed, but the other parts have not. This means that even if future research improves upon the accuracy of K_g in the Kendall-Maugis model, the part accounting for polymer properties will remain unchanged.

1.2.3 The Importance of Surface Free Energy

As discussed in section 1.1.2, the exact nature of the surface interactions between the dry adhesive and its target surface are still under debate. Nevertheless, literature does agree that the strength of these interactions can be quantified by the surface free energy of the bulk material, as suggested by Kendall-Maugis[18][23]. This was partially supported by the experimental results of Kizilkan and Gorb[20], who used an air plasma treatment to alter the surface free energy of the pillar tips. They found pull-off force to be related to $\sqrt{\gamma} \cdot A_{det}$, where A_{det} is the area of the pillar tip at detachment. Their results showed that after a plasma treatment, A_{det} also changed, leading to a larger change in pull-off force than suggested by Kendall-Maugis in eq. (1.9). Kizilkan and Gorb propose that this is a secondary effect of altering the surface free energy, however as plasma treatment affects surface roughness, this is likely at least partially responsible for the unexpected change in both A_{det} and adhesion.

This was shown by Simaite and Spenko[29], who did not use air plasma treatment and found no unexpected change in adhesion and did not note a change in A_{det}. They controlled the surface free energy by altering the chemical composition of their silicone elastomers, which had the drawback of also altering the viscoelastic properties of the polymer. Therefore they did not manage to isolate the effect of γ, although they did find a linear relation between adhesion and $\sqrt{E\gamma}$, as proposed by the Kendall-Maugis model.

Chen et al.[11] used this knowledge to create a reversible adhesive. They covered the pillar tips in n-isopropylacylamide (NIPAAm), a material that drastically changes it surface free energy with temperature. For flat, unstructured polystyrene covered in NIPAAm, the water contact angle dropped from about 80° at 25°C to roughly 40° at 50°C, indicating a large change in surface free energy. In the same temperature range, the viscoelastic properties of polystyrene (the structural polymer in this dry adhesive) stays relatively constant[2]. Therefore, it can be concluded that a large part of the adhesion decrease at 50°C, a factor of 10, is due to the decreased surface free energy, highlighting the importance of the surface chemistry of the pillar tips.

In short, the exact nature of the surface interactions is not yet discovered, however a strong relation between $\sqrt{\gamma}$ and adhesion is indicated by multiple studies. The difficulties in isolating this polymer property ensures that this relation has not been proven conclusively.

1.2.4 The Importance of Bulk Polymer Stiffness

The Kendall-Maugis model poses that material stiffness directly influences adhesive strength, and adhesion scales linearly with $\sqrt{E}$. Studies of amongst others, Kizilkan and Gorb[20] have reported such behaviour for silicone elastomers exhibiting almost purely elastic behaviour.

Knowing that adaptability is the key to dry adhesion, it at first seems counterintuitive that a stiffer material improves adhesive performance. However, adaptability and material stiffness are two separate parameters. Adaptability quantifies how well an adhesive (a 3D object) can adapt to surface roughness and depends on both the stiffness of the bulk material and, more importantly, on the geometry of the surface topology. Bulk material stiffness on the other hand, is a measure of how a material (shapeless and dimensionless) deforms upon loading and therefore purely depends on the polymer architecture of the material. It is therefore perfectly possible to construct a highly adaptable dry adhesive from a stiff polymer. Why this is beneficial is explained in the widely accepted theory proposed Jagota and Bennison[15], which will be shortly summarized in the next paragraphs.

As detailed earlier, creating a large energy difference is the key to forming a strong adhesive bond during the contact phase. However, the energy changes during the pull-off phase are just as important. During this phase, an external load is applied to the adhesive, stretching the pillars until they detach. This stretching increases the elastic strain energy in the pillar, until it becomes high enough to break the surface interactions at the pillar tip. Once the pillar detaches, it returns to its original shape, thereby shedding all its elastic strain energy. As all this energy has to be supplied by a mechanical load, increasing the elastic energy inside of the pillar before detachment increases the magnitude of the required detachment load. It is here that the bulk material stiffness comes into play: the stiffer a material, the more elastic energy it can store for the same deflection. Although it has to be noted that the adaptability of the microstructure puts limits on how stiff the material can be[32].

Where the microstructure is of great help in lowering the elastic energy during contact, it does not greatly affect strain energy during pull-off. In the contact phase, contact splitting ensures that each slender pillar deforms as little as possible, be it by stretching, compressing, bending or even buckling. Therefore, the adaptability helps lower the minimum stored elastic energy in each pillar. However upon pull-off, a pillar only detaches once it has elongated to a fixed length, where the stored elastic energy is strong enough to overcome the surface interactions. In such a case, the level of stored elastic energy is set by the material stiffness and strength of the surface interactions, and is unaffected by the adaptability.

Therefore, a good dry adhesive can make use of its intricate microstructure to increase adaptability and minimize elastic strain energy during the preloading phase, while making use of the bulk material stiffness to maximize elastic strain energy during pull-off, thereby ensuring that the mechanical energy applied to detach the adhesive is a large as possible.

Since then, Castellanos et al.[10] have shown that not only the elasticity, but also the viscous behaviour of the polymer affects adhesion. They found that differences in elongation and energy dissipation during pull-off greatly affected adhesive performance. Viscoelastic behaviour consist of an elastic part, depending on the storage modulus, and a viscous part, depending on the loss modulus. The elastic energy is stored inside of the material in the form of displacements and internal stresses. The viscous energy however is dissipated as heat, making it effectively "lost energy". Similarly to the elastic energy stored in the pillars, the dissipated viscous energy also has to be supplied as mechanical energy during detachment. This means that by increasing the viscous behaviour in the form of the loss modulus can further increase adhesive performance. A more detailed explanation of the mechanical behaviour of a viscoelastic material can be found in section 4.1.

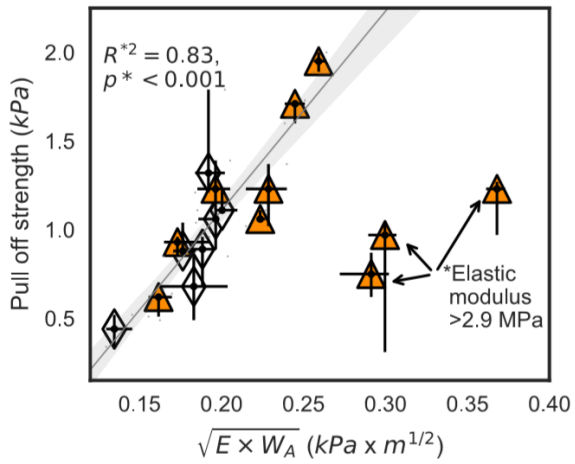

Figure 1.6: Experimental results of Kizilkan and Gorb[20] showing the relation between stiffness and surface free energy and adhesion for several silicone elastomers. The adhesives with a stiffness above $2.9MPa$ likely have much lower adhesion do to their limited contact adaptability. All polymers used in this study had loss factors below 0,12.

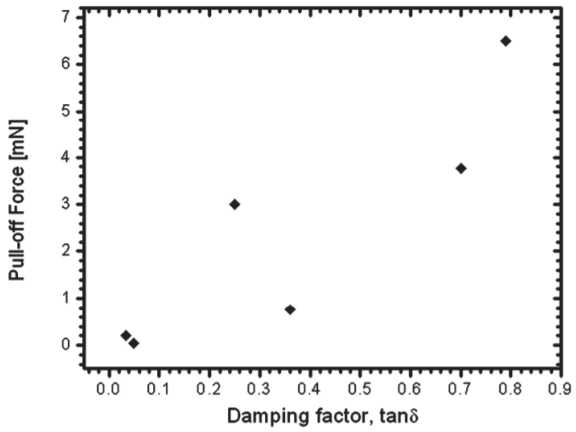

Figure 1.7: Experimental results of Castellanos et al.[10]. Each datapoint corresponds to a specific mixing ratio of two epoxies. The two points with the lowest pull-off are both the stiffest ($2.3GPa$) and the softest polymer ($2.3MPa$), indicating that stiffness does not accurately predict adhesion in viscoelastic dry adhesives.

This was further supported by studies on the effects of pull-off speed[1] and environmental temperature[6], both factors that influence the viscoelasticity. Increasing the pull-off speed strengthens the effects of viscoelasticity, as more viscous energy is dissipated at higher velocities. It is important to note here that although Sitti and Abusomwan[1] reported adhesion to significantly increase with pull-off speed, they did not attribute this to viscoelastic behaviour, nor did they quantify the changes in mechanical behaviour at the relevant velocities. Yet, their explanation for the increase in performance indirectly relied on mechanical polymer behaviour changing with the velocity, which only occurs in viscoelastic polymer, as an ideal, purely elastic polymer is not affected by deformation speed.

The effects of environmental temperature were investigated by Barreau et al.[6]. They proposed that dry adhesion was strongest around the glass transition temperature (T_g) of the used polymer. This is the temperature at which the polymer transitions from more glass-like behaviour (stiff and predominately elastic) to more rubbery behaviour (softer and more viscous). At the T_g, the pillar still has the stiffness of the glassy phase, but it combines this with the viscous behaviour from the rubbery phase, and the loss modulus is roughly equal to the storage modulus. This means that upon deformation, the energy that is dissipated as heat is roughly equal to the elastic energy stored/released, thereby doubling the energy lost during detachment when compared to similar polymers with predominately elastic behaviour. This coincides with Jagota and Rennison[15] who argued that an increase in the required input for deformation leads to better adhesion. Barreau et al.[6] showed that for PU, the highest adhesion was indeed reached slightly above T_g. PDMS and perfluoropolyether dimethacrylate (PFPEdma) have a T_g below the tested temperature range, but both showed a decrease in adhesion as temperature increased, which is consistent with the theory that adhesion is highest around T_g. This point was further supported by Lakhera et al.[21], who tuned the cross-linking density in methacrylates and temperature in order to control viscoelastic properties. Doing this, they were able to prove that their polymers showed the best adhesion around their T_g, and that the adhesion increase around T_g is more pronounced for lower cross-linking densities. Another interesting result of their study is that they found the polymers with a lower cross-linking density to adhere better. These polymers are noticeably softer than their highly cross-linked counterparts, showing an effect contrary to what the Kendall-Maugis model predicts.

Although they did not measure/publish the loss moduli for their polymers, it can be assumed that the ones with a low cross-linking density will have a much more significant viscous element than the highly

cross-linked polymers. This further suggests that the Kendall-Maugis model is incomplete and that viscous behaviour should not only be accounted for, but can actually be key in further improving dry adhesive performance.

1.3 Research Gap

In conclusion, an interesting research gap in dry adhesive research was found. As mentioned in section 1.2.1, investigating how polymer design can affect adhesion shows great promise for further improvements in dry adhesion. While current models can adequately explain how the properties of an linearly elastic polymer affects adhesion, experimental results seem to indicate that viscoelastic polymer would outperform their purely elastic counterparts. Therefore, the aim of this research project was to show how to design a viscoelastic polymer for optimal adhesion.

However, altering even a single parameter in the polymer architecture often has multiple effects on the behaviour of the polymer, all of which might affect adhesion in a different way. In order to fully understand how the polymer architecture affects adhesion, the relation between polymer properties and adhesion had to be studied first. As the relation between polymer architecture and polymer properties is fairly well understood, this will help separate the effects and clarify how exactly each architectural parameter affects adhesion. Therefore, while the research objective of this project is:

Investigating how the polymer architecture can be altered to improve dry adhesion

This cannot be done without first fulfilling the secondary objective:

Quantifying the relation between the polymer properties of viscoelastic polymers and dry adhesive performance.

2 Sample Manufacturing

This chapter discusses how the samples were manufactured. It first discusses which polymers were chosen and why in section 2.1. Next, the process used to create the microstructure and give the samples their dry adhesive properties, is discussed in section 2.2.

2.1 Using Thermoplastic Polyurethanes

While most dry adhesive studies use silicon elastomers such as PDMS, this research project made use of thermoplastic polyurethanes. In section 2.1.1, the reasons for this choice are discussed. This is done by first offering a short introduction to the nature of thermoplastic polyurethanes, followed by its benefits to dry adhesion and this research project. The last part of this subsection discusses which chemical compositions were used, and why these compositions were chosen. Furthermore, section 2.1.2 details the process used to synthesize these polymers.

2.1.1 Material Choice

Introduction to Thermoplastic Polyurethanes

Thermoplastic polyurethanes are uncross-linked polymers, characterised by urethane bonds between the monomers. Its polymer chains consist of alternating hard and soft segments. Due to phase separation, the hard segments of multiple chains group together and crystallise, thereby forming hard blocks. This is where the TPU differs from most thermoplastic polymers.

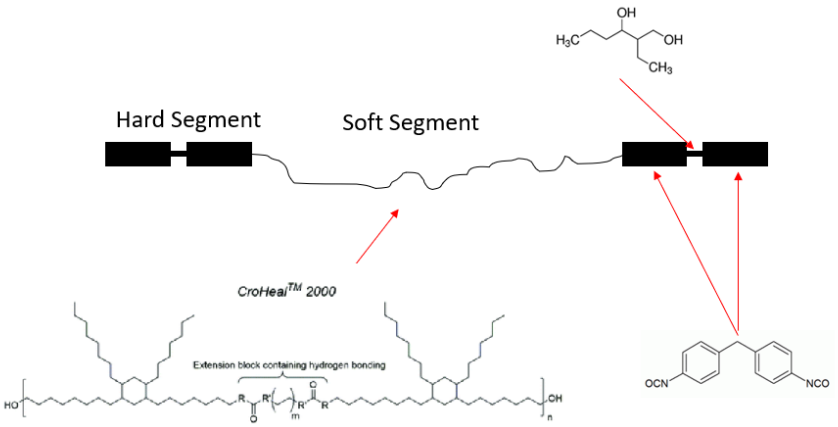

Figure 2.1

In regular thermoplastics, structural integrity results from the long polymer chains being entangled and therefore difficult to move with respect to each other. This allows for small elastic deformations, as the chains can bend, stretch or otherwise deform. However, at higher deformation strains, the chains start to slip their entanglements, which leads to plastic deformation, meaning that the polymer does not return to its original shape upon unloading. In a TPU on the other hand, structural integrity results from the hard blocks, as they are crystal structures bonding multiple chains together. Upon loading, the soft blocks can deform by stretching and aligning the chain segments, while the hard blocks stay rigid and inhibit the chains slipping with respect to each other, as shown in fig. 2.2. This means that phase separation in the TPU allows for large elastic deformation, since the chains cannot slip and therefore have to return to their original shape.

This behaviour is similar to thermosetting elastomers, where strong cross-links inhibit slipping. However, whereas cross-linking relies on a small amount of very strong bonds, the crystal structure of the hard blocks relies on a large amount of weaker bonds. While the total strength of the bonds is similar, the lower individual strength of the hard blocks means that they can be broken at much lower temperatures. This means that the crystal structure of the hard blocks can be dissolved at temperatures that do not degrade the polymer itself, which is impossible for conventional cross-links. By dissolving the hard blocks, the PTU becomes very soft and liquid-like, meaning that it can be formed into a new shape, which it will keep upon cooling. This combination of thermoplastic behaviour and an elastomeric nature is why phase separated TPUs are called thermoplastic elastomers.

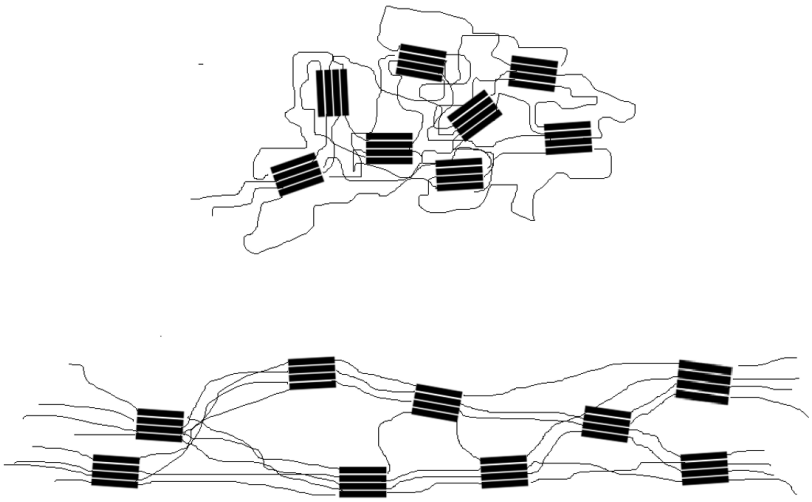

Figure 2.2: Deformation behaviour of a thermoplastic elastomer, where the straight, thick black lines denote the hard segments, and the curved, thin black lines represent the soft segments. The upper figure shows a relaxed elastomer, with the hard segments grouped together in hard blocks and the soft segments in a relaxed, coiled state. The lower figure shows a stretched elastomer, where the soft segments are stretched and aligned, greatly increasing the length of the polymer. However, since the hard blocks do not deform, the individual chains cannot slip, meaning that once the soft segments go back to their relaxed, coiled state, the polymer returns to its original shape.

The benefits of using TPU in dry adhesives

Investigating the effects of polymer architecture on adhesion requires a large amount of control over this architecture. Previous studies[10][29], achieved this control by altering the cross-linking density or even mixing several polymers together. Altering the cross-linking density allows for great control over the stiffness of the polymer, and simultaneously affects the loss factor. Creating composite polymers by mixing several different polymers together further increases the range of polymer properties that can be achieved, therefore allowing for more interesting studies.

Although these methods allow for adequate control over the polymer properties, only a single parameter of the polymer architecture is varied, either the cross-linking density or the mixing ratio. This has two significant drawbacks: first of all, lack of control over individual polymer properties, and secondly, this method sheds little light on how the polymer architecture should be optimised for dry adhesion.

The first drawback is caused by the complex relation between polymer properties and polymer architecture. Changing a single parameter in the polymer architecture affects multiple properties, which makes it impossible to for example increase the stiffness without affecting the loss factor and/or the surface free energy of the polymer. When multiple parameters in the polymer architecture can be controlled, this can be used to counteract undesired effects, and thereby altering only a single polymer property by making multiple changes in the polymer architecture. However, cleverly choosing the polymers that are being mixed can at least partially overcome this hurdle as shown by Castellanos et al.[10]. They managed to cre-

ate polymers with not only a wide variety in stiffness and viscous behaviour, but more importantly, also a wide variety in the combination between those properties.

The second drawback is of a more general nature. Understanding how polymer properties affect adhesion is very useful, and gives a good indication as to which polymers will perform well in a dry adhesive. However, as there are multiple ways to alter each property, all of which affect other properties, optimising the polymer architecture based on desired polymer properties can be a complex process. However, if the direct relations between changes in polymer architecture and dry adhesion were to be known, the process becomes infinitely more simple.

With thermoplastic polyurethanes, the polymer architecture can easily be altered in multiple ways. Not only the ratio between hard and soft blocks, but also the molecular weight, composition and even crystallinity of these blocks can be controlled. This not only leads to more control over the polymer properties and their frequency and temperature response, but a large amount of information on how each of those parameters affects adhesion. This is why TPU are a highly suitable material for this study. Of course, there is a limit to this control, as the copolymerization happens randomly.

Furthermore, TPU shows excellent self-healing properties[25], which could be used to extend the lifetime of the dry adhesive, which couples well with the repeatable nature of the adhesion. Although the scope of this study did not allow for any self-healing research, the developed manufacturing and experimental methods open the door for future studies on self-healing dry adhesives.

Limits of the Polymer Architecture

The thermoplastic polyurethanes used in this study were made from three compounds: a polyol, a diisocyanate and a chain extender. The isocyanate group reacts with the hydroxil group of the polyol to form the urethane bonds that define the polyurethane. Since the polyol is much longer than the diisocyanate, a chain extender was used to connect multiple isocyanates together. This way the polymer chain consists of alternating soft segments (made from the long polyol) and hard segments (made from multiple isocyanates connected by a chain extender), as shown in fig. 2.1.

A previous, unpublished study within the NovAM group showed that a TPU synthesized from MDI (4,4'-Methylene diphenyl diisocyanate), chain extender EHD (Ethylene hexane diol) and CroHeal™ 2000 exhibited promising adhesive properties. This polymer was taken as the starting point for this study. In order to investigate the effects of the polymer architecture on dry adhesion, a carefully chosen group of polymers around this base polymer were used.

As to the chemical composition, three parameters where varied, leading to three groups of at least three polymer compositions. The first parameter was the hard-/soft block ratio, which is denoted by the first number in the polymer name. This ratio could not be lowered very much, as this would make the polymer too soft/viscous and diminish the structural integrity of the micropillars. Therefore, M0,8P2 was the lowest attainable ratio. M2P2 was chosen as the upper limit, as M3P2 pillars were too stiff and hard to demould without damage. M1,5P2 was taken as an intermediate composition, such that at least three polymers were available in this group, in case M0,8P2 turned out to have inadequate structural integrity.

The second parameter was the length of the soft blocks, which was controlled with the molecular weight of the polyol and denoted by the last letters/numbers of the name. This is the only group that did not contain the base polymer, M1P2. The reason for this is that both M1P1,2 and M1P1,2/2 were very viscous polymers, which meant that at room temperature, the pillars would slowly flow and lose their shape. Therefore, M2P2 was chosen as the base polymer for this group. In M2P2, all the polyol molecules have a molecular weight of $2kDa$. In M2P1,2 a similar polyol was used, albeit with a molecular weight of only $1.2kDa$. For M2P1,2/2, a 50/50 molar mixture of both polyols was used.

The last parameter was the aromaticity of the hard blocks. In M1P2, each hard segment contains two aromatic rings, as it consists of MDI. Replacing MDI by HDI, removed those rings, which means that the hard blocks in H1P2 are fully aliphatic. In H/M1P2, a 50/50 molar mixture of HDI and MDI was used, meaning that half of the hard segments contain aromatic rings, while the other half is aliphatic.

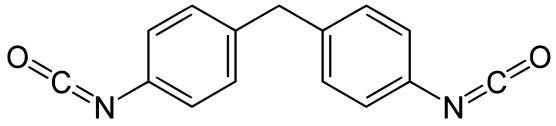

Figure 2.3: The MDI molecule used in this study.

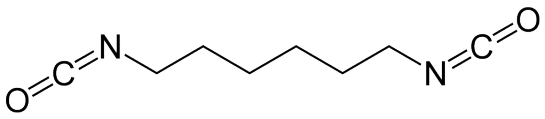

Figure 2.4: The HDI molecule used in this study.

Name	Ratio	Isocyanate	Polyol	Comment
M1P2	1 : 0,6 : 1,7	MDI	$2kDa$	Base Polymer
M0,8P2	1 : 0,5 : 1,6	MDI	$2kDa$	Lowest hard-/soft block ratio
M1,5P2	1 : 0,85 : 1,95	MDI	$2kDa$	Intermediate hard-/soft block ratio
M2P2	1 : 1,1 : 2,2	MDI	$2kDa$	Highest hard-/soft block ratio
M2P1,2/2	1 : 1,1 : 2,2	MDI	$1,2/2kDa$	Mixture of short and long soft blocks
M2P1,2	1 : 1,1 : 2,2	MDI	$1.2kDa$	Shorter soft blocks
M1P2	1 : 0,6 : 1,7	MDI	$2kDa$	Base Polymer
H/M1P2	1 : 0,6 : 1,7	HDI/MDI	$2kDa$	Mixture of aliphatic and aromatic hard blocks
H1P2	1 : 0,6 : 1,7	HDI	$2kDa$	Aliphatic hard blocks

Table 2.1: Chemical composition of the used polymers. Here, the ratio shows the molar ratios between polyol, isocyanate and chain extender. In the polymer name, the *M* stands for MDI, the *H* for HDI and *P* for the polyol.

2.1.2 Polymer Synthesis

The polymers were synthesised according to the method proposed by Montano et al.[25]. Important to note here is that an estimated 10% of isocyanate was left behind in the cups during the process, which is why 110% of the quantity mentioned in table 2.1 was used in the polymer synthesis. The final synthesis was done via one-shot bulk polyaddition, however the entire process consisted of 7 steps, which are discussed here. In case a mixture of polyols was used, both polymers were stored in the same cup. This was done mainly as the high viscosity would have lead to a large and uncontrolled amount of polyol to remain in one of the cups, thereby disturbing the stoichiometry.

First of all, the polyol was heated to 80°C. This was done in order to increase the flow and allowed for the correct amount of polyol to be measured. The desired quantity of polyol was put into a cup and kept at 55°C such that the viscosity was still low enough for proper mixing.

Secondly, the isocyanate was taken out of the freezer and allowed to acclimatise to room temperature before its container was opened. Opening the cooled container in a room temperature environment would have caused significant condensation. Since isocyanates degrade in the presence of water, this was to be kept to a minimum.

After about 40 minutes, the isocyanate was measured, put into a closed cup and heated to 55°C. This was done to melt the isocyanate in the case of MDI, and to ensure all precursor chemical were at the same temperature.

Next the chain extender was measured and added to the polyol, before being returned to the 55° oven.

Once the isocyanate had completely melted and all components had reached the desired temperature, it was added to the cup with the polyol and chain extender and mixed using a vacuum assisted speed mixer (SpeedMixerTM DAC400.2 VAC-P). This process consisted of 2 minutes without any movement, such that

the mixture could be degassed and a $20mbar$ air pressure could be reached. This was followed by 45 seconds of mixing at $1800rpm$.

The next step consisted of pouring the mixture into a preliminary mould. This mould had a simple cylindrical shape, with a $60mm$ diameter and the mixture was poured until a thickness of about $5mm$. While the shape of the mould was of little importance as blank disks with the desired diameter were cut out before forming, the thickness had to be carefully controlled to not impede the thermoplastic forming process, discussed in the next section.

After pouring, the filled moulds were put into the oven, and cured overnight at $60°C$. The next morning, the polymers could be taken out of the oven, cooled to room temperature and removed from their moulds. Here it should be noted that the polymers that contained HDI needed to remain at room temperature for at least 1 hour before they fully solidified and could be demoulded.

2.2 Thermoplastic Forming

Since the polymer synthesis was a part of this project, it would have been possible to use the manufacturing methods designed for thermosetting polymers, although early testing did show issues with viscosity and degassing, which required a tweaked process. Using such a process would have had two main benefits, the first of which is the lower viscosity. As mentioned before, it takes around 10-15 hours for all the monomers to react and form long polymer chains. Before this time, the mixture is much more liquid than the eventual polymer will be even in molten state. With this lower viscosity, the mixture would have been much easier to form into a dry adhesive, as it would have taken the shape and detail of the mould a lot quicker. Secondly, most dry adhesive research is done with PDMS or other silicone elastomers, all of which are thermosetting polymers. As a result, manufacturing processes for thermosetting polymers are well-developed. This means that an existing manufacturing process could have been used with only minor tweaks.

Despite those benefits, thermoplastic forming was still the preferred method. First and foremost due to the shorter and more time-efficient process. As mentioned before, the polymer synthesis, even without curing is a lengthy process, taking several hours. If one were to use a process designed for thermoset polymers and cure the polymer in the mould, it would mean that for every dry adhesive sample, the entire polymer synthesis process had to be performed, after which the mould would have to be used for the overnight curing. This means that only a single dry adhesive sample could have been made per day. However with a thermoplastic forming process, polymer synthesis and dry adhesive manufacturing could be separated. A large batch of every used polymer composition could be made simultaneously, meaning that only a single day of polymer synthesis was required. Creating dry adhesives from those polymer then only required heating, forming and cooling, a process taking only around 2 hours. This meant that instead of one dry adhesive per day, up to 4 or 5 could be created. Therefore, using thermoplastic forming lead to a much quicker and more flexible process than in-mould curing.

Secondly, manufacturing processes for thermoplastic dry adhesives are scarce and often only applicable to a certain group of polymers. As interest into the effects of polymer properties on dry adhesion is growing, dry adhesives will be created from a larger variety of polymers, including thermoplastics. This created the need for a universally applicable manufacturing process that did not rely on resistance against oxidation or a low viscosity after T_m. Therefore, the time spent developing such a method was not wasted and aid future research into thermoplastic dry adhesives.

Due to the low sample size and wide variety of polymer compositions, all pillar for this research were be manufactured using compression moulding. Although injection moulding is a faster process, the process optimisation required for each polymer only makes sense for larger sample sizes.

During the compression moulding process, both heating and pressure were provided by a hydraulic press with heated pressure plates, the Joos Press. The full mould was enclosed in a vacuum bag, to allow

for a vacuum environment, which the hydraulic press could not provide. It is important to note here that the moulds used during the testing and optimising of the manufacturing process were provided by INM-Saarbrucken and the final moulds used to manufacture the used samples were based on their moulds, keeping the pillar geometry which had been shown to lead to high adhesion[24].

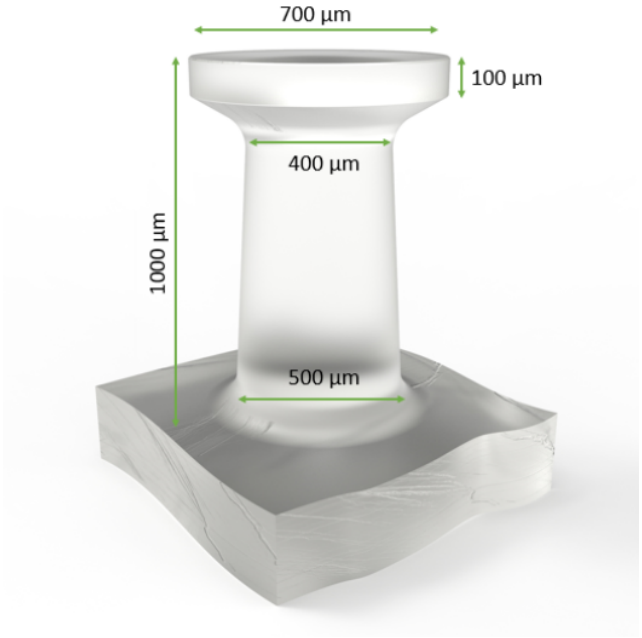

Figure 2.5: The dimensions of the micropillars used in this study.

Vacuum Environment

The manufacturing process used in this study required a vacuum environment for two reasons. First and foremost, heating up the TPU for an extended period in atmospheric conditions would lead to oxidation of the polymer, thereby altering the properties in a hard to control way. In a vacuum environment, there is not enough oxygen present for the polymer to oxidate in any measurable way.

Secondly, the relatively high viscosity of the molten polymer meant that it could not flow into the negative pillar shape if this void was already occupied by air. When using a less viscous fluid, the air would be able to flow out while the polymer flows in, however if the polymer becomes to viscous this does not occur. Therefore, a vacuum environment was required to ensure that no air was left in the mould, allowing the polymer to easily flow into the voids.

For this procedure, the use of a vacuum bag was chosen over a vacuum oven. Although using a vacuum oven is also possible, this is less suitable. First of all, the vacuum oven has to use radiation to heat up the sample, which is much slower than the conduction heating of the steel plates in the Joos Press. Secondly, applying pressure inside of the vacuum oven would require a construction with weights or clamps. This not only adds complexity, but also increases the mass inside the oven, further slowing down the heating process. Thirdly, both heating and cooling can be done in a quick and controlled manner in the Joos Press, allowing for more control over the process. The only drawback of the Joos Press was that it did not supply a vacuum environment. This problem was solved by using a vacuum bag that could withstand both the temperatures and pressures of the process.

Delayed Pressure Application

However, due to the atmospheric pressure outside of the bag and the vacuum inside of it, the bag already applies a certain amount of pressure on both the male and female mould. As a result, the mould is fully closed and the polymer hermetically seals the holes before all air can be evacuated. This problem could

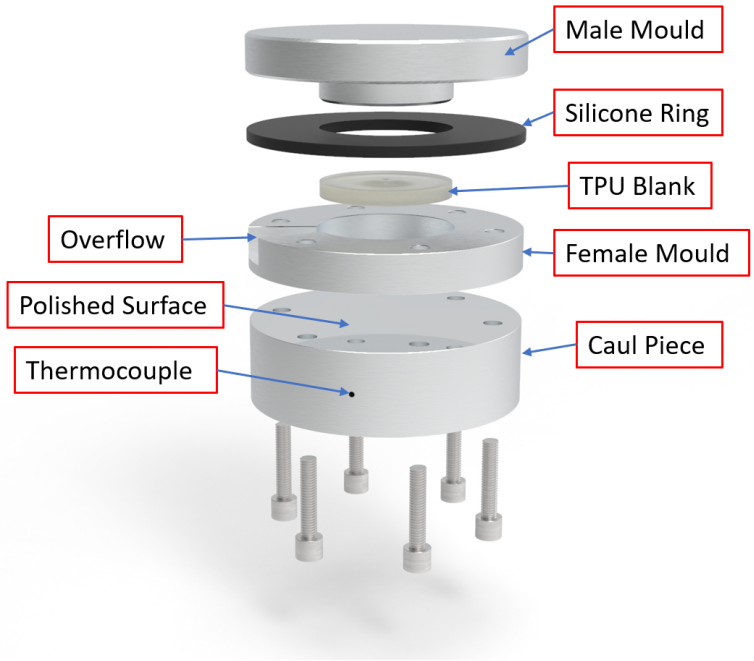

Figure 2.6: Moulding setup for the thermoplastic processing. The bolts on the bottom were used to ensure a tight connection between the caul piece and female mould.

have been solved by first heating up the polymer and only applying vacuum and pressure afterwards, but as explained earlier this would have lead to oxidation and degradation of the polymer. Therefore, one has to be able to apply vacuum and still keep the mould open. This was done by placing silicone elastomer rings between the male and female mould. The force applied by the pressure difference in- and outside the bag is not enough to deform these rings and close the mould. However, once the Joos Press applied extra hydraulic pressure, the rings started deforming and the mould closed. Using this method, the application of pressure could be decoupled from that of the vacuum.

Figure 2.6 shows the entirety of the mould setup going into the vacuum bag. The need for the caul piece (**2**) might not seem obvious at first. This piece solves three issues, the first of which is mould manufacturing. Due to the shape and size of the micropillars, the holes needed to form them cannot be made blind. This means that contrary to cylindrical holes, which can be drilled from one side, these holes require two-sided access. As a result, both sides of the holes are open, which means that under temperature and pressure, the TPU would leak out of the mould. The caul piece is therefore used to ensure the TPU fills up the holes instead of pouring through. The second issue is that of surface roughness. In order to ensure repeatable and reliable results, the surface finish of the mushroom caps has to be controlled. If this surface is too rough, effects such as mechanical interlocking come into play and distort the data. As the TPU copies the surface finish of the mould, this means that the mould itself has to be polished. Once again, both the size and shape of the holes makes it almost impossible to polish their inside. Have a large, flat and accessible surface renders polishing and controlling the surface finish much easier. The third issue is a demoulding issue. Once again, this is an issue caused by the shape of the pillars. As the mushroom caps are wider than the narrowest part of the hole, the pillars are not easily pulled out of the mould. Dissolving the mould after each process[35] is much too expensive and is difficult to scale up for commercial applications. However, the flexibility of the TPU means that if there is room for the cap to deform, demoulding becomes possible. By removing the caul piece, the mushroom caps are given this room, and they can fold inwards (comparable to the reverse of a flower opening).

The mould setup was fairly straight forward. The caul piece was bolted to the female mould, after

which a thin disk of polymer was put into the female mould. The silicone ring was then inserted between the male and female mould to finish the setup. Strategically placed pieces of tape were used to ensure the male and female mould stuck together. This was done as misalignment between both could have occured during the transport from the preparation table to the hydraulic press. If pressure were to be applied in such a case, both parts of the mould would have been irrevocably damaged. Figure 2.7 shows how the mould setup looks inside of the vacuum bag, both in open and closed condition.

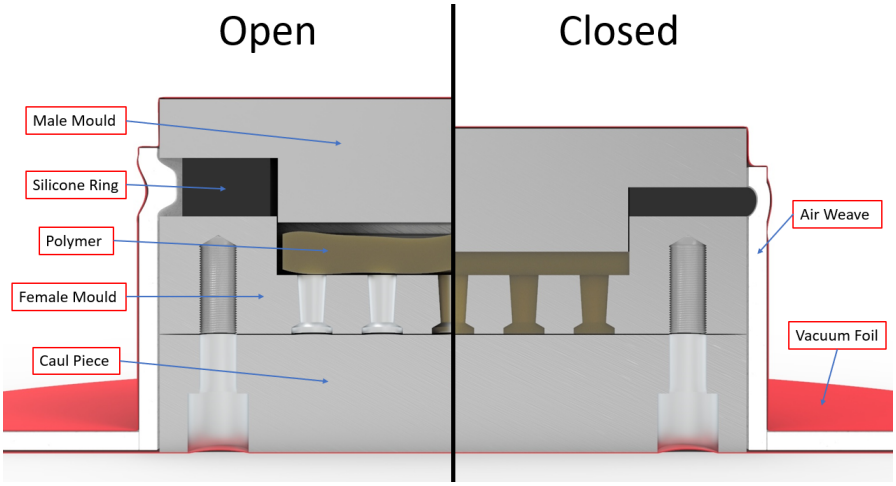

Figure 2.7: The mould setup in open and closed condition inside of the vacuum bag.

Demoulding was done by first removing the caul piece and male mould. Next, the sample could be pulled out of the mould. Thanks to the flexibility of the polymer, the mushroom caps ($\varnothing 700 \mu m$) could be pulled through the thinnest part of the hole ($\varnothing 400 \mu m$) without any damage. One has to keep this in mind when designing the microstructure, as the stiffer the polymer becomes, the smaller the maximum cup to pillar diameter ratio becomes. After a quick rinse with acetone and ethanol the mould is ready to be reused. To ensure easy demoulding, all three pieces of the mould setup were coated in (Tridecafluoro-1,1,2,2-tetrahydrooctyl) trichlorosilane.

Forming Process

With the moulding setup constructed and put into a vacuum bag, the forming process could commence. As discussed, this was done entirely in the hydraulic press, which supplied both heating and pressure, while an external vacuum pump allowed for a vacuum environment. The forming process is shown in fig. 2.8. While the basis of the process consisted of simply heating up to polymer, forcing it into the desired shape, and cooling down again, some additional steps were needed.

The first of these additional steps was step **2**, where a $3kN$ pressure was applied. This pressure was required to ensure good contact between the heating plates and the mould, while also being low enough to not close the mould. Next, the process was kept at the processing temperature and $40kN$ pressure for 30 min in step **5**. This was done to compensate for the high viscosity of the polymer, and ensure the polymer could flow and relax into the desired shape, ensuring as little internal stress as possible. Lastly, in step **8**, the polymer was kept at room temperature, yet under the $40kN$ for around 45 minutes. This was only necessary for the polymers containing HDI, as these did not solidify immediately at room temperature, and needed some time before they were stiff enough to demould.

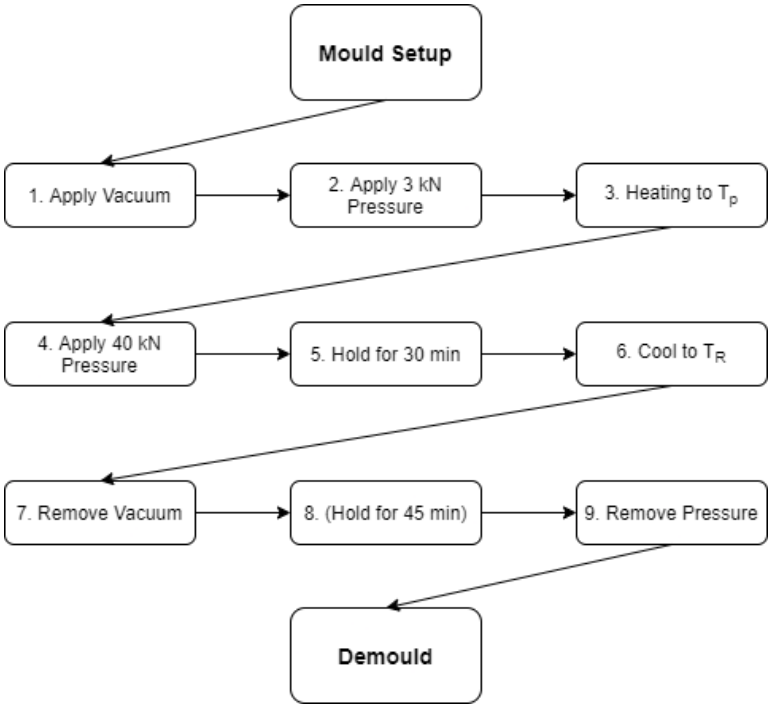

Figure 2.8: The forming process used to create synthetic dry adhesives from thermoplastic polyurethanes.

3 Experimental Setup

3.1 Adhesion and Rheology Measurements

3.1.1 Physical Setup

The adhesion measurements required a setup that allowed for highly accurate control of the axial force in the mN range, the displacement in the $mm - \mu m$ range and the environmental temperature. As the available DMA (TA Instruments RSA G-2) fulfilled those requirements, creating a dedicated device such as proposed by Yu et al.[34] was not necessary. Although the DMA was designed for oscillation strain-controlled experiments, the software also allows for highly accurate control based on force, displacement or even strain-rate. These methods of controlling the head movement allowed for the desired loading profile, as explained in section 3.1.2.

As the normal adhesion of individual pillars was tested, all forces and displacements were applied and measured perpendicular to the target surface and parallel to the pillar. The target surface in question was a glass microscope slide, mounted on a $2mm$ thick aluminium plate that could be mounted into the static DMA fixture. The micropillar was mounted to the DMA actuator head as shown in fig. 3.1. This fixture consisted of two parallel aluminium plates, the first of which was bolted to the DMA head, while the second was connected to the first with 4 bolts. These bolts allowed for control over the angling of the bottom plate, to counteract for small deviations in the angle of the micropillar. This micropillar was connected to the bottom plate by a $200\mu m$ thick piece of double sided tape.

3.1.2 Adhesion Measurement Parameters

Loading Profile

In literature, a wide variety of loading profiles has been used for normal adhesion tests. Despite their difference, each profile consists of two main phases: the preloading phase and the pull-off phase. During the preloading phase, the dry adhesive is put into contact with the target surface, and a compressive force is applied to ensure good contact between both. Next, the dry adhesive is pulled away until the critical pull-off force is reached and the adhesive detaches.

As to the preloading phase, there are four parameters to be controlled. The first is the temperature, which is a general parameter for the entire adhesion test and is therefore discussed seperately, later in this section. The other three parameters are preloading force, deflection and holding time. Several studies[33] have shown adhesion to scale with preloading force, making it an important parameter to control. Due to this clear relation and the easy application, most studies use a fixed preloading force.

However, as the deflection is a measure of how much the pillar tip has adapted to the target surface, pillar deflection is much more reliable way of controlling the preloading phase. Certainly when it comes to pillars with large differences in stiffness, preloading should be done according to the deflection instead of the force.

Unfortunately, due to the scale of the micropillars, the optimal deflection is often in the μm range. As this is similar to the variation in backing layer thickness introduced during manufacturing, controlling the deflection by forcing the DMA head to a fixed position becomes impossible. Therefore, it would be required to find the compressive force corresponding to the desired deflection in order to ensure uniform deflection for all pillars in all circumstances. Due to the large variety in mechanical properties and temperatures used in this study, such a process would be extremely time-consuming and therefore falls outside of the scope of this project.

Instead, $0.03N$ was chosen as a fixed preloading force, applied to all pillars under all circumstances. This value was chosen as it was the highest force that could be applied to the softest pillars at high tem-

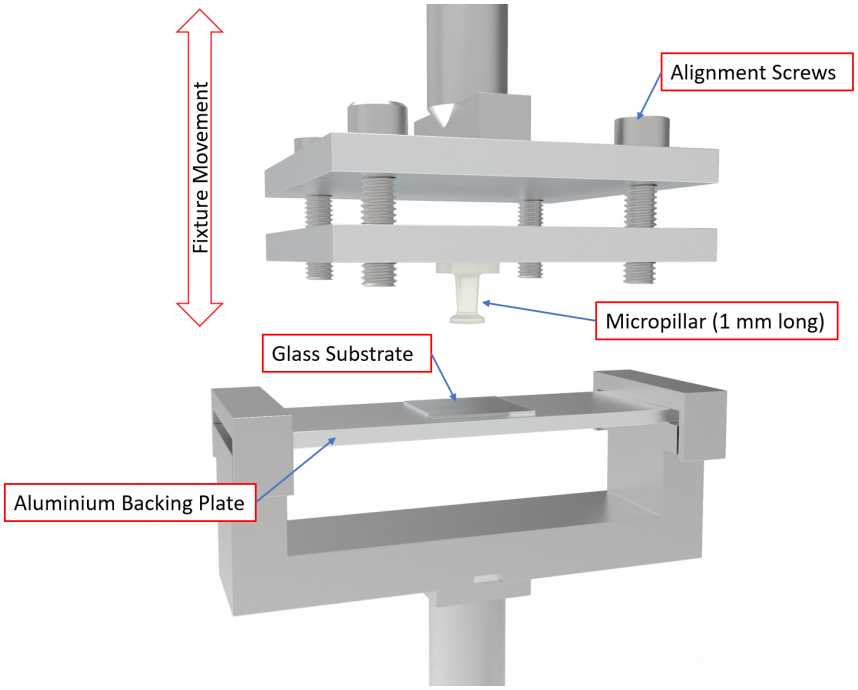

Figure 3.1: Fixture used to connect the micropillar and its substrate to the DMA.

peratures without damaging them. The effect of opting for a fixed preloading force instead of deflection further investigated in appendix A.

As to the holding time, this is a relatively underexplored parameter, as most silicone elastomers used in dry adhesion research are mostly elastic and therefore fairly time-independent. However, as this study focused heavily on the effects of viscoelastic behaviour, it was important to choose the correct holding time.

The longer the holding time, the more a viscoelastic polymer can relax its internal stresses, which should be beneficial to the adhesive performance (see section 5.2). Therefore, a long holding time should magnify the differences between the viscoelastic and the purely elastic polymers and make the results easier to interpret. To make use of this effect, a holding time of 5 seconds was chosen, which was long enough to let the viscoelastic polymer relax partially, but short enough to not greatly increase the required time per experiment. Furthermore, software limitations lead to the approaching phase (discussed later in this section) shortening the actual preloading phase with $1-3s$. Since this resulted in a $2s$ variation in the holding time, the holding time had to be long enough to ensure this variation did not affect performance. For this reason, the holding time in the software was set to $10s$, as the amount of stress relaxation for even the most viscous polymers did not change significantly whether the effective holding time was 7 or $9s$.

During the pull-off phase the pull-off velocity and tensile force are the key parameters. A shown by [1], the pull-off velocity can significantly affect adhesion and therefore has to be accurately controlled. Furthermore, in order to investigate the effects of viscous polymer behaviour, which is highly frequency-dependant, it is important to measure at a wide range of retraction speeds. Therefore, both in this research project and most other dry adhesive studies, the pull-off phase is driven by a fixed retraction speed, while the force required to maintain that velocity is measured.

The entirety of this loading cycle is shown in fig. 3.2, where the fastest experiment ($1000\mu m/s$) and the slowest ($10\mu m/s$) are both shown. This figure also shows the approaching phase, which is of no significant importance to the performance, but was added to counteract issues with the software. During this approaching phase, the DMA head moved to a position where the pillar tip is almost touching the glass substrate, yet no load is applied. This shortened the distance the DMA head had to travel in order to apply

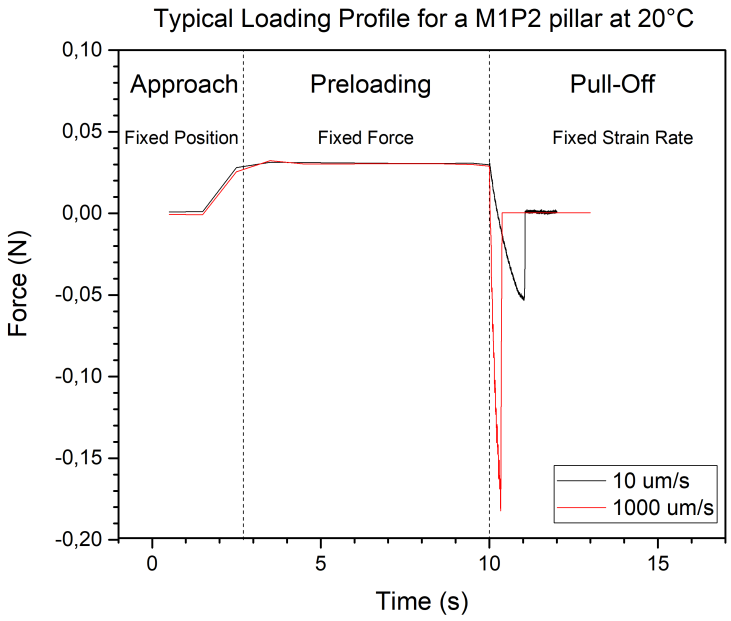

Figure 3.2: Loading profile used during the adhesion experiments.

the fixed preload. Without this phase, the DMA head would have automatically moved at a much faster rate before contact, and the initial contact force would have been both uncontrollable and much too high, which would have added a great deal of inaccuracy to the adhesion measurements.

Parameter Limits

As mentioned before, the adhesion measurements where performed at a wide range of pull-off rates and temperatures. This section explains what the limits of those ranges were and why they were chosen.

First of all, the adhesion tests were performed at velocities of $10, 100, 300, 400, 500$ and $1000 \mu m/s$. These velocities were converted into strain rates according to eq. (3.1), where $\dot{\epsilon}$ is the strain rate, V_{PO} the pull-off speed and h the pillar length. This conversion allowed the adhesive performance at a certain velocity to be linked to the mechanical properties of the pillar at the corresponding frequency. For this reason, the terms frequency, strain rate and pull-off velocity can all be used to describe the same measurement parameter, and are treated as interchangeable in this report. $10 \mu m/s$ was chosen as a lower limit as these experiments gave a good impression of the adhesion at low frequencies ($0.01 Hz$). Slower experiments ($1 \mu m/s$ or $0.001 Hz$) were performed for some polymers, however the performance was similar to that at $10 \mu m/s$ and as the experiments took almost 10 times longer, this would have greatly increased the total time needed for the experiments.

$$\dot{\epsilon} = \frac{V_{PO}}{h} \tag{3.1}$$

The upper limit on the other hand was limited by the measurement frequency of the physical setup. At strain rates above $1 Hz$, the pull-off phase for most polymers happened so quickly that the DMA couldn't accurately measure the adhesion peak anymore. As the pull-off time depended on the pillar stiffness, measurements at $1,5$ or possibly even $2 Hz$ could have been possible for the softest polymers. However, finding the upper frequency limit for each polymer is a time-consuming process and was not expected to result in any information that could not already be deducted from measurements at $1 Hz$.

The measurement temperature varied between -5 and $45°C$, with $5°C$ increments. $45°C$ was chosen as an upper limit since the micropillars lost too much structural integrity at $50°C$ and above. At $50°C$, the

pillars deformed plastically during both the preloading and the pull-off phase. This irrevocably damaged the pillars and made repeated measurements impossible.

The lower limit varied from polymer to polymer and was defined for multiple reasons. As will be discussed later, all polymers exhibited their stiffest behaviour at the low end of the temperature range. Due to the high stiffness, the pull-off phase happened very quickly, even at retraction speeds of $100\mu m/s$ and came close to the limit posed by measurement frequency. Next to that, most polymers showed little to no adhesion in that same range as the pillars showed little viscous behaviour at those temperatures. This meant that it became increasingly difficult to decide whether the polymer did not adhere, or if adhesion could simply not be measured.

Another reason for setting the lower temperature resulted from the DMA being designed as strain-controlled machine. Due to both the scale and the stiffness of the pillars at low temperatures, both the required displacement and the allowed error in that displacement became increasingly small. Certainly for the stiffer polymers, keeping a constant preload of $0,03N$ below this temperature limit was impossible (more information in appendix A.

Experimental Matrix

Ideally, measurements would be done at all possible temperatures, frequencies and combinations thereof. Unfortunately, this would have resulted in at least 48 different experiments for every single pillar, which would have greatly exceeded the time limit of this study. Therefore, it was decided to perform measurements at $20°C$ for each frequency, and at $0,1Hz$ for each temperature, thereby eliminating all other combinations of frequency and temperature. This reduced the amount of experiments per pillar from 48 to only 13, thus greatly reducing the total required time.

$0,1Hz$ was chosen as the frequency for the temperature sweep, since it was fast enough to show the effects of viscous behaviour, while also slow enough to ensure that even for the stiffest polymers, the pull-off phase was not too fast to capture. Increasing this frequency would have shown the effects of viscoelasticity more clearly, yet would also have upped the lower temperature limit, thereby decreasing the available temperature range.

$20°C$ was chosen as the temperature for the frequency sweep, as it was simultaneously below the T_g of some polymers and above the T_g of others. This allowed for greater insight into the effects of glassy and rubbery behaviour on dry adhesion. Doing this sweep at a lower temperature would have decreased the upper frequency limit for several polymers, thereby decreasing the available frequency range. Measuring at a higher temperature was possible, and since this would have ensured that all polymers were above their respective T_g, this would have enabled a more direct comparison of the absolute maximum adhesion for each polymer. However, the goal of this report was to investigate the effects of polymer architecture and properties, and the benefits of more varied mechanical behaviour outweighed those of finding the absolute strongest dry adhesive in the most optimal circumstances. Next to that, measuring at $0,01Hz$ at higher temperatures would have lead to an extremely long pull-off phase for the softest polymers. Since each measurement was repeated at least 5 times for each pillar, and at least 3 pillars were measured for each datapoint, this would have drastically increased the total measurement time.

Temperature	10 μ m/s	100 μ m/s	300 μ m/s	400 μ m/s	500 μ m/s	1000 μ m/s
-5 °C		Tested*				
0 °C		Tested*				
5 °C		Tested*				
10 °C		Tested				
15 °C		Tested				
20 °C	Tested	Tested	Tested	Tested	Tested	Tested
25 °C		Tested				
30 °C		Tested				
35 °C		Tested				
40 °C		Tested				
45 °C		Tested				

Table 3.1: Experimental matrix for this study. The experiments indicated by a * were only performed for M0,8P2 and M1P2 as they were the only ones soft and viscous enough.

3.1.3 Rheology Measurement Parameters

As mentioned earlier, rheology measurements were done in the DMA using the same physical setup as used for the adhesion measurements. As adhesion and retraction relies on linear deformation, rheology was done using oscillating compressive loading at maximum oscillation strain between 0,3 and 2%, depending on the linear viscoelastic regime of each polymer. The rheology in this project differed from more conventional rheology on two main points. First of all, it was performed on the micropillars themselves. Secondly, the temperature ramp was performed at $0,1Hz$ instead of the usual $1Hz$.

The rheology was performed on the micropillar in order to measure the pillar stiffness as accurately as possible. Instead of measuring the bulk polymer stiffness and simulating the deflection behaviour of the complex pillar shape, a simple measurement suffised. Furthermore, the same physical setup as for the adhesion tests could be used and no additional sample manufacturing had to be done, thereby saving significant amounts of time. Secondly, as all pillars had identical dimensions, all differences in pillar stiffness resulted from the bulk polymer stiffness, therefor making pillar rheology an adequate measure for comparing mechanical polymer behaviour. In order to calculate E' and E'' from the oscillation strain and force, the pillar was assumed to be a $1mm$ long cylinder with a $450\mu m$ diameter. This is why E', E and E^* were used interchangeably in this report.

Secondly, the temperature was performed at $0,1Hz$ instead of $1Hz$, as this corresponded to a pull-off velocity of $100\mu m/s$, which is the speed at which the adhesion temperature ramp was performed. This allowed for more honest comparison between polymer properties and adhesive performance.

3.2 Surface Free Energy Measurements

All surface free energy data was based on water contact angle measurements. These measurements were performed on flat pieces of bulk polymer. The temperature was controlled in two ways, depending on whether the required temperature was below or above room temperature. Heating was done by simply laying the sample on a heating stage. A thermocouple was inserted directly into the polymer in order to get an accurate temperature reading.

As to cooling, a slightly more complex setup was used. Instead of a heating stage, the sample was laid ontop of the cooling side of a Peltier element. The other side of the element was connected to a solid block of steel, which acted as a heat sink. In order to ensure that the steel block remained cold for the entire duration of the measurements, it was placed in a bath of ice-water. This had the added benefit of keeping the block's temperature constant, therefore requiring little variation in the settings for the Peltier element.

4 Results

In this chapter, the experimental results are discussed. Before moving on these results, an explanation on the mechanical behaviour of viscoelastic materials is given in section 4.1. Next, the ageing of the polymers and how this affected performance is discussed in section 4.2, as this was an unintentional extra parameter that was discovered and had to be controlled. The polymer properties of the different compositions are shown in section 4.3. while the adhesive strength of the micropillars is detailed in section 4.4.

4.1 What is Viscoelastic Behaviour

As most polymers, the thermoplastic polyurethanes used in this research project are viscoelastic materials. Before going into detail on the viscoelastic behaviour of the polymers and how it affects adhesion, a short introduction to this viscoelasticity is in place.

Viscoelastic materials combine the behaviour of viscous and elastic materials. Their respective behaviour is illustrated by their response to a simple step loading in fig. 4.1. A purely elastic material deforms instantaneously upon loading, similarly to how an ideal spring would behave. Depending on the stiffness of the material, this is either a large deflection (eg. rubber bands) or a small deflection (eg. steel). A viscous material on the other hand shows more liquid behaviour, and gradually flows to adapt to the applied load. Here, the viscosity of the liquid decides whether this is a quick and large deflection (eg. honey) or a much slower and smaller deflection (eg. tar). Viscoelastic materials show both an almost immediate (elastic) deflection and a slower (viscous) deflection.

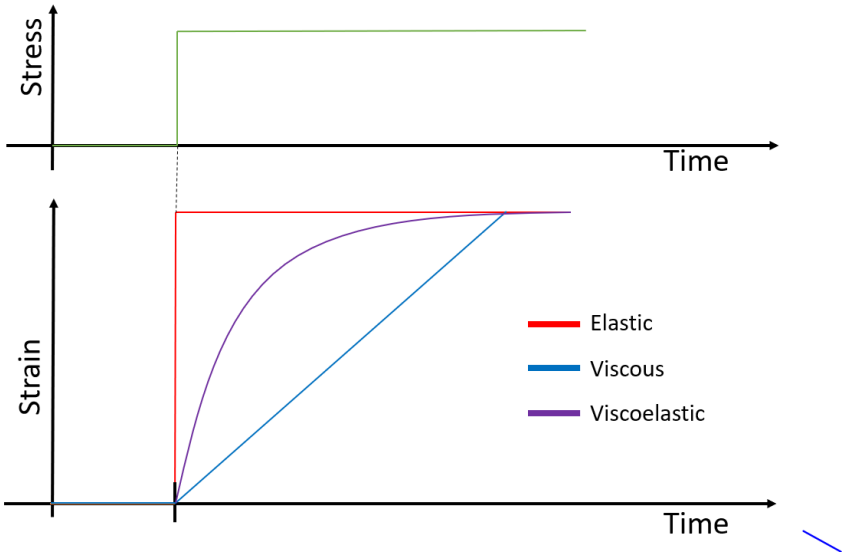

Figure 4.1: The mechanical response of various materials when subjected to a simple step loading. The blue line shows the instantaneous deformation of a purely elastic materials. The red line shows how a viscous material deforms in a linear, gradual manner. Lastly, the purple line shows how a viscoelastic material combines a large, quasi-immediate deformation with a slower, more gradual deformation.

As mentioned in section 1.2.4, viscous and elastic deflection not only takes place at a different pace, but also transform the applied deformation energy in different ways. In elastic materials, the individual atoms and molecules are well-connected to their neighbours, for example by a strong crystal structure (eg. metals) or with the help of a strongly cross-linked polymer network (eg. siloxane elastomers). This means that upon deformation, these connections bend, stretch or compress, thereby allowing the material to

deflect. Once the load is removed, the connections will return to their original state, meaning that the material regains is undeformed shape. This means that the energy used to deform the material is stored during deformation, and afterwards used to move the material back to its original form. Therefore, in a purely elastic material, deformation energy is stored.

In viscous materials on the other hand, the individual molecules are not well-connected to their neighbours. This means that when a mechanical load is applied, the molecules are moved instead of deformed. Depending on the size and shape of the molecules, significant friction can occur when they are moved. This friction is what gives the materials their resistance against deformation. As a result, the material does not return to its original shape when the load is removed, meaning that the deformation energy does not get stored. Instead, the friction leads to the mechanical energy being transformed into heat, which in turn gets dissipated into the environment. Therefore, in a purely viscous material, deformation energy is dissipated, or lost.

In viscoelastic materials, a combination of both systems is used. For example in a semi-crystalline polymer, where the crystal structure acts as a strong connection that deforms elastically, while the amorphous part of the polymer relies on friction and deforms viscously. Even fully amorphous, uncross-linked polymer can exhibit viscoelastic behaviour. In such cases, the polymer chains are long enough to entangle, and these entanglements partly immobilise the chains, causing them to deform as well as slip. Upon unloading, the chains return to their original shape, however as they have slipped with respect to each other, they do not return to their original location. This means that the material partly returns to its original shape. Therefore, in a viscoelastic material, the deformation is part elastic and part viscous, leading to a portion of the deformation energy to get stored, while the rest gets dissipated.

While the terms elastic, viscous and viscoelastic describe how a material deflects, they do not quantify how easily it deflects. For that reason, the storage modulus (E') and the loss modulus (E'') are used. The storage modulus denotes how much stress is needed to elastically deform a material one strain unit, while the loss modulus quantifies the same for viscous deformation. Viscoelastic materials therefore have both a storage and a loss modulus. The storage modulus depends on elastic deformation, and is therefore unaffected by deformation speed. The loss modulus on the other hand relies on friction, which is highly velocity-dependant. Therefore, a loss modulus is always given in combination with the frequency at which it was measured. Measuring at a higher deformation speed leads to more friction, which in turn leads to a higher loss modulus.

In viscoelastic materials, a loss- or damping factor is often used. This is the ratio between the loss- and storage modulus, and therefore a good measure of how much of the deformation happens viscously. For a perfectly elastic material, the loss modulus is zero, which means that the loss factor is also zero. In a perfectly viscous material on the other hand, the storage modulus is zero, which means that the loss factor is infinite. For the TPUs used in this research project, the loss factor varies between 0.2 and 1.3, meaning that the mechanical behaviour varies from predominately elastic to more viscous than elastic. As will be explained more fully in section 5.3, the behaviour at low temperatures is mostly elastic, leading to low loss factors. This behaviour is often called glassy behaviour, due to the high stiffness and lower toughness. At a certain temperature, called the glass transition temperature (T_g), the polymer transitions to viscoelastic behaviour, leading to intermediate to high loss factors. This is called the rubbery phase, due to the lower stiffness and high thoughness. Increasing the temperature further causes the polymer to melt, leading to high loss factors. In order to retain structural integrity, the storage and loss factors for the used polymers were not measured close to and above the melting temperature.

To summarise, viscoelastic behaviour means that upon consecutive loading and unloading, a material partly regains its original shape. This is because part of the deformation gets stored in the material, while the rest gets dissipated as heat. The loss factor ($tan\delta$) indicates the ratio between both parts, where 0 means that all energy gets stored and 1 means that equal amounts of energy get stored and dissipated.

Viscoelasticity is highly frequency dependent, resulting in higher loss factors when measurements are performed at higher frequencies. The TPU used in this project show mostly elastic behaviour below the glass transition temperature, and transition to viscoelastic behaviour after T_g, until finally, after melting they are mostly viscous.

4.2 Ageing and Heat Treatment

An interesting effect was found when measuring a M1P2 pillar after it was kept undisturbed at room temperature for a month. This effect can be seen when comparingfig. 4.2 **A** to fig. 4.2 **B**. The location, sharpness and height of the $tan\delta$ peak all changed. Combined with the frequency response, as shown in fig. 4.2 **C** and **D**, this indicates that after ageing the pillar for 1 month at room temperature, the pillar will exhibit less viscous behaviour and become stiffer.

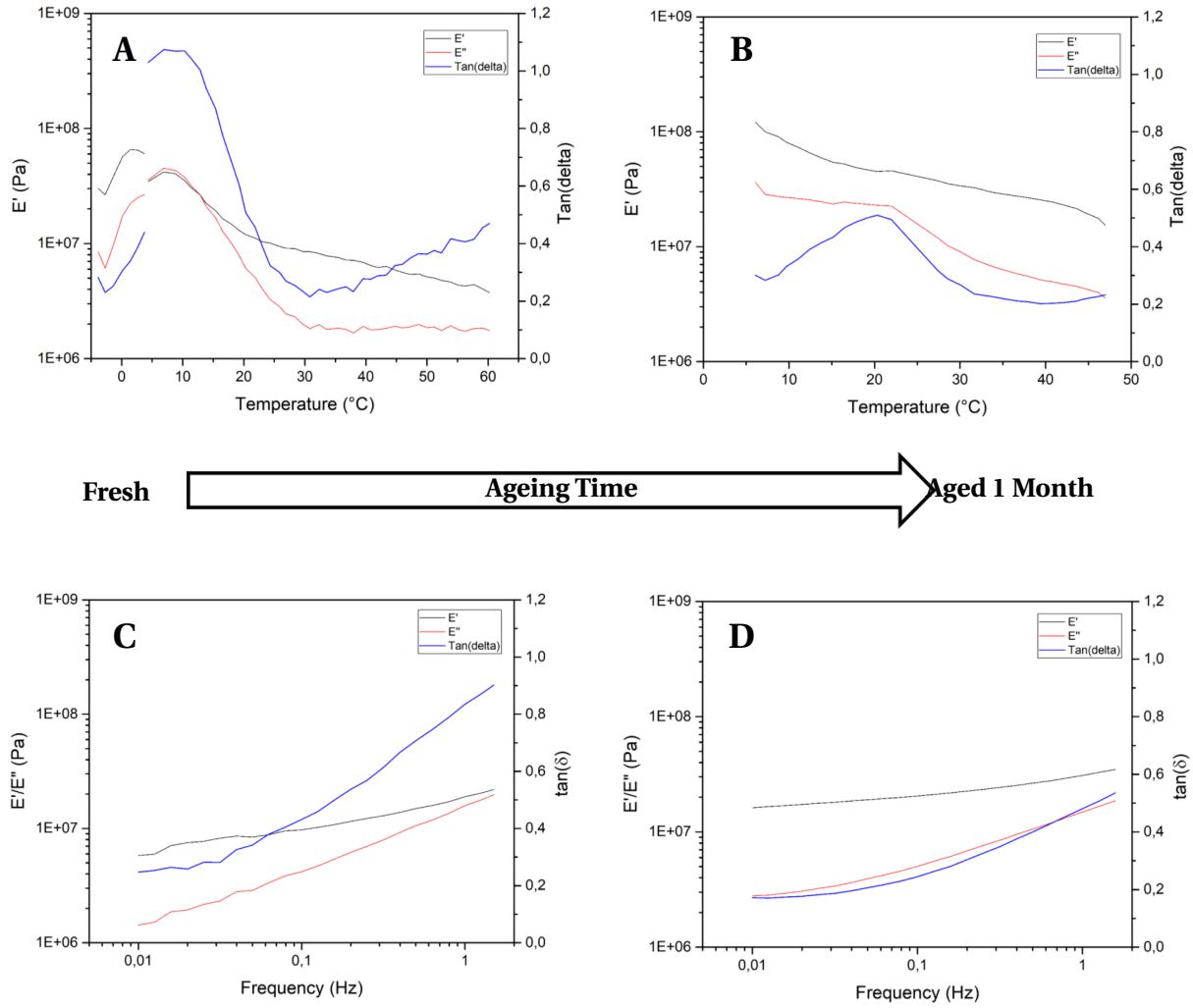

Figure 4.2: The effects of ageing on the mechanical properties of the bulk polymer. **A** shows the rheology at $0,1Hz$ for the unaged polymer, which has recently been heat-treated. **B** shows the same for a pillar made from the same polymer, that has been aged for 1 month. **C** shows the frequency response at $20°C$ for the fresh polymer and **D** shows the same for aged.

Due to time constraints, the rheology measurements before and after ageing were only possible for M1P2. However, surface free energy measurements at $20°C$ were performed for multiple polymers (fig. 4.5), all showing a significant decrease in surface free energy after ageing, indicating that a similar behaviour

takes place in all of the polymers.

This effect was also clearly reflected in the adhesive properties of the pillar. Looking at fig. 4.3, the aged pillar showed greatly decreased adhesion, with the difference increasing with pull-off speed. This figure also shows that the ageing of the pillar is fully reversible with a simple heat treatment. This heat treatment consisted of 20 minutes at 45°C, after which the pillar was allowed to cool down to room temperature. Figure 4.3 shows that although the heat treatment greatly affected the adhesive properties of the aged pillar, the same cannot be said for a newly made pillar. This supports the idea that the heat treatment does indeed reverse the ageing process.

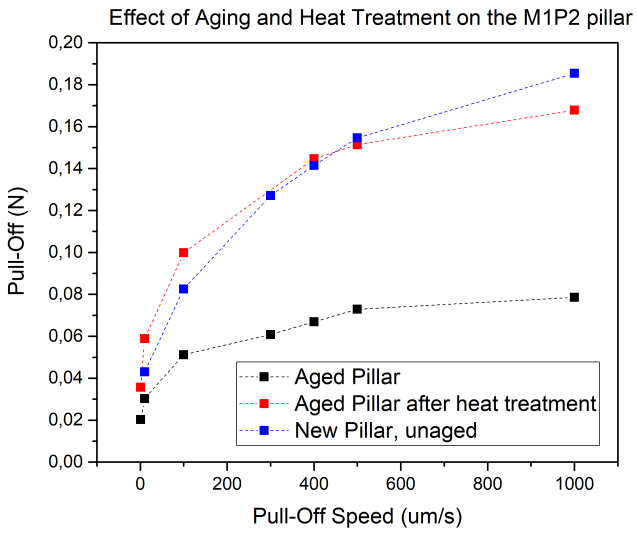

Figure 4.3: Adhesive performance of a single pillar after ageing and heat treatment. This shows how a heat treatment can return the pillar back to its unaged performance.

A similar ageing behaviour was found by Petidier[26] and attributed to crystallisation in the soft blocks. These soft blocks were constructed from the CroHeal™ 2000, which is in a solid, crystallised state at room temperature. It is theorised that incorporating this polyol into a TPU lowered its mobility and thereby slowed the crystallisation process, which is why the ageing process took a full month.

A crystal structure in the soft blocks would not only align the long chains, but also bond them together. As this would lower the mobility of the chains further, it would lead to a stiffer, less viscoelastic polymer, which is indeed what the result show. Furthermore, by heating the polymer up to 45°C, this crystal structure should get dissolved, thereby returning the polymer properties to their pre-aged state. It can thus reasonably be assumed that the behaviour shown by M1P2 during ageing and heat treating is consistent with the formation and dissolution of a crystal structure in the soft blocks.

This theory is further supported by the presence of an endothermic peak in the Differential Scanning Calorimetry (DSC) measurements of an aged M1P2 pillar, as shown in fig. 4.4. This peak concides with those found by Petidier[26], which were between $40,5-45,5°C$. The reason for their peaks being at a slightly lower temperature and more pronounced is likely due to the lower heating rate ($5°C/min$ vs $10°C/min$).

As expected, repeating the measurements 13 days after the heat treatment showed no significant endothermic peak, indicating the crystal structure has not been able to reform in any significant way. While after 1 month, a clear endothermic peak has reappeared. This indicates that the crystal structure does indeed grow, albeit slowly. Due to time restrictions, a measurement 3 months after heat treatment was not possible, however it is expected that the intensity of the endothermic peak would be similar to that of a pillar that has never been heat treated and has been ageing for 3 months.

This means that heat treatment and ageing could be used to reversibly control the crystallinity in the

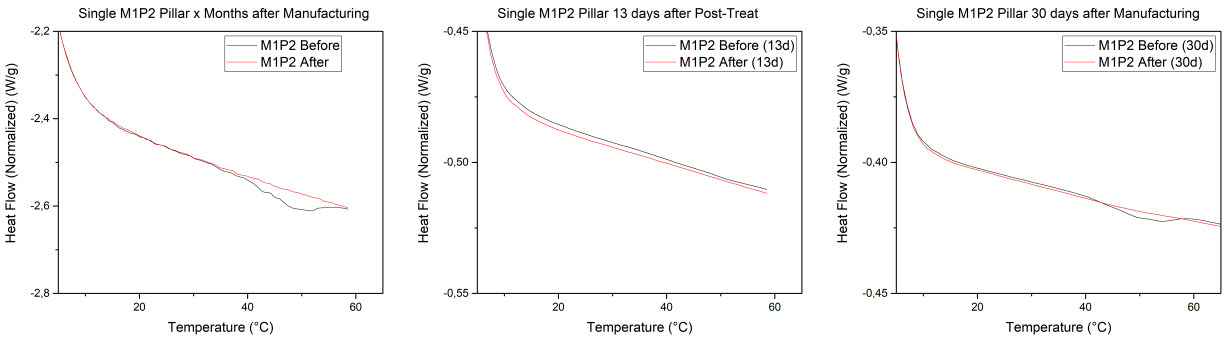

Figure 4.4: DSC results for a M1P2 pillar in different stages of the ageing process. This shows the endothermic peak disappearing after heating above 45°C, and slowly reappearing after 1 month.

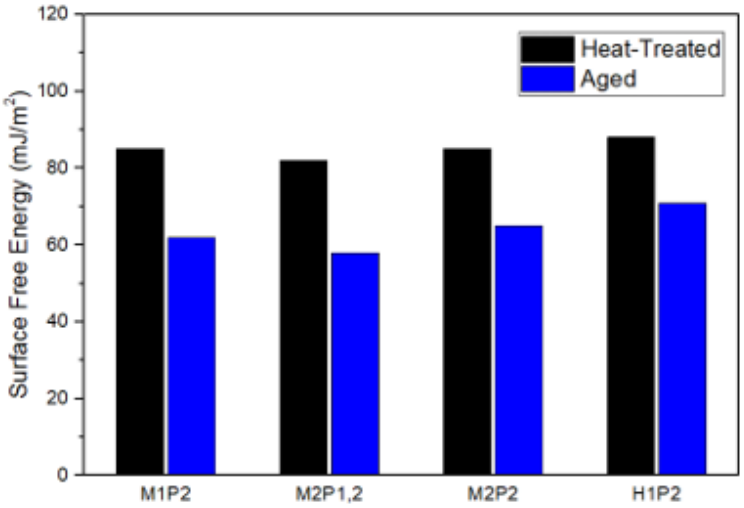

Figure 4.5: Surface free energy for recently heat-treated and aged polymers, indicating that a change to the polymer architecture occurs for most of the polymers.

soft blocks, without damaging the micropillars. This not only allowed for additional control over the viscoelastic properties, but more importantly over the surface free energy of the pillars.

The presence of this behaviour in all of the other polymers has noth been investigated with DSC and rheology measurements, however the clear change in surface free energy before and after heat-treatment indicates that it occurs in most of the polymers. Furthermore, the results of Petidier[26] indicate that at least for the polymer with long soft blocks, crystallinity in some form is likely to be present. Their results also show that the ageing time varies greatly with polymer architecture, which means that for some of the polymers, the crystal structure might reform in a matter of days instead of weeks. As the presence of this crystallinity can greatly affect adhesion, all pillars were heat treated before any experiments. This removed a parameter that was difficult to measure and control without detailed investigation, thereby increasing repeatability and reliability of the results and ensuring fair and obective comparison. Since the $1,2kDa$ polyol has a similar architecture to its $2kDa$ alternative, the assumption was made that crystallisation was possible for M1P1,2 and M1P1,2/2 and these pillars were also heat treated before any testing.

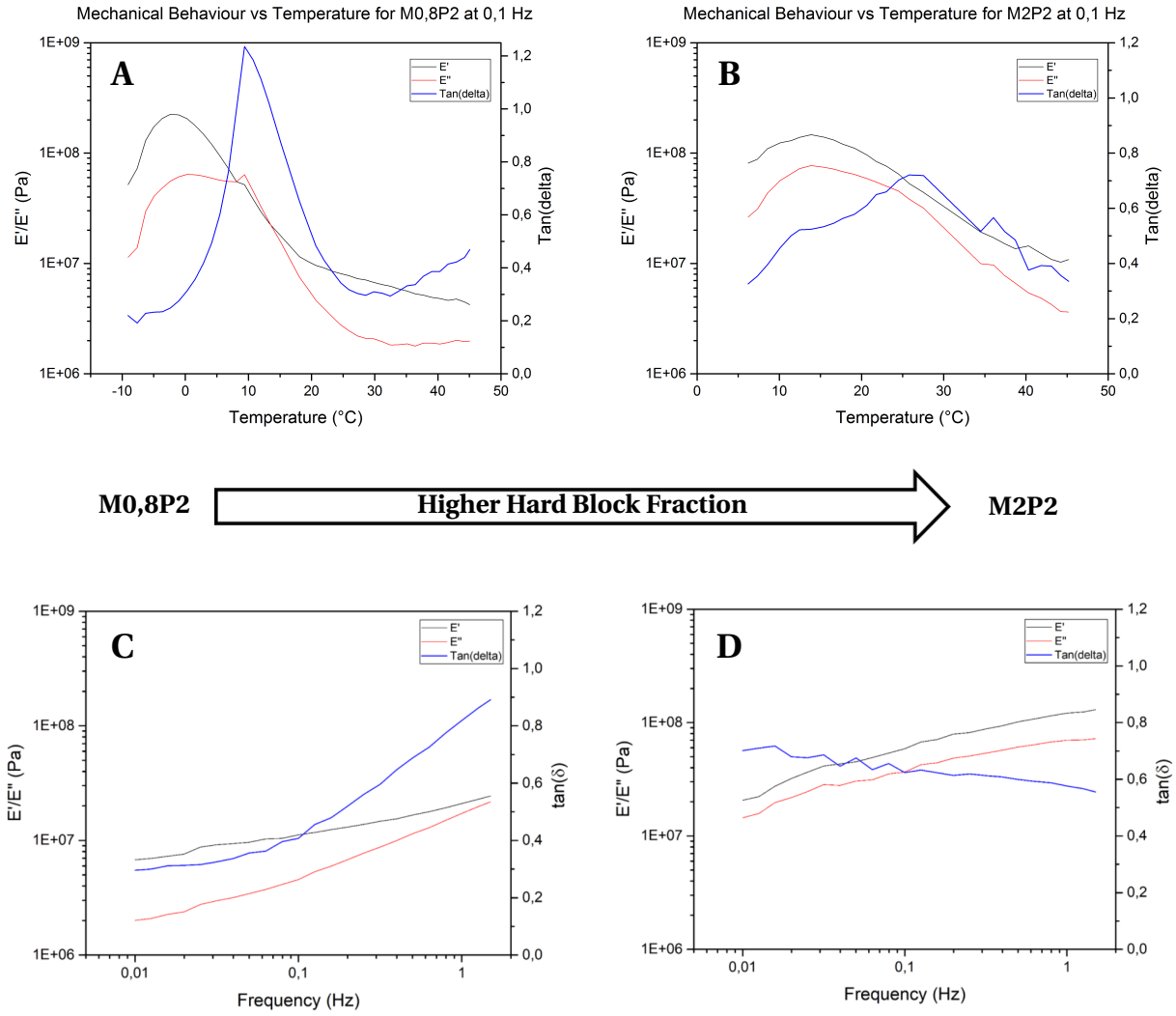

Figure 4.6: The effects of hard block fraction on the mechanical properties of the bulk polymer. **A** shows the rheology at $0,1Hz$ for the lowest hard block fraction, with the isocyanate being 16,9% of the total mass, for M0,8P2. **B** shows the same for the highest hard block fraction, with the isocyanate making up 20,3% of the total mass for M2P2. **C** shows the frequency response at $20°C$ for M0,8P2 and **D** shows the same for M2P2.

4.3 Properties of the Compositions

4.3.1 Mechanical Behaviour

This section shows the mechanical behaviour of the polymers, based on the DMA results. All data shown here resulted from compressive oscillation rheology on individual pillars. For clarity reasons, the rheology data of the polymers was grouped according to the parameter in which they vary.

Hard Block Fraction

The two main effects of hard block fraction on mechanical properties can be seen in fig. 4.6. First of all, the loss factor peak becomes significantly lower as the hard block fraction increases. From around 1,25 for the lowest hard block fraction to only about 0,75 for the highest.

Secondly, the glass transition temperature shift by approximately $17°C$. This is not only visible in the horizontal location of the loss factor peak in fig. 4.6 **A** and **B**, but also in the frequency response in **C** and **D**. At $20°C$, M0,8P2 with its low hard block fraction is below its T_g and highly sensitive to frequency changes, shown in the damping factor increasing from 0,3 at $0,01Hz$ to 0,9 at $1,5Hz$. M2P2 with the highest hard

block fraction on the other hand is below its T_g and much less frequency-sensitive. While its stiffness does increase, the loss factor stays fairly constant, with the decrease likely being caused by measurement inaccuracies.

Soft Block Length

The three main effects of soft block length on mechanical properties can be seen in fig. 4.7. First of all, the loss factor at T_g becomes lower as the soft segments increase in length. M2P1,2 with the shortest soft blocks reaches a $tan\delta$ of about 1.1, while M2P2 with the longest only reaches 0,75. Secondly, the loss factor peak also broadens. While the peak for M2P1,2 is clearly defined and steep, that of M2P2 is much wider and flatter. Next, the stiffness below T_g is visibly higher for the polymers with shorter soft segments. While this difference does not seem immense due to the logaritmic scaling, the storage modulus for M2P1,2 is roughly two times larger than that for M2P2.

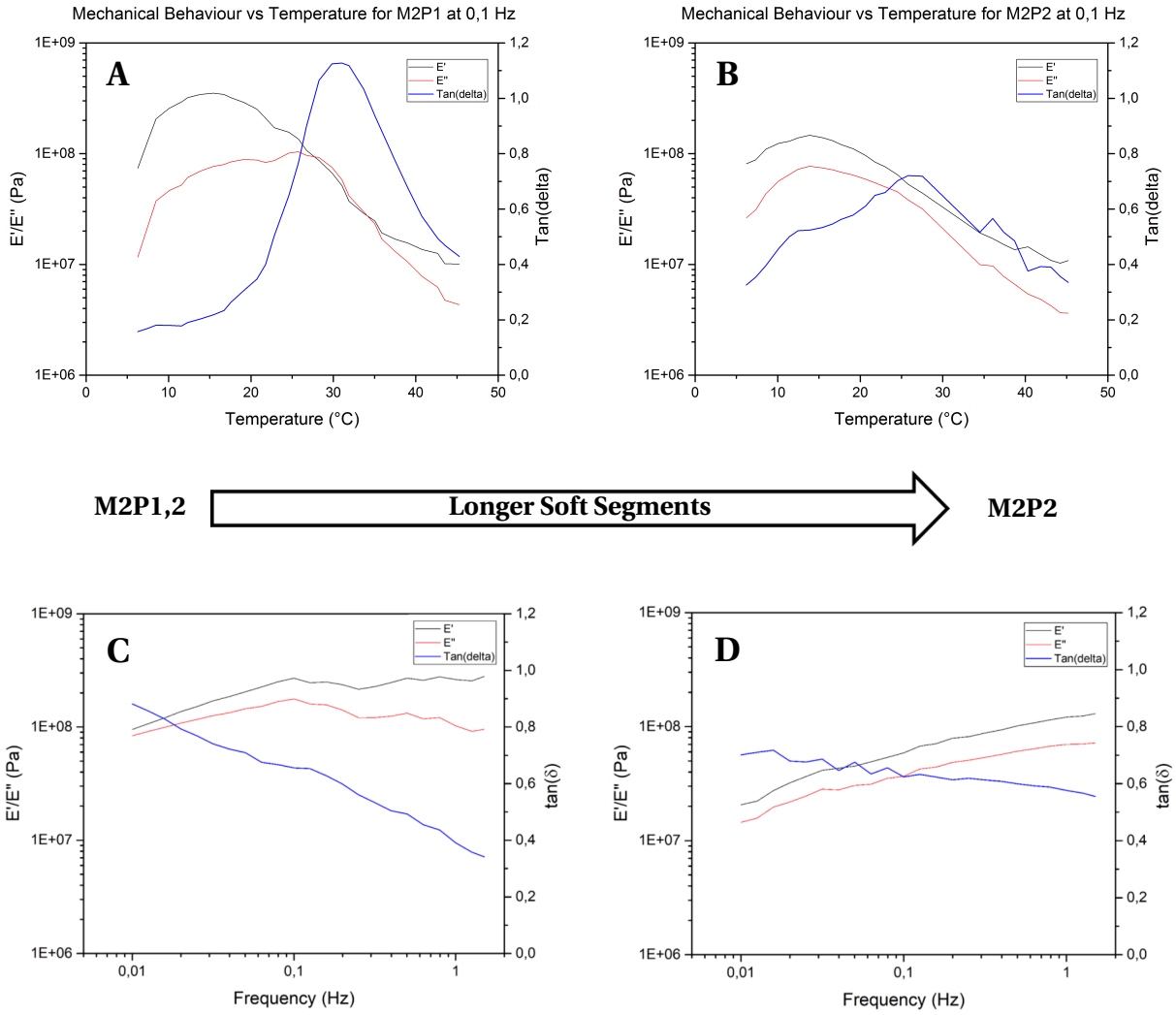

Figure 4.7: The effects of soft segment length on the mechanical properties of the bulk polymer. **A** shows the rheology at $0,1Hz$ for the shortest soft segments, with the average polyol molecular weight being $1,2kDa$ for M2P1,2. **B** shows the same for the longest soft segments, with the polyol having an M_w of $2kDa$ for M2P2. **C** shows the frequency response at $20°C$ for M2P1,2 and **D** shows the same for M2P2.

Hard Block Aromaticity

The effects of hard block aromaticity are very clear when looking at fig. 4.8. For H1P2 with its aliphatic hard blocks, there is a clear absence of glass transition. Over the entire temperature range, the loss factor barely changes until it reaches 30°*C*, after which it only gradually increases as the polymer approaches the melting temperature at 55°*C*. Furthermore, a noticeable difference in stiffness before the glass transition is present. The storage modulus for H1P2 is roughly half that of M1P2.

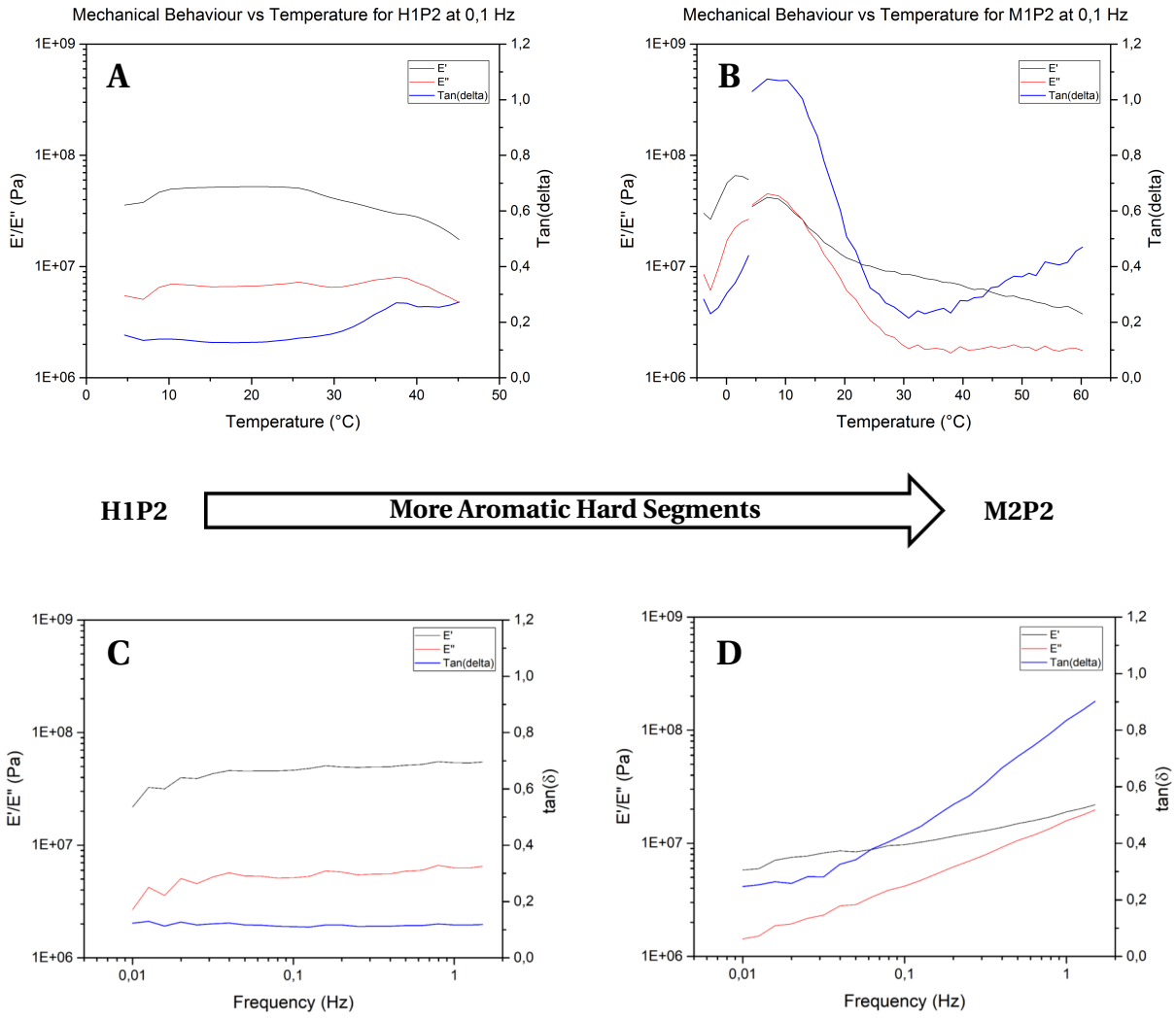

Figure 4.8: The effects of the hard block aromaticity on the mechanical properties of the bulk polymer. **A** shows the rheology at $0,1 Hz$ for completely aliphatic hard segments, with HDI being the only isocyanate for H1P2. **B** shows the same for purely aromatic hard segments, with MDI being the only isocyanate for M1P2. **C** shows the frequency response at 20°*C* for H1P2 and **D** shows the same for M1P2.

4.3.2 Surface Free Energy

Figure 4.10 shows how little γ varied between the compositions. Between 10 and 25°*C*, the γ decreased seemingly linearly, while after 25°*C* it increased again for all of the polymers. It is likely that these changes are related to the mobility and position of the hydrophobic branches of the polyol (fig. 4.9). However, while the surface free energy changes by about 30% over the entire temperature range, the stiffness changes by almost an entire order of magnitude for most polymers, and loss factors rangeing between 0,3 and 1,25. It is therefore reasonable to say that the changes in surface free energy, both between polymers and over the

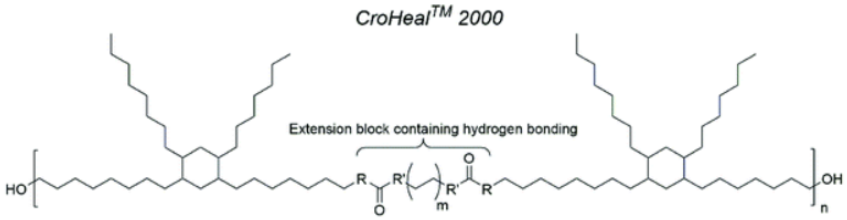

Figure 4.9: Polymer architecture for the polyol used in this project. While this is a long and mostly linear polymer, there are 4 branches on each repeating unit.

temperature range for a single polymer, are negligible when it comes to dry adhesion.

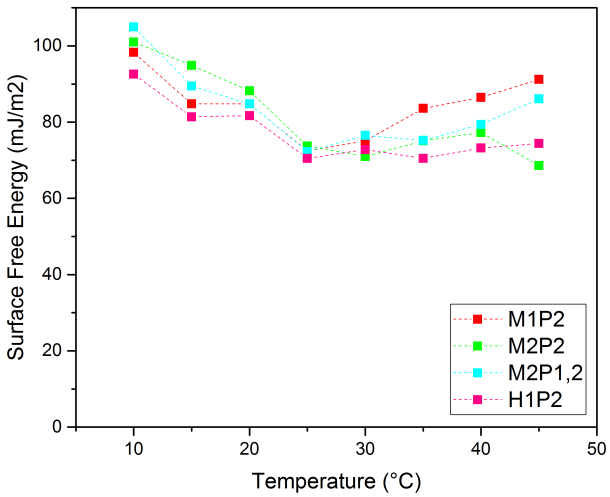

Figure 4.10: Surface free energy changes over the relevant temperature range for M1P2. All results came from water contact angle measurements.

4.4 Micropillar Adhesion

This section shows the adhesive performance of the micropillars. Each adhesion value in this section is the average of at least 3 pillars with identical geometry, chemical composition and measurement setting unless mentioned otherwise. For each individual pillar, each measurement was repeated at least 5 times to ensure that the adhesion was repeatable, constant and reliable.

Polymer compositions with similar adhesive behaviour were grouped and discussed together. This lead to three groups with decreasing adhesive performance. The first contained polymers that showed a clearly defined peak in adhesion between $10-15°C$: M0,8P2, M1,5P2 and M1P2. The second group contained stiffer polymers that peaked around $30-35°C$: M2P1,2 and M2P2 and their intermediate polymer M2P1,2/2. Lastly, the third group contained the two polymers without a clear adhesion peak: H1P2 and H/M1P2.

4.4.1 Polymers peaking around $10-15°C$

This first group showed excellent adhesion at at low temperatures and a large frequency-dependency at $20°C$. For M0,8P2 a single pillar could support $0,17N$ at $20°C$ and $1000\mu m/s$. Seeing as the tip surface was only $0,385mm^2$, this resulted in an adhesive strength of around $440kPa$, a similar order of magnitude to

other state-of-the-art pillars[19][9]. However when making this comparison, two important factors have to be taken into account.

First, it has to be noted that the results shown here are for individual pillars, while those reported by for example Drotlef et al.[12] ($300kPa$) or Del Campo et al[9] ($170kPa$) were for complete pads. It is expected that incorporating the pillars used in this study into a dry adhesive pad will lower the total adhesive strength. Secondly, studies[32] have shown that the performance of the dry adhesive increases as the pillars become smaller. This is due to the increased contact splitting improving adaptability. As the pillars used in this project were fairly large ($700\mu m$ diameter compared to eg. $67\mu m$ for Drotlef et al. and $10\mu m$ for Del Campo et al), they are expected to perform better when scaled to a similar size. Therefore, incorporating the pillars used in this project into dry adhesive pads similar to state-of-the-art concepts is expected to result in a similar, if not better performance.

As to the temperature response, fig. 4.11 shows that adhesion increased rapidly with temperature below T_g, yet once the glass transition has occurred, adhesive strength started to decrease with temperature, yet even at higher temperatures, the adhesion was still stronger than below T_g.

Looking at fig. 4.12, the pillar adhesion was greatly increased by speeding up the pull-off phase, although the increase was not linear and indication of an upper limit is visible. The decrease at $1000\mu m/s$ for M1,5P2 was likely due to a measurement error caused by the high speed coming close to the sampling frequency of the DMA.

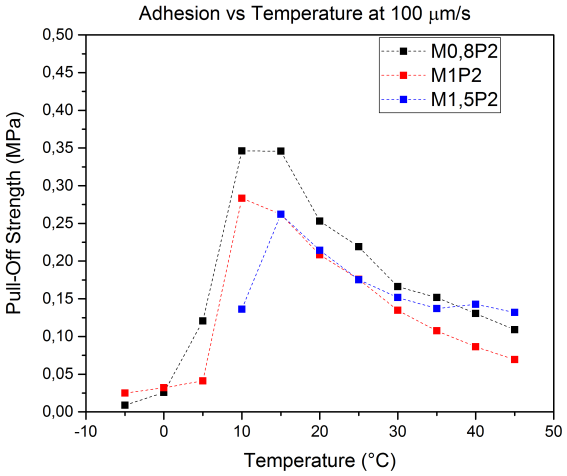

Figure 4.11: Adhesion versus temperature at a $0,1Hz$ strain rate ($100\mu m/s$) for polymers with varying levels of hard-/soft block ratios and/or soft block crystallinity.

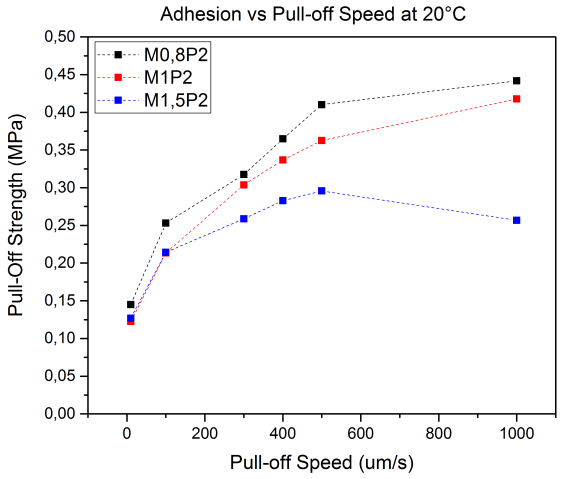

Figure 4.12: Adhesion versus strain rate at $20°C$ for varying levels of hard-/soft block ratios and/or soft block crystallinity.

4.4.2 Polymers peaking around $30-35°C$

For the polymers in this group, the maximum adhesion was significantly lower than for the previous group. Once again, this adhesion peak is found around T_g. At the high end of the temperature range, they show similar performance to the previous group.

Looking at the frequency response in fig. 4.14, it becomes clear that the adhesion at $20°C$ was barely, if at all, affected by adhesion. Furthermore, the adhesion at $1000\mu m/s$ was several times lower than that of the previous group.

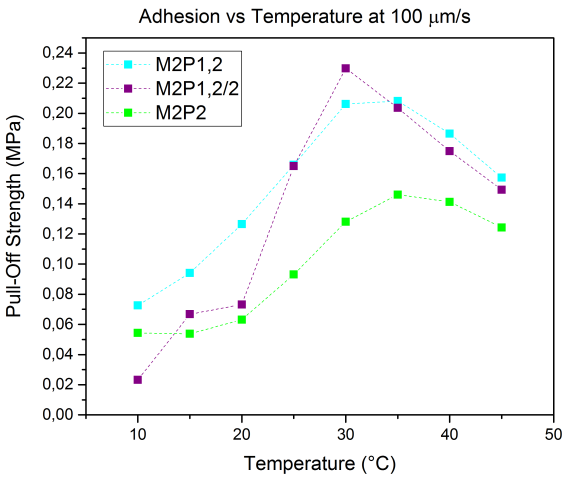

Figure 4.13: Adhesion versus temperature at a $0,1Hz$ strain rate ($100\mu m/s$) for polymers with varying soft segment lengths.

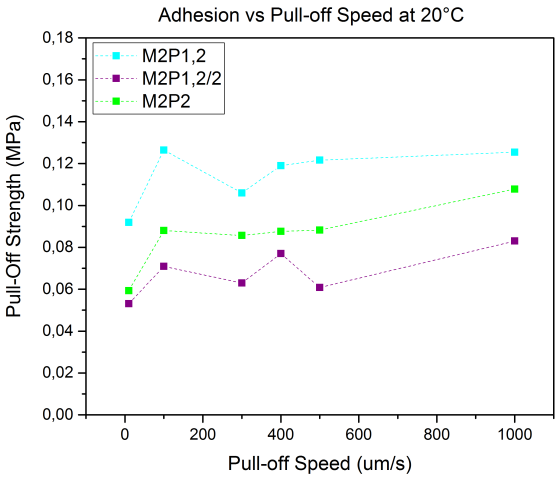

Figure 4.14: Adhesion versus strain rate at $20°C$ for polymers with varying soft segment lengths.

4.4.3 Polymers without a clear peak

This last group performed relatively poorly. Below $30°C$, adhesion was almost non-existent. Only once this temperature was reached, did adhesion slowly start increasing. At $45°C$, its adhesion comes close to that of the previous two groups, albeit still visibly lower (around $0,04N$ compared to $0,05-0,06N$).

Figure 4.16 shows that while adhesion did seem to increase slightly with pull-off speed at $20°C$, the absolute value of this adhesion is very low compared to that of the first group.

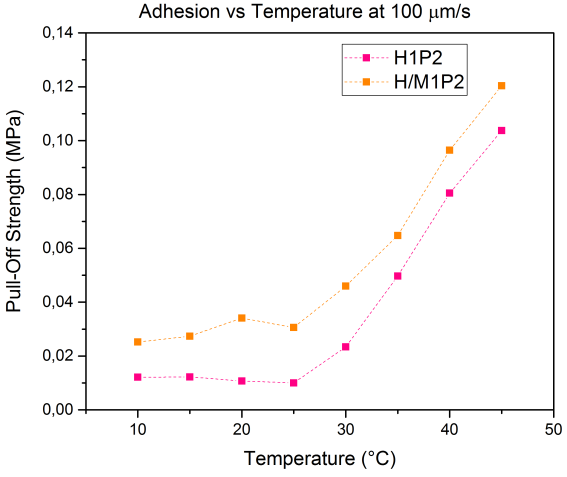

Figure 4.15: Adhesion versus temperature at a $0,1Hz$ strain rate ($100\mu m/s$) for polymers with varying hard block aromaticity.

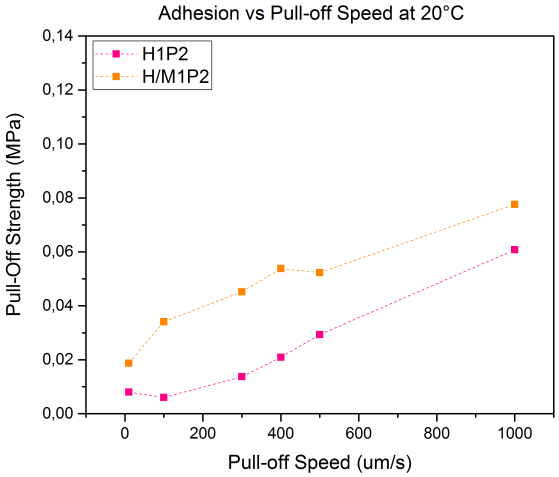

Figure 4.16: Adhesion versus strain rate at $20°C$ for polymers with varying hard block aromaticity.

5 Discussion

5.1 Accuracy of the Kendall-Maugis model

One of the main assumptions of the Kendall-Maugis model was fully linear elastic deformation. Therefore, this model could not be applied to polymers with pronounced viscoelastic behaviour such as TPUs. However, below the glass transition temperature, even semi-crystalline polymers exhibit predominately elastic behaviour. This meant that the Kendall-Maugis should reasonably accurately predict the adhesive performance of the micropillars below T_g.

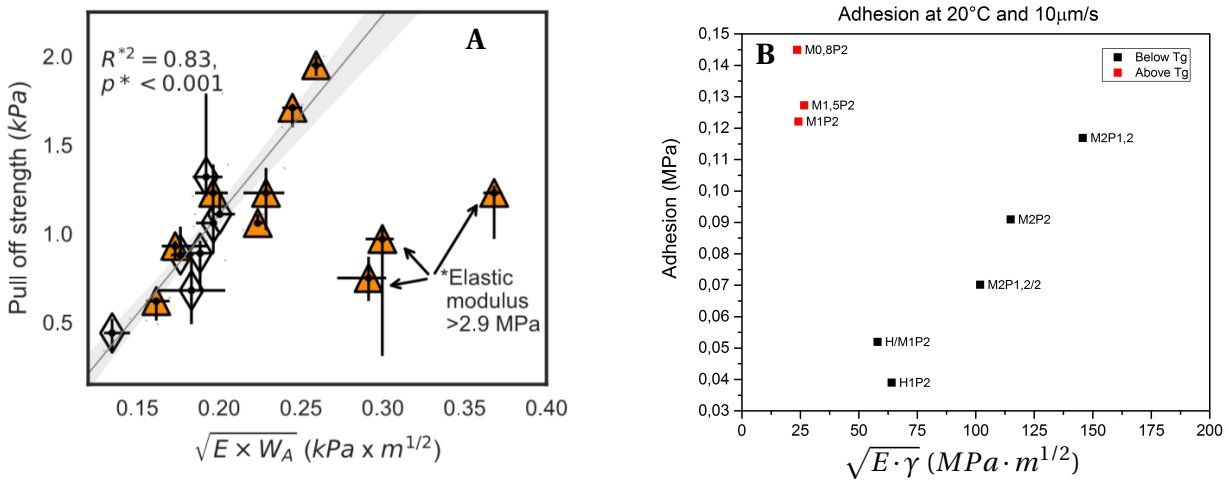

Figure 5.1: Adhesion vs $\sqrt{E\gamma}$ for varying polymers. **A** shows the results of this research project, where each represents the performance of a different polymer at 20°C. **B** shows the results of Kizilkan et al.[10], where each datapoint represents the performance of a certain polymer at room temperature.

This hypothesis was tested by looking at the adhesive performance well below the T_g at the lowest possible pull-off rate. The low temperature was used to ensure the pillar had the lowest possible viscous component. However, even at those temperatures, the polymers could still show some viscous behaviour, which is why only adhesion at the lowest possible frequency, where the effects of viscous behaviour is kept to a minimum, were looked at.

Interestingly, section 5.1 shows a clear linear relation between $\sqrt{E^*\gamma}$ and adhesion. This indicates that even for semi-crystalline polymers such as TPU, the Kendall-Maugis model could be used to predict adhesive performance at low pull-off rates and well below T_g. However, the red datapoints show clearly that for polymers that were above their T_g, the model becomes highly inaccurate and adhesion was much higher than expected.

Although section 5.1 does provide strong proof for the validity of the Kendall-Maugis model, it is important to look at the isolated relations between adhesion and both of the polymer properties used in that model. This is done in the next two sections, where the effects of stiffness are substracted from adhesion to investigate those of surface free energy and vice versa.

5.1.1 Scaling with $\sqrt{\gamma}$

Both surface free energy and bulk polymer stiffness result from the polymer architecture of the material. These parameters are therefore highly interdependent, and impossible to control independently. In order

to isolate the effects of γ, those of E^* had to be accounted for. This was done by dividing the adhesive force by the relevant pillar stiffness, which should nullify the effects of stiffness. This so called corrected adhesion should scale linearly with $\sqrt{\gamma}$, as predicted by the Kendall-Maugis model.

Section 5.1.1 shows that this was not the case. At first sight, this would indicate that the relation between surface free energy and adhesion as proposed by Kendall-Maugis does not hold for TPUs, even below T_g. However, the seemingly random spread was likely caused by the changes in γ being negligible when compared to those in stiffness. Take for example M2P1,2 at 20°C and M2P2 at 10°C, two points from opposite side of the available γ-range. Whereas the surface free energy for M2P2 is 28% higher, the stiffness increased by roughly 400%. As adhesion is supposed to scale with the square root of both, this means while the adhesion increased by roughly 150%, only 13% was caused by the change in surface free energy. As the change in adhesion was thus mainly driven by stiffness increasing, the measurement errors in both adhesion and stiffness created too much noise when trying to isolate the effects of surface free energy.

Therefore, the results of this study could not be used to validate the $P \sim \sqrt{\gamma}$ relation proposed by Kendall-Maugis, due to the small surface free energy range. Properly investigating this relation using TPU micropillars as proposed in this report require dedicated polymer design and temperature settings such that the surface free energy range can be increased, while the E' is kept as small as possible. Figure 4.5 shows that ageing the pillars could result in a large change in surface free energy, which could help increase the range. However, adhesion measurements for aged pillars were only performed on M1P2 at 20°C, where the polymer is highly viscoelastic, meaning the Kendall-Maugis model is invalid. Yet, with both the aged and the fresh polymer being above T_g at 20°C, some form of comparison can be done.

Figure 4.3 shows that at higher frequencies, the difference in performance between the pillars is large. As will be discussed later in this chapter, this likely resulted from the lower viscous behaviour of the aged pillar. However, at the low end of the velocity range, there is still a clear difference and the unaged pillar still outperforms its aged counterpart. While this is again likely due in part to the lower viscous behaviour of the aged pillar, the 25% decrease in surface free energy has probably further increased the difference. Therefore, while not at all conclusive, these measurements do indicate that a positive relation between surface free energy does indeed exist, and that ageing could be used to further investigate this behaviour.

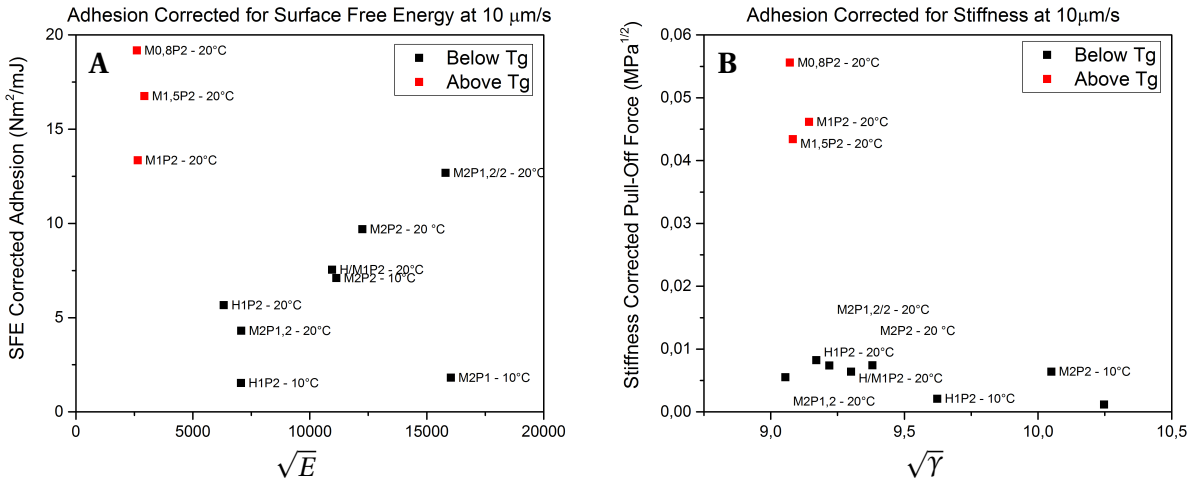

Figure 5.2: Plots showing the isolated effects of surface free energy and storage modulus. **A** shows the corrected adhesion vs surface free energy, where the corrected adhesion is $P/\sqrt{E'}$, **B** on the other hand shows the corrected adhesion vs the storage modulus, where the corrected adhesion is $P/\sqrt{\gamma}$

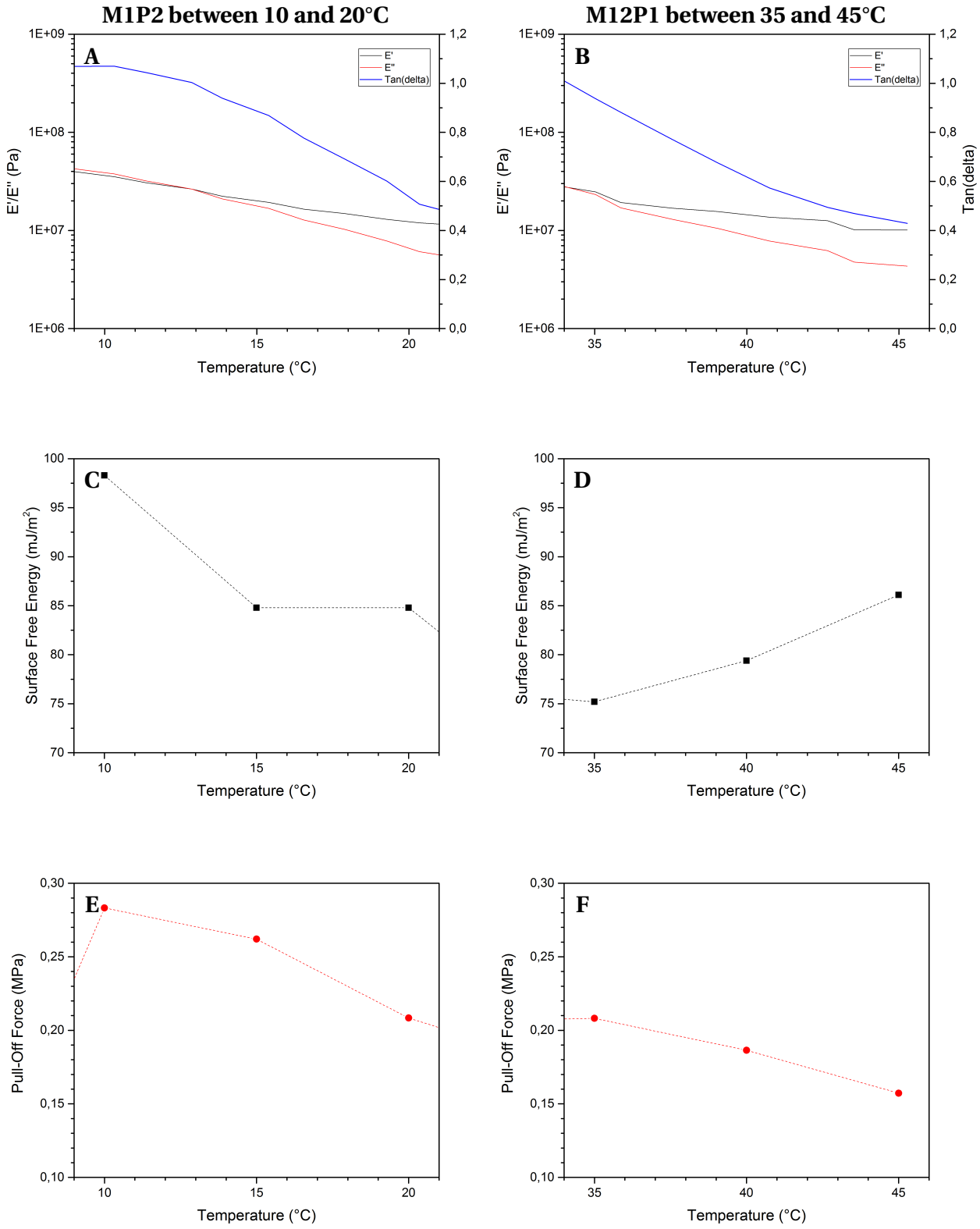

Figure 5.3: A comparison between viscoelasticity, surface free energy and adhesion for M1P2 and M2P1 at respectively $10-20°C$ and $35-45°C$. **A** shows the rheology results for M1P2 in that temperature range, while **B** shows the same for M2P1. **C** shows how the surface free energy for M1P2 varies, while **D** shows the same for M2P1. **E** shows the adhesion for M1P2 in that range, while **F** shows the same for M2P1.

While investigating the effects of surface free energy in the glassy regime was not possible, a comparison could be made in the rubbery regime. Two polymers, M1P2 and M2P1 had similar viscoelastic properties in the temperature range between, respectively $10-20°C$ and $35-45°C$, as shown in section 5.1.1. This meant that any difference in adhesive performance was likely caused by difference in surface free energy. Looking at section 5.1.1, two interesting conclusions can be made. First of all, while the surface free energy and adhesion for M1P2 follow the same trend and both decrease with adhesion, this is not the case for M2P1. This does however not prove that surface free energy and adhesion are unrelated. Instead, looking at the rheology results shows that both storage modulus and damping factor decrease with temperature for both polymers. Next to that the change in surface free energy over the temperature range is much smaller than the change in mechanical properties, which is why the shape of the adhesion-temperature curve is predominately decided by the viscoelasticiy.

However, section 5.1.1 **E** and **F** do show that for M1P2, where the surface free energy decreases with temperature, the adhesion decrease with temperature is stronger than for M2P1, where the opposite occurs. This suggest that while the changes in surface free energy were too small to dominate the adhesive performance, they were strong enough to affect the slope of the curve. Therefore, even though the surface free energy and adhesion do not follow similar trends, it seems plausible that adhesive strength scales with the surface free energy.

Secondly, the adhesion for M1P2 is noticeably higher than for M2P1. With their similar viscoelastic properties, this difference is therefore likely caused by the surface free energy differences. Section 5.1.1 **C** and **D** show clearly that for most of the temperature range, the surface free energy of M1P2 is higher than that of M2P1. This once again suggest that the surface free energy does have an important effect on adhesive properties. Therefore, while it was impossible to conclusively proof that adhesion scales with $\sqrt{\gamma}$, the results of this study do seem to support this theory.

5.1.2 Scaling with $\sqrt{E^*}$

Since the changes in surface free energy were almost negligible to those in pillar stiffness, isolating the effect of $\sqrt{E^*}$ on adhesion was fairly straightforward. Similarly to before, this was done by dividing the adhesive force by $\sqrt{\gamma}$.

Section 5.1.1 **A** shows that except for a single outlier, most datapoints follow one clear line. This suggests that there is indeed a strong relation between adhesion and pillar stiffness. Combined with the results shown in section 5.1 and in section 5.1.1**B**, this proves that the Kendall-Maugis accurately predicts the relation between stiffness and adhesion for polymers with mostly elastic behaviour.

5.2 Importance of Viscoelastic Behaviour

As indicated in the previous section, the Kendall-Maugis model did not prove accurate for polymers above the glass transition temperature. Not only did this model greatly underestimate adhesive strength, section 5.1 also showed how polymer above T_g were able to greatly outperform those in the glassy regime, despite significantly lower stiffness. This section discusses how and why this was the case.

5.2.1 Hypothesis

Looking at the results of temperature changes on dry adhesion and polymer properties (eg.fig. 5.4 and fig. 5.5), it quickly becomes clear that adhesion does not always simply scale with stiffness. At low temperatures, a decrease in stiffness lead to a strong increase in adhesion, while the inverse is true at higher temperatures. Interestingly, the temperature at which this inversion takes place is around the T_g of each polymer, indicating that viscoelastic behaviour plays a role. Therefore, $\sqrt{E}$ does not seem like a good indicator of adhesive performance in viscoelastic materials.

However, both of these plots show that the adhesion is highest around the glass transition temperature. This supports initial findings by Barreau et al.[6], whose results indicated that adhesion is best close to the glass transition temperature. Looking at this adhesion at T_g, section 5.2.1 **B** shows a clear, linear correlation

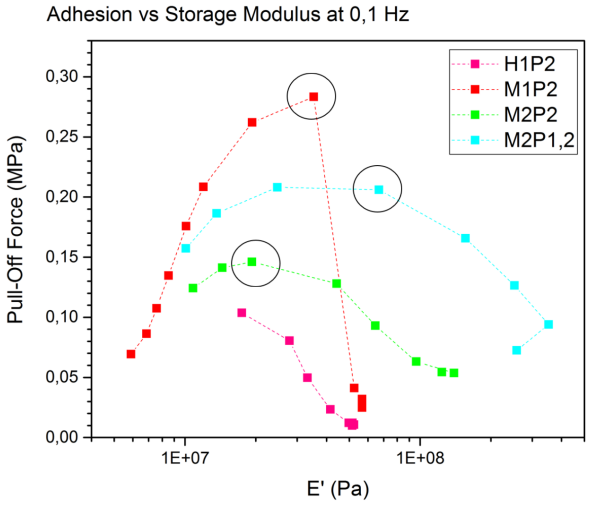

Figure 5.4: Adhesion versus Storage modulus at $0.1Hz - 100\mu m/s$ and varying temperatures for various polymer compositions. The black circles highlight the measurement at the glass transition temperature. H1P2 does not a clearly defined T_g.

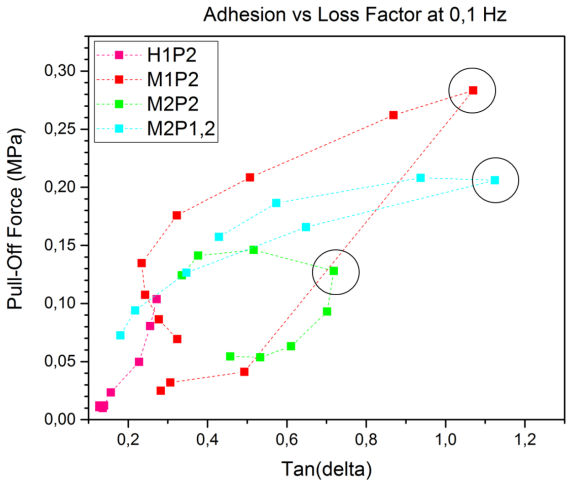

Figure 5.5: Adhesion versus Loss Factor at $0.1Hz - 100\mu m/s$ and varying temperatures for various polymer compositions.The black circles highlight the measurement at the glass transition temperature. H1P2 does not a clearly defined T_g.

between adhesion and loss factor. A similar relation was found by Castellanos et al.[10], albeit at room temperature. This indicated that for viscoelastic materials, $tan\delta$ would be a better indicator of adhesion than stiffness.

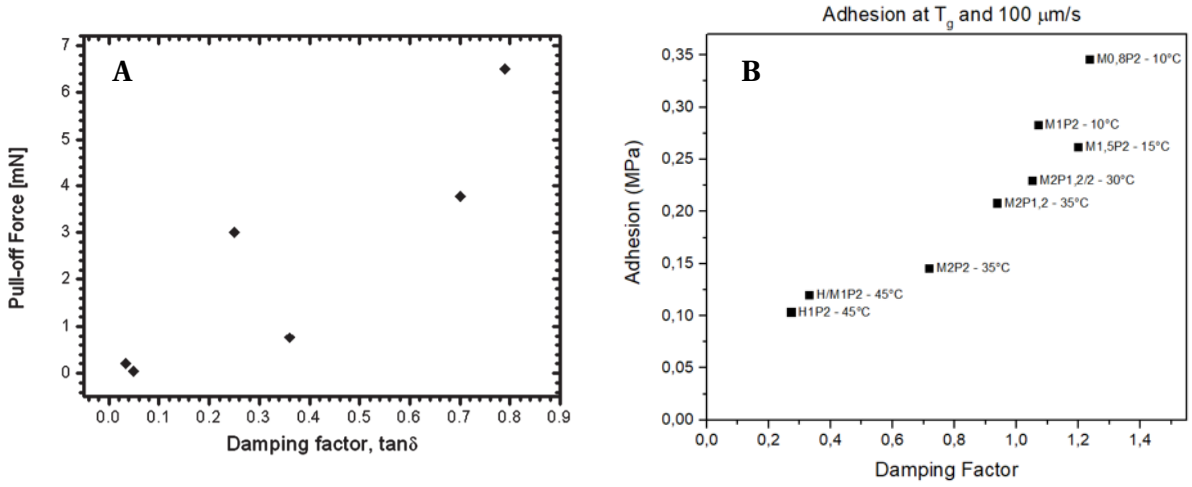

Figure 5.6: Adhesion vs Loss factor for varying polymers. **A** shows the results of this research project, where each datapoint was taken at the T_g of the respective polymer. **B** shows the results of Castellanos et al.[10], where each datapoint represents the performance of a certain polymer at room temperature.

For all of the polymers, adhesion is strongest at the glass transition temperature. Below the T_g adhesion increases together with the loss factor, while above T_g, adhesion and $tan\delta$ both decrease. The difference in the vertical position of the $tan\delta$ - adhesion line below and above T_g could be explained by the effects of the preloading phase, see appendix A. Since the loss factor is a measure of how viscous the polymer's behaviour is, this indicates the importance of viscous behaviour in dry adhesion.

Furthermore, the effects of frequency on dry adhesion provide additional support for this theory. As both the loss factor and the adhesion increase with frequency, it was likely that they are connected. Next

to that, the increase of adhesion with frequency was much stronger for polymers with a high viscous component, while for mostly elastic polymers below their T_g, this increase was almost negligible.

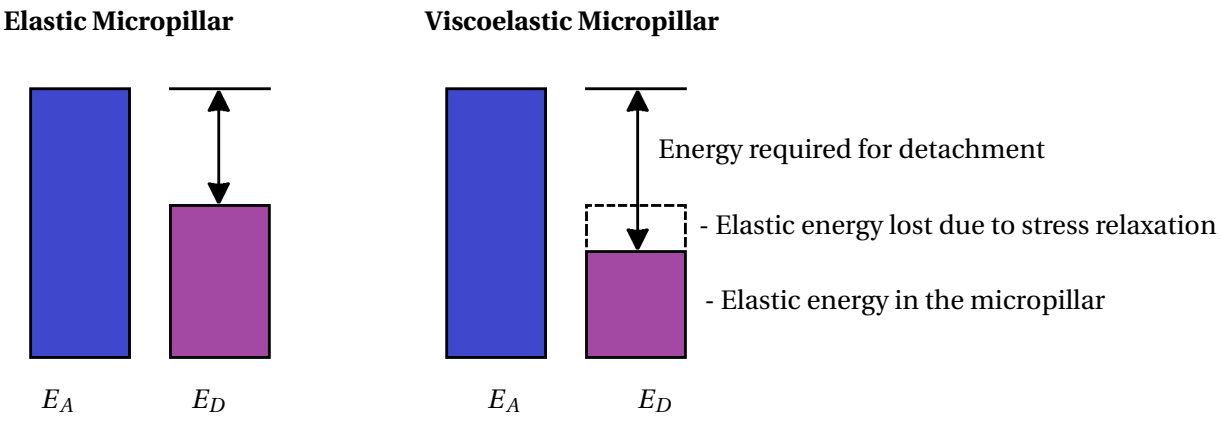

Figure 5.7: The energy balance for an attached micropillar with pure elastic behaviour and viscoelastic behaviour, where E_A is the attachment energy, or the energy required to break the surface interactions, and E_D is the detachment energy, or the energy working to return the pillar to its undeformed (and detached) state.

These results reinforce both theory[15] and experimental results[10][6], which, as mentioned in section 1.2.4, suggested that dry adhesion does not simply scale with $\sqrt{E}$ and viscous behaviour should not be neglected. Therefore, this research project suggest that the $tan\delta$, or the loss factor, is a much more suitable indicator of dry adhesive performance than the stiffness.

Viscous behaviour affects adhesion in two ways: it improves the adaptability and increases the energy consumption during pull-off. The better adaptability is caused by the stress relaxation during the preloading phase, while the required energy during pull-off is increased by the polymer transforming mechanical deformation energy into heat, that gets dissipated.

Firstly, as both JKR and Kendall-Maugis explain, the adhesive strength results from the close-range surface interactions being stronger than the internal stresses caused by deformation. In dry adhesives, this is normally achieved by improving the adaptability, and thus lowering the internal stresses, with the use of contact splitting in the microstructure. However, viscoelastic polymers also exhibit stress relaxation, which over time lowers the internal elastic stress. Therefore, this stress relaxation increases the difference between the energy required to break the surface interactions and the elastic energy stored in the polymer, as shown in fig. 5.7. This means that a larger mechanical energy input is required to detach the pillar. A larger mechanical energy requires a stronger pull-off force, which is why stress relaxation is beneficial to adhesive performance.

Secondly, as proposed by Jagota et al.[15], viscous behaviour leads to energy dissipation during the pull-off phase. A purely elastic polymer fully converts the mechanical energy input into internally stored energy. Upon unloading, the polymer returns to its original shape and the energy is released. A viscoelastic polymer however is better represented by a spring-damper system. In such a system, part of the mechanical energy is converted into heat and dissipated into the environment. This means that a larger mechanical energy (and thus force) is required to achieve the same deformation as in a purely elastic polymer. Therefore, increasing the stored energy in a pillar to the level at which detachment occurs, a viscoelastic polymer requires a larger amount of external mechanical energy, as it is partly dissipated, as shown in fig. 5.8. Once again, a larger required mechanical energy translates to a stronger pull-off force. As damping depends on the deformation velocity, this effect only increases with a faster pull-off phase.

These effects not only add up, but also reinforce each other. The stress relaxation leads to more mechanical energy having to be applied, which means even more energy is dissipated and and even stronger

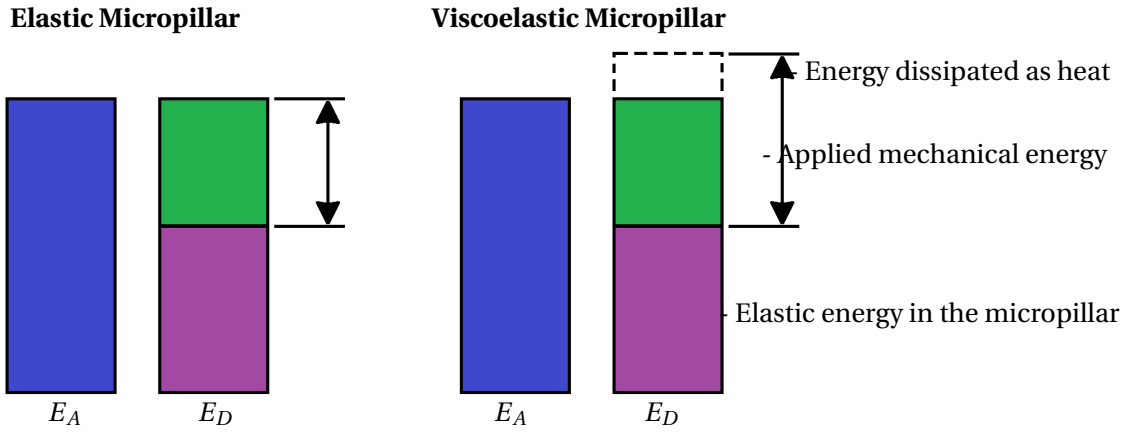

Figure 5.8: The energy balance for at detachment for micropillars with pure elastic behaviour and viscoelastic behaviour, where E_A is the attachment energy, or the energy required to break the surface interactions, and E_D is the detachment energy, or the energy working to return the pillar to its undeformed (and detached) state.

pull-off force is required. As shown in fig. 5.9, a viscoelastic pillar therefore requires a much higher energy input in order to detach. This is why, all else being equal, viscoelastic polymers greatly outperform elastic polymers in dry adhesives.

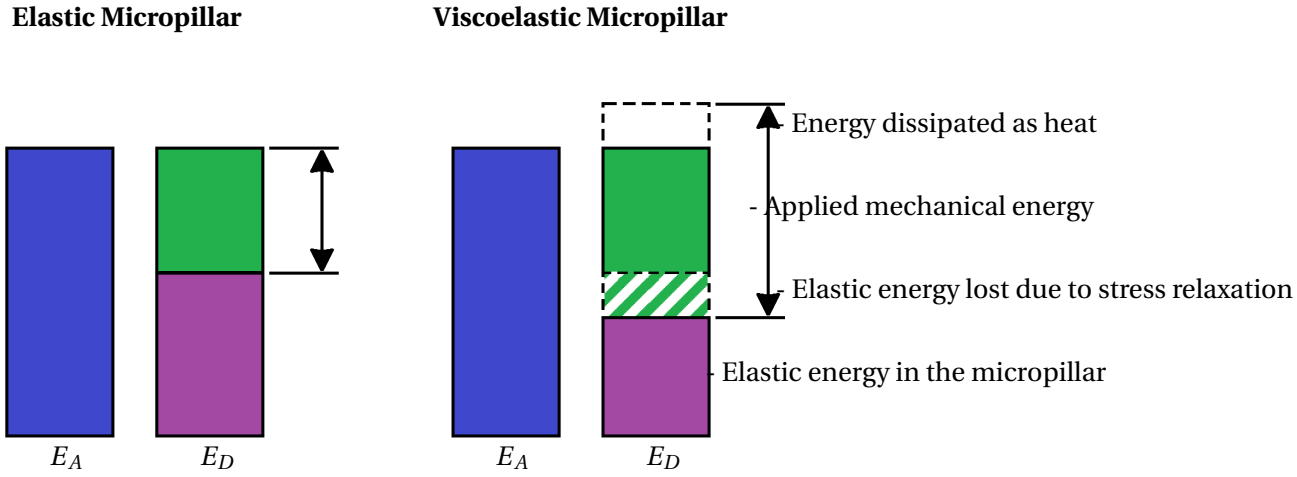

Figure 5.9: The energy balance for at detachment for micropillars with pure elastic behaviour and viscoelastic behaviour, showing the effects of both stress relaxation and energy dissipation. Here E_A is the attachment energy, or the energy required to break the surface interactions, and E_D is the detachment energy, or the energy working to return the pillar to its undeformed (and detached) state.

In order to better interpret how the loss factor affects adhesion, it is important to differentiate between dry adhesion in the glassy phase (below T_g) and the rubbery phase (above T_g). This was done by looking at specific polymers in specific temperature ranges. For the behaviour below T_g, all polymers with a T_g above $20°C$ were used. This was done for two reasons: first of all, as their T_g was above $20°C$, this meant that the frequency measurements were done in the glassy phase for these polymers, thereby giving insight into the frequency-dependent adhesion for polymers below T_g. Next to that, their high T_g ensured that for a significant part of the temperature range, they were below T_g. This created a good amount of datapoints for those polymers. All measurements ranging from the lowest available temperature to right below their T_g were included in the plots for this category. For the behaviour above T_g, all polymers with a glass

transition below 20°C were taken for the same reasons. In this case, all measurements at temperatures ranging from right above their T_g to the highest available temperature were taken.

5.2.2 Behaviour below T_g

Below the glass transition temperature, the mechanical behaviour of the polymer is dominated by the storage modulus and is mostly elastic. In this region, increasing the temperature has two effects. Firstly, an increasing temperature softens the polymer, which according to Kendall-Maugis should decrease adhesion. Secondly, it increases the viscous behaviour of the polymer as the temperature approaches T_g. This is clearly visible in fig. 4.7, where between $10-30°C$, the stiffness of M2P1,2 greatly decreased, while its loss factor increased to a maximum.

Plotting adhesion vs stiffness for polymers in the glassy regime (fig. 5.10) shows that the expected relation between stiffness and adhesion was completely overshadowed by the increasing loss factor. Figure 4.7 shows that between 10 and 30°C M2P1,2 goes from a low loss factor, almost purely elastic behaviour, to their peak loss factor, where its behaviour is extremely viscous. This increase in viscous behaviour greatly affected adhesive performance, making adhesion scale with the loss factor in the glassy phase.

Figure 5.11 shows that independent of their stiffness and surface free energy, most polymers follow a single adhesion-$tan\delta$ curve below T_g. This is in stark contrast to fig. 5.10, where each polymer follows a separate curve, albeit with a similar slope. The reason for these separate curves is exactly the loss modulus. At the low end of the temperature range, the polymers are mostly elastic and their adhesion simply scales with stiffness, which is why M2P1,2 outperforms H1P2 at 10°C. However, with increasing temperature, the polymer softens and becomes more viscous. This is why for M2P1,2/2 close to its T_g reaches a similar stiffness to H1P2 at 10°C. Yet, where H1P2 is almost purely elastic at that temperature, M2P1,2/2 is highly viscoelastic at 30°C, leading to much stronger adhesion.

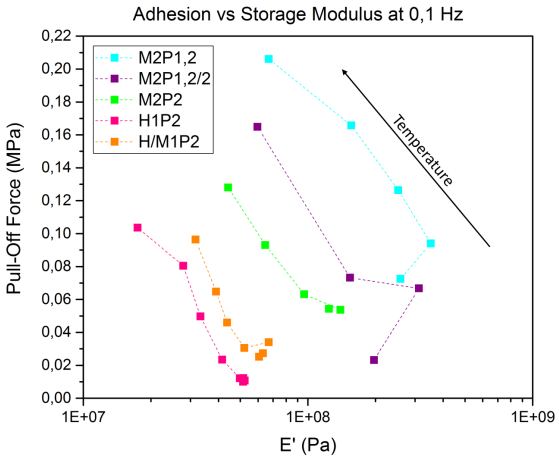

Figure 5.10: Adhesion versus Storage modulus at a 0.1Hz and temperatures varying up to T_g for polymers with that exhibited glassy behaviour for a significant part of the temperature range.

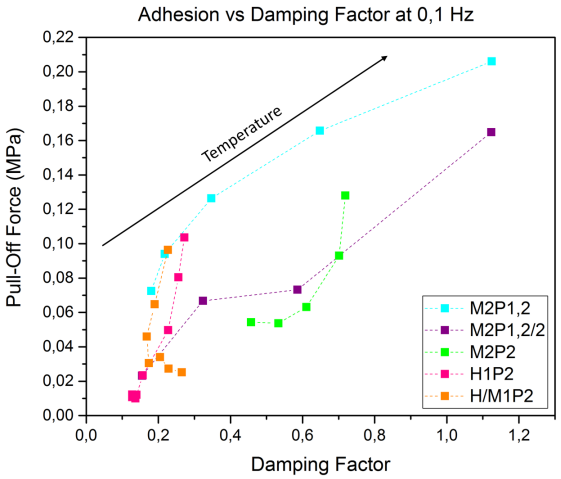

Figure 5.11: Adhesion versus Loss Factor at a 0.1Hz and temperatures varying up to T_g for polymers with that exhibited glassy behaviour for a significant part of the temperature range.

Furthermore, as glassy polymers behave elastically, there is (almost) no energy dissipated as heat during the pull-off phase, and as the magnitude of this energy dissipation is frequency dependant, the glassy polymers show no adhesion increase at higher frequencies. This is visible in fig. 5.12, where neither E' nor adhesion varied with much with frequency changes. At 20°C, most polymers shown here are at least $10-15°C$ below their glass transition temperature, which means that viscous behaviour is much less dominating than at higher temperatures. As a result, fig. 5.12 and fig. 5.13 show that adhesion scales both with increasing stiffness and increasing loss factor. As discussed in section 4.3.2, the $tan\delta$ in the frequency

domain should here be taken with a grain of salt, and are likely much lower. This means that for several polymers at 20°C, the viscoelastic behaviour is negligible enough for adhesion to become mainly stiffness driven.

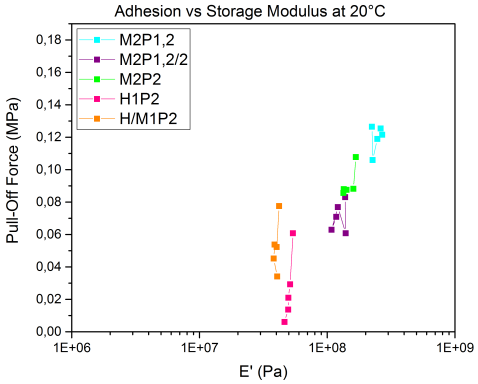

Figure 5.12: Adhesion versus Storage modulus at 20°C and varying frequencies for polymers that are in the glassy regime at 20°C.

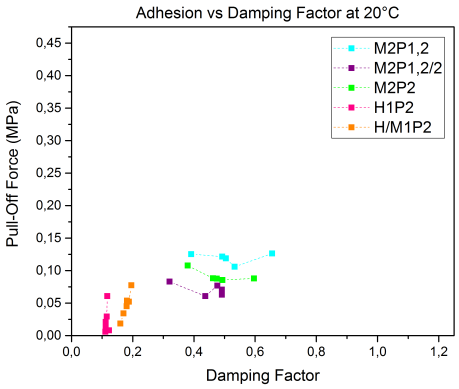

Figure 5.13: Adhesion versus Loss Factor at 20°C and varying frequencies for polymers that are in the glassy regime at 20°C.

5.2.3 Behaviour above T_g

Above the glass transition temperature the polymer exhibits clear viscous behaviour. The results of varying the frequency show how frequency-dependant the behaviour is in this phase. For example, fig. 4.8 shows that M1P2, in its rubbery phase is not only much softer than H1P2, in its glassy phase, but both its stiffness and loss factor greatly increase with frequency.

In this region, increasing the temperature greatly softens the polymer until the polymer reaches its most liquid state. As the polymer cannot become more viscoelastic, increasing temperature mostly affects how stiff the polymer is, and therefore does not further improve the effects of viscoelasticity on adhesion. Instead, the lower stiffness means that a lower force is required to apply the mechanical energy needed to detach the polymer, as detailed in the Kendall-Maugis model. Therefore, when it comes to temperature changes, adhesion does scale with stiffness in the rubbery phase, yet it also scales with $tan\delta$. Looking at fig. 5.14 and fig. 5.15, it becomes clear that this was indeed the case, and adhesion scaled with both E' and $tan\delta$. Here it can again be seen that while all polymers follow a similar P~E' slope, their curves do not coincide. However, when looking at fig. 5.15, all polymers come close to following the same curve, although some spread can be found at higher $tan\delta$-values.

The frequency response shown in fig. 5.16 and fig. 5.17 show the immense effect of pull-off rate on adhesion. This highlights once again the importance of the viscous behaviour and its damping during the pull-off phase. Similar effects were found by Abusomwan and Sitti, when investigating how retraction speed affected adhesion. Although they did not directly attribute this effect to viscoelastic behaviour, they did propose a theory that relied on velocity-dependent mechanical behaviour.
In short, in the temperature range around T_g, adhesion was not governed by E, but by the loss factor. This was due to viscous behaviour greatly improving adhesion. This increase resulted from both the stress relaxation in the contact phase and the energy dissipation during the pull-off phase.

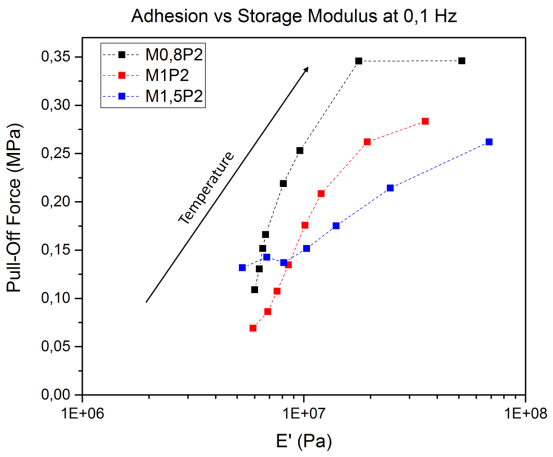

Figure 5.14: Adhesion versus Storage modulus at a $0.1Hz$ and temperatures varying from T_g onwards for polymers with that exhibited rubbery behaviour for a significant part of the temperature range.

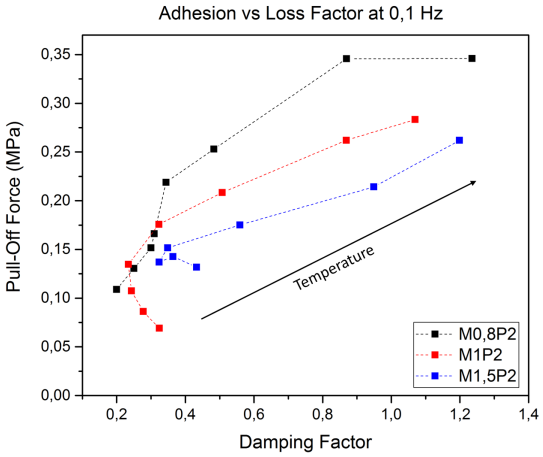

Figure 5.15: Adhesion versus Loss Factor at a $0.1Hz$ and temperatures varying from T_g onwards for polymers with that exhibited rubbery behaviour for a significant part of the temperature range.

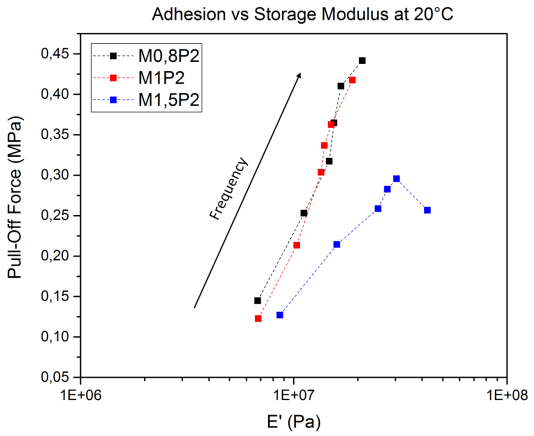

Figure 5.16: Adhesion versus Storage modulus at $20°C$ and varying frequencies for polymers that are in the rubbery regime at $20°C$.

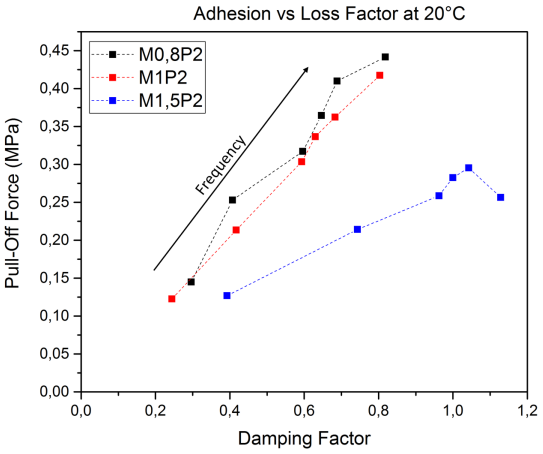

Figure 5.17: Adhesion versus Loss Factor at $20°C$ and varying frequencies for polymers that are in the rubbery regime at $20°C$.

5.2.4 Why the Adhesion-Loss Factor Curve shifts upwards after T_g

Looking at both fig. 5.19 and fig. 1.7, there is a clear difference in adhesion above and below T_g, whether the damping factor is controlled by the temperature or the chemical composition. While adhesion does scale with the loss factor in both temperature ranges, the adhesion-$tan\delta$ curve shifts upwards once T_g has been passed. As this behaviour has been found for all polymers, it is important to understand it.

It is believed that this behaviour results from the experimental setup. As discussed in section 3.1.2, preloading had to be done at a fixed force instead of a fixed strain value. As the strength of the interface depends on how much the pillar tip has deflected and adapted to the target surface, only measurements with an identical strain during preloading will have a similar interfacial strength.

However, when using a fixed preload, the softer, viscoelastic polymers will have a higher strain value, leading to better contact and a stronger interface. This is shown in fig. A.1, where the soft M1P2 reaches strong adhesion (indicating a strong interface) at a preload of only $0,03-0,04N$. However, at that same temperature, M2P1,2 is still below its T_g and therefore much harder. As a result M2P1,2 pillar only reaches a high enough strain value at around $0,10N$. It is expected that once M2P1,2 exceeds its T_g, this value will

drop to one closer to the chosen preload of $0,03N$.

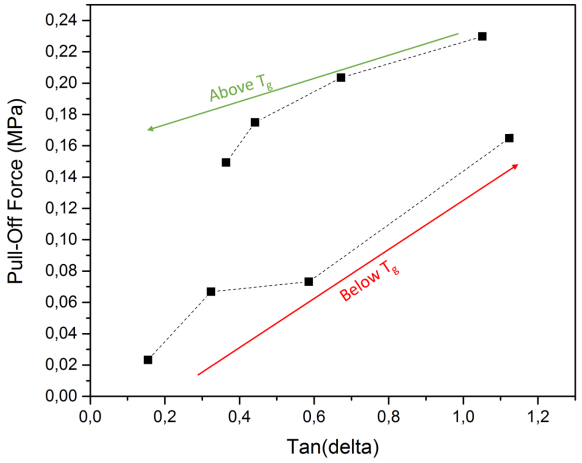

Figure 5.18: Adhesion versus Loss Factor at $0,1Hz/100\mu m/s$ and varying temperatures for M2P1,2/2 at a fixed preloading force.

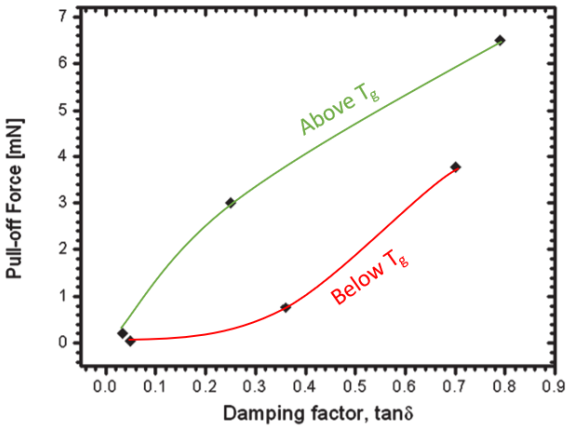

Figure 5.19: Adhesion versus Loss Factor for varying polymer compositions at a fixed preloading force[10]. The green and red line were not a part of the original publication, but were added here for clarity.

This means that the interface below T_g is likely to be significantly weaker due than above T_g, which in turn leads to lower adhesion. It is believed that this is the reason for the adhesion-$tan\delta$ curve shifting upwards. Although this effect relies on the behaviour of the polymer, it results from the loading profile, and not the intrinsic strength of the dry adhesive. Therefore, it is expected that when preloading is done according to a fixed strain value, the adhesion-$tan\delta$ curves above and below T_g will coincide. This theory is further supported by the fact that Castellanos et al.[10], whose results show similar behaviour also used a fixed preloading force.

5.3 Effects of Polymer Architecture

The understanding of the effects of polymer properties on dry adhesion was used to investigate how the polymer architecture affected adhesive performance. As discussed in section 4.3.2, the variations in surface free energy between the different polymers was negligible when compared to those in mechanical behaviour. Therefore, this section aims to explain the differences in adhesive performance by looking at the mechanical behaviour of each polymer. For this reason, the link between mechanical properties and polymer architecture is first discussed in section 5.3.1. Next, the link to dry adhesion is made for each of the parameter: starting with the hard block fraction, to the average soft segment length and ending with the hard block aromaticity.

5.3.1 The Mechanical Properties of Thermoplastic Polyurethanes

In a TPU, the hard blocks are crystalline domains, while the soft blocks rely on entanglements for structural integrity. These entanglements lead to significant stiffness at low temperatures, where the chains have low mobility. This means that once the deformation load is removed, the polymer returns to its original shape and little to no permanent deformation remains. The behaviour of the polymer at low temperatures is therefore stiff and predominately elastic, which is why this is called the glassy stage. Due to the low chain mobility, there is very little viscous behaviour in this stage.

As temperature increases, so does chain mobility. In the hard blocks, this mobility is countered by the hydrogen bonds, and the mechanical properties of the hard blocks only changes very little. The soft segments on the other hand do not have these bonds, and the increased mobility makes it much easier to deform the chains. Therefore it the polymer is still predominately elastic, but much softer in this phase, which is why it is called the rubbery stage. The transition between the glassy and the rubbery stage is grad-

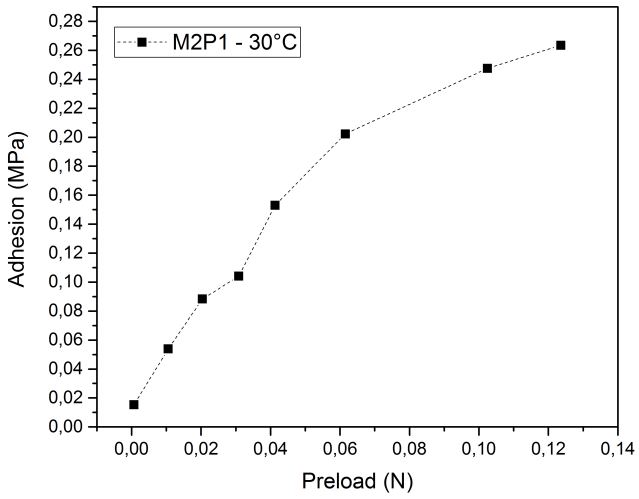

Figure 5.20: The effect of preloading on the adhesive strength of a M2P1,2 pillar at 100 $\mu m/s$, measured at 35°C.

ual and occurs over a range of temperatures, however for clarity, often a single, easily defined temperature inside of that range is called the glass transition temperature, or T_g. In the rubbery stage, the high soft segment mobility leads to significant viscous behaviour, therefore the polymer is viscoelastic in this stage.

When the temperature increases even further, the hydrogen bonds in the hard block crystals start to break, turning the hard blocks from rigid and crystalline into soft and amorphous domains. Since the hard blocks kept the polymer chains from slipping and gave the polymer its elastic behaviour, their dissolution removes most of the structural integrity of the polymer. In this phase, the polymer's behaviour can be classified as soft and even (semi-)liquid. This is why the temperature at which the hard block crystals dissolve is called the melting temperature, or T_m. Once molten, the polymer behaves as a predominately viscous polymer.

5.3.2 Hard Block Fraction

The hard block fraction was controlled using the ratio between polyol, chain extender and isocyanate. Increasing the amount of isocyanate used during synthesis leads to more hard segments per chain, which in turn results in a higher hard block fraction. The four polymers in this group have hard block mass fractions ranging from 16,2% (M0,8P2) to 20,3% (M2P2). While this seems like a small range, a large variety in adhesive performance was found within that range.

Increasing the molar fraction of diisocyanate during synthesis has two effects: first and foremost, it increases the amount of hard blocks per chain, and secondly, it is likely to increase the amount of isocyanates in the soft blocks, as both copolymerization and phase separation are imperfect.

The effect of the amount of hard blocks per chain affects both the temperature and the intensity of the glass transition. Once T_g is reached, the hard blocks are responsible for the stiff and elastic behaviour of the polymer, while the un-crosslinked and amorphous nature of the soft segments accounts for the viscous behaviour. Therefore, a thermoplastic polyurethane consisting of only crystalline hard blocks does not show lower stiffness after T_g, as their are no soft blocks in which the mobility is increased, as shown in fig. 5.21. Such a polymer would remain stiff and highly elastic until the crystals dissolve at T_m, meaning no clear glass transition or viscoelastic behaviour takes place.

For a thermoplastic polyurethane consisting purely of amorphous soft blocks, the exact opposite would

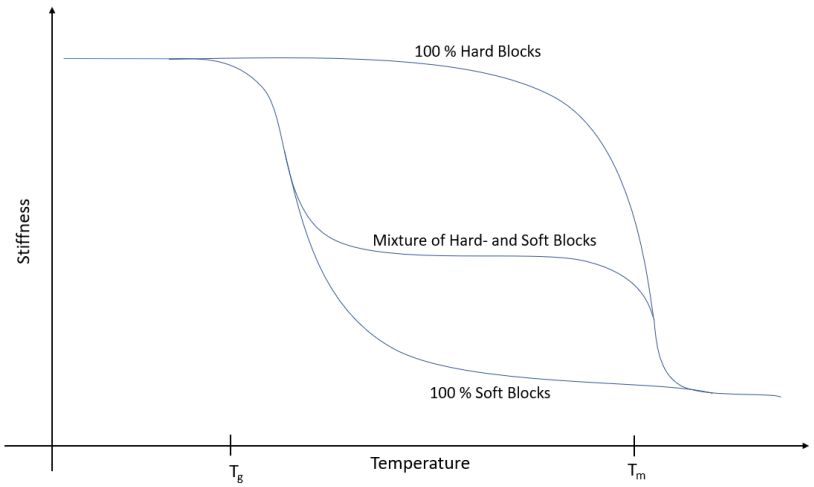

Figure 5.21: Visualisation of the temperature affects the behaviour at T_g and T_m for polymers with varying levels of hard block fractions.

occur. While stiff and mostly elastic below T_g, there are no rigid hard blocks to ensure structural integrity after T_g, which results in an extremely soft and viscous liquid-like polymer. In such a polymer, there are no crystal structures to dissolve, meaning the glass transition and the melting point coincide and the polymer does not show elastic behaviour after T_g. Adding hard blocks to such a polymer would gradually increase the structural integrity after T_g, thereby increasing the stiffness and the elastic behaviour. The more hard blocks there are, the lower the drop in stiffness and the more elastic the polymer will be after T_g. Next to that, the level of mobility in the soft segments at which the stiffness drops noticeably also increases, as there are more hard blocks forcing the soft segments to retain their shape. This higher level of mobility translates to a higher temperature, which means that the glass transition temperature increases. However, tuning the molar fraction of isocyanates during synthesis had a secondary and unintended effect. Since both copolymerization and phase separation were imperfect, some of the isocyanate ended up in the soft blocks. Since the isocyanate in this case was MDI, a stiff and short molecule with two aromatic rings, this likely increased both the stiffness and the order of the soft blocks. However, due to the random copolymerization, some soft blocks might contain much more MDI than others, leading to non-uniform polymer chains, which is called polydispersity. This polydispersity means that some of the polymer chains are much softer than the average, while other are much stiffer. This difference in mechanical behaviour also means that each chain reaches the critical drop in stiffness at a different temperature. This means that for the entire polymer, the change in mechanical behaviour happens more gradually, leading to a less sharply defined T_g, which is reflected in a broader $tan\delta$-peak.

Therefore, it can be said that an increase in hard block fraction leads to an increase in T_g, but also in lower viscous behaviour after T_g and a broader, less pronounced glass transition. These effects are clearly visible in fig. 4.6.

First of all, the higher T_g is visible in the temperature at which the adhesion peaks. Figure 5.22 shows that for the lowest hard block fraction, this is around $10-15°C$, while for the highest hard block fraction this increases to $35-40°C$. This results from adhesion being highest at T_g due to the combination of high stiffness and strong viscoelastic behaviour. Next to that, parts **C** and **D** of fig. 5.22 clearly show that at $20°C$, the polymer with the low hard block fraction shows a great improvement in adhesion at higher pull-off rates, while this is not the case for the high hard block fraction. This is due to the former polymer being above T_g at that temperature, and therefore showing excellent damping behaviour, which only increases with the deformation speed. For the latter polymer however, there is little to no damping, as this polymer is still well below its T_g. This means not only that adhesion is visibly lower, but also does not increase with

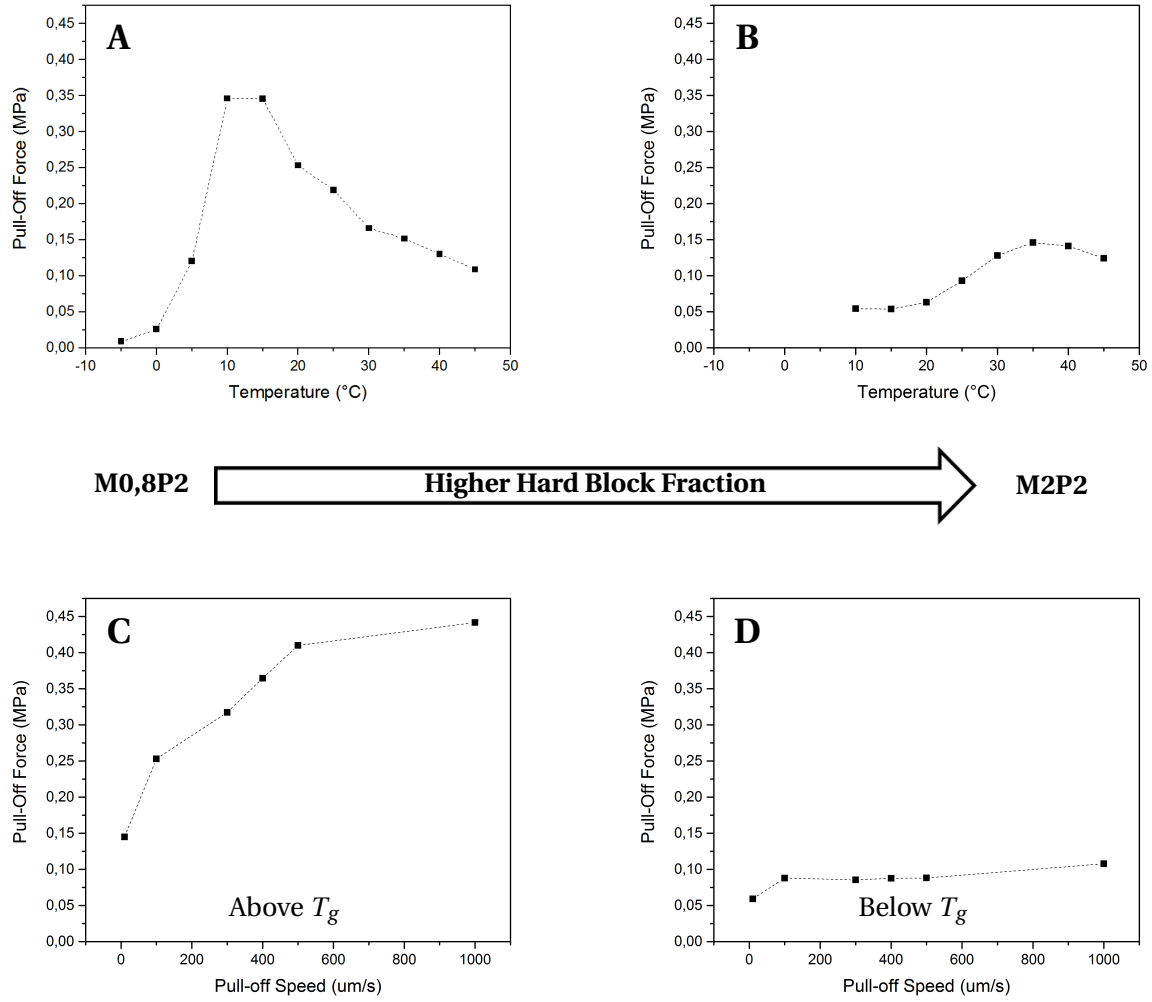

Figure 5.22: The effects of the hard block aromaticity on the adhesive performance. **A** shows the adhesion for a retraction speed of $100\mu m/s$ for the lowest hard block fraction, with the isocyanate being 16,9% of the total mass, for M0,8P2. **B** shows the same for the highest hard block fraction, with the isocyanate making up 20,3% of the total mass for M2P2. **C** shows the frequency response at $20°C$ for M0,8P2 and **D** shows the same for M2P2.

pull-off speed.

Secondly, the less pronounced glass transition is reflected in the lower temperature sensitivity of the adhesive performance. For the polymers with lower hard block fractions, the adhesion peak at T_g is much steeper and higher than that for the high hard block fractions. Whereas M0,8P2 peaks at around $0,35MPa$, M2P2 only reaches $0,15MPa$. This was caused by the higher crystallinity and therefore lower viscoelastic behaviour at T_g when the hard block fraction is increased. Furthermore, the wider $tan\delta$ peak likely also lowers the intensity of this peak. This is because the gradual glass transition leads to a suboptimal combination of medium stiffness and daming instead of the high stiffness and strong damping of a more rapid transition.

In short, increasing the hard block fraction not only increases the optimal temperature for adhesion, but also decreases the maximum adhesion the polymer can reach. While this does lower the overall performance, controlling the hard block fraction could be used to tune the adhesion to the desired operating temperature.

5.3.3 Soft Segment Length

The length of the soft segments was controlled using the molecular weight of the polyol. Keeping the molar ratios of the compositions the same, a larger Mw lead to longer soft segments. The three polymers in this group were synthesised using only $1,2kDa$ polyol (M2P1,2), only $2kDa$ polyol (M2P2) and a 50/50 molar mix between both (M2P1,2/2).

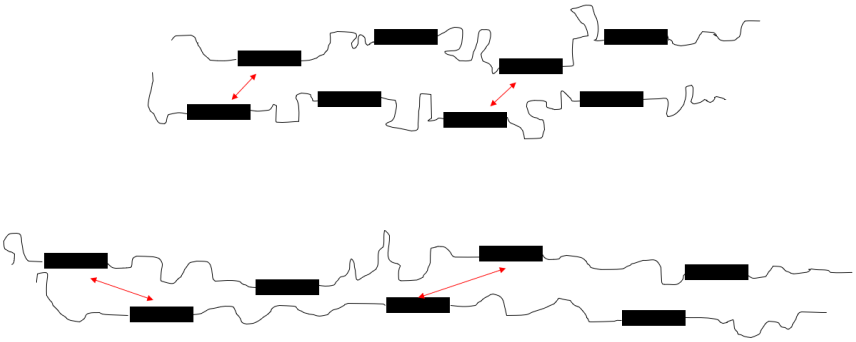

Figure 5.23: The upper figure shows two polymer chains with short soft segments, while the lower shows two chains with longer soft segments. The red arrows indicate how the distance between their respective hard segments increases if the chains are not yet properly aligned.

Increasing the average soft segment length mainly affects mechanical behaviour by increasing the distance between hard segments in a chain. This has two effects: first of all it increases the crystallinity, and secondly it improves the phase separation.
The first effect of this change is a less organised chain system. With the short soft segments, the distance between the hard segments inside of the polymer chain is fairly short. This also means that the average distance between the hard segments of multiple chains is fairly short, as shown in fig. 5.23. Due to this short distance, it is fairly easy for the hard segments to form hydrogen bonds and crystallise into organised hard blocks. When the soft segments are lengthened, this distance increases, which in turn makes it harder for organised crystal structure to form. Therefore, the polymers with shorter soft segments are more crystalline. The higher crystallinity leads to a stiffer and less viscous polymer.

Counterintuitively, this also leads to a more pronounced glass transition. In general, a more crystalline polymer relies more on hydrogen bonding between the chains, and less on entanglement for its structural integrity. As the increased mobility at T_g only affects the strength of the entanglements, the drop in stiffness is less pronounced for polymers with a higher degree of crystallinity. However, elastomeric TPUs rely heavily on phase separation, which adds a secondary effect. The phase separation turns the polymer from a mixture of crystalline and amorphous domains into a composite of both. In a mixture, both the crystalline and amorphous parts are intermixed and have to be deflected equally. However, in the composite, all of the deformation is taken up by the large soft blocks, while the hard blocks remain relatively undeformed. This means that while a polymer without phase separation has a stiffness that is roughly the weighted average of its crystalline and amorphous domains, a phase separated polymer has a stiffness that is much closer to that of the amorphous domains. As the stiffness of both domains is fairly similar below T_g, it is only after the glass transition that a phase separated polymer is much softer than its intermixed counterpart. This means that when phase separation occurs, the change in mechanical behaviour over T_g is much more pronounced. As the longer soft segments lead to a less organised polymer, this decreases the phase separation and thereby lowers the effect of T_g, despite its lower crystallinity.

Therefore, it can be said that increasing the average soft segment length leads to lower stiffness below T_g, where the crystallinity dominates, and a less pronounced T_g, due to the lower phase separation. These effects are clearly visible in fig. 4.7.

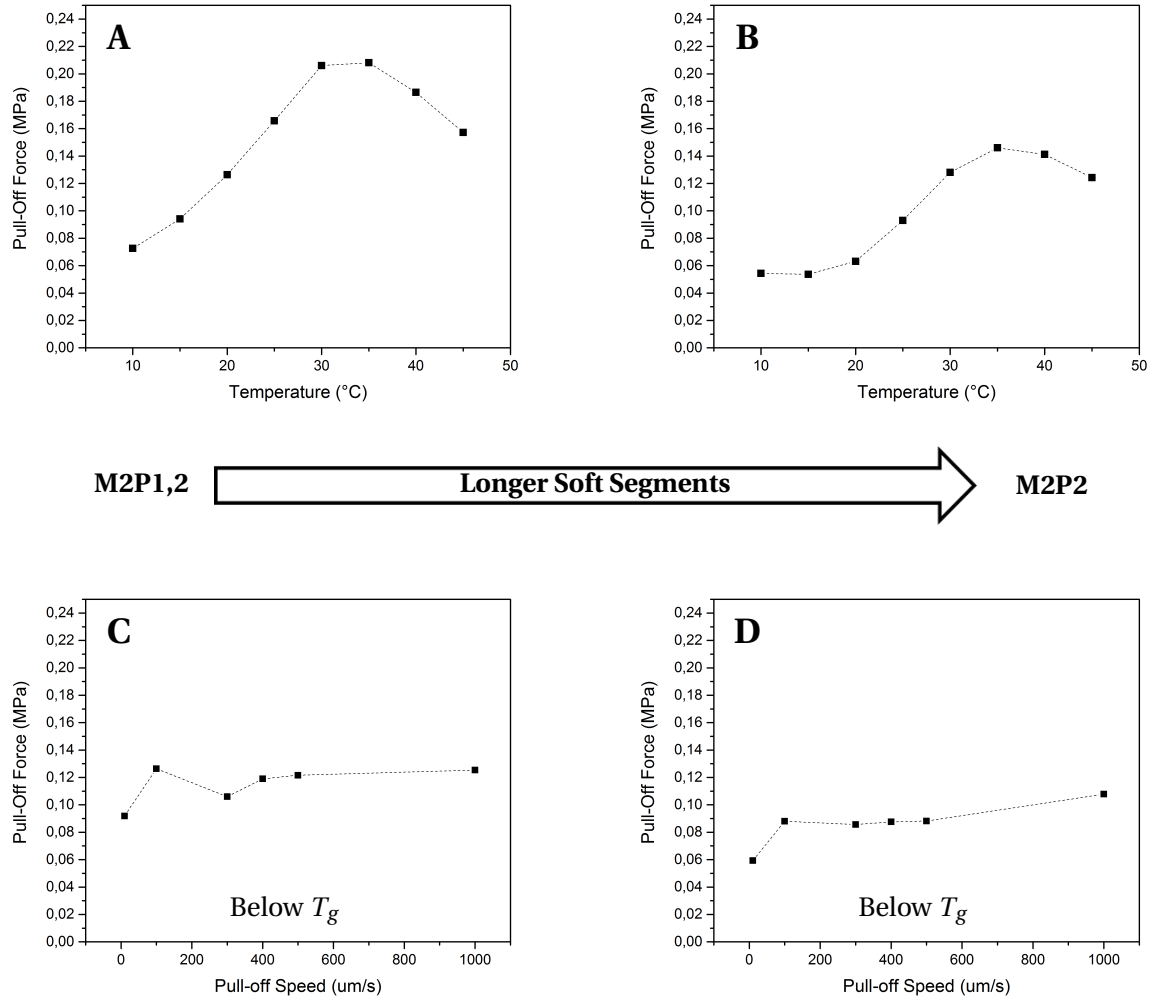

Figure 5.24: The effects of soft segment length on the adhesive performance. **A** shows the adhesion at $100\mu m/s$ for the shortest soft segments, with the average polyol molecular weight being $1,2kDa$ for M2P1,2. **B** shows the same for the longest soft segments, with the polyol having an M_w of $2kDa$ for M2P2. **C** shows the frequency response at $20°C$ for M2P1,2 and **D** shows the same for M2P2.

As to the lower stiffness below T_g, this is best shown in the frequency response. At 20°C both the polymer with the short and the long soft segments are well below their T_g, which is reflected in the limited adhesion increase at higher pull-off speeds. Figure 5.24 **C** and **D** clearly show that the polymer with the shorter soft segments has an adhesive strength of around $0,12MPa$, while the polymer with the longest soft segments only reaches $0,09MPa$. This was a direct result of the lower crystallinity caused by the longer soft segments.

Next, the less pronounced glass transition shows in the temperature response. Figure 5.24 **A** and **B** show that both at and around the T_g, M2P1,2 with its short soft segments clearly outperforms M2P2 with the long soft segments. While the width of the peak does not seem to vary as much, the intensity does. Whereas M2P1,2 reaches around $0,21MPa$, M2P2 only reaches $0,15MPa$. This was caused by the lower degree of phase separation leading to a less pronounced glass transition.
In short, increasing the length of the soft segments negatively affects adhesion. Both at lower temperatures, where the polymers are mostly elastic and after the glass transition, where viscoelastic behaviour dominates, do the shorter soft segments lead to better adhesion.

5.3.4 Hard Block Aromaticity

The aromaticity of the hard blocks was controlled by using different isocyanates during the polymer synthesis. For M1P2, only MDI was used, which lead to each hard segment containing two aromatic rings. For H1P2 on the other hand, only HDI was used, which resulted in aliphatic hard segments. For H/M1P2, a 50/50 molar mixture of both isocyanates was used, which resulted in 50% of the hard segments being aromatic, and 50% being aromatic. The aromatic rings in the hard segments have two important effects. First of all, it leads to stiffer hard blocks due to a stronger crystal structure. Secondly, they increase the phase separation in the TPU.

The extra strength of the crystral structure results mainly from $\pi-\pi$ stacking of the aromatic rings[28]. The chain structure of the aliphatic HDI is simple an symmetrical, which enables the hard segments to form hydrogen bonds and crystallize. The same occurs when using the MDI, however instead of simple hydrogen bonding, the aromatic rings stack on top of each other and form additional, stronger bonds, this is called $\pi-\pi$ stacking. Not only are there more bonds per hard segment, but the bonds themselves are stronger, which in turn results in a crystal structure that is harder to deform. Therefore, increasing the amount of aromatic hard segments leads to a stiffer polymer. An additional effect of this $\pi-\pi$ stacking is that a much higher temperature is needed to dissolve the crystal structure, which translates into much higher melting temperature (ca. 50°C for H1P2 and ca. 160°C for M1P2).

More importantly, adding aromatic rings to the hard segments increases the phase separation. For H1P2, with only aliphatic hard segments, no noticeable phase separation takes place. This means that once T_g is reached, the polymer does not become elastomeric, thereby greatly decreasing the change in mechanical behaviour over T_g. Instead, the polymer gradually softens until the melting temperature is reached. This is reflected in both low viscoelastic behaviour and a barely visible glass transition. However, once aromatic rings are added to the hard segments, there is clear phase separation and the polymer becomes highly elastomeric after T_g, as shown in fig. 5.25.

In short, the addition of aromatic rings to the hard segments increases stiffness and greatly improves the viscoelastic behaviour of the polymer. However, due to the large difference in reactivity between HDI and MDI, controlled copolymerisation with both isocyanates is difficult, leading to the intermediate polymer (H/M1P2) acting very similarly to the polymer containing only HDI, H1P2. The same effect was found by Infante[26], who investigated the effect of isocyanate mixtures on the properties of thermoplastic polyurethanes.

Looking at the lower temperature range in, a clear difference in adhesive performance can be seen. While both polymers perform quite badly, M1P2 with its aromatic hard blocks shows at least some adhesion, whereas the adhesion for the aliphatic H1P2 is negligible. This difference was caused by the $\pi-\pi$

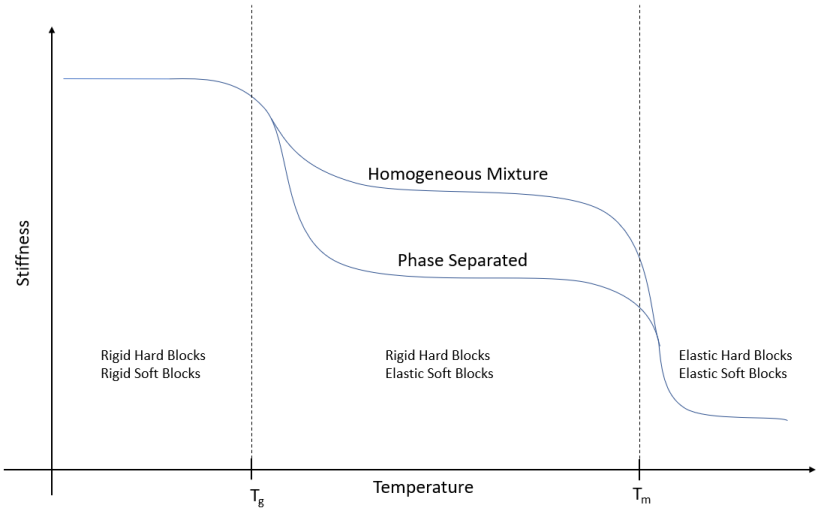

Figure 5.25: The temperature response at T_g and T_m for polymers with and without phase separation.

stacking in the aromatic hard blocks leading to additional stiffness.

Secondly, the adhesion for the polymer with purely aliphatic hard blocks shows no clear peak and only starts to increase when the polymer starts to approach its melting temperature (ca. 55°C). The polymer with aromatic hard blocks on the other hand shows a very strong peak right around its T_g. This resulted from the lack of phase separation in H1P2, which lead to a highly crystalline polymer without a clear glass transition. Furthermore, the frequency response at 20°C indicates that H1P2 shows at least some viscoelastic behaviour, which is consistent with it being a non-phase separated, yet semi-crystalline polymer instead of a thermoplastic elastomer.

In short, the addition of aromatic rings to the hard blocks massively improves the adhesion. This holds true both at low temperatures where the higher stiffness is beneficial and at higher temperatures where the phase separation leads to elastomeric behaviour.

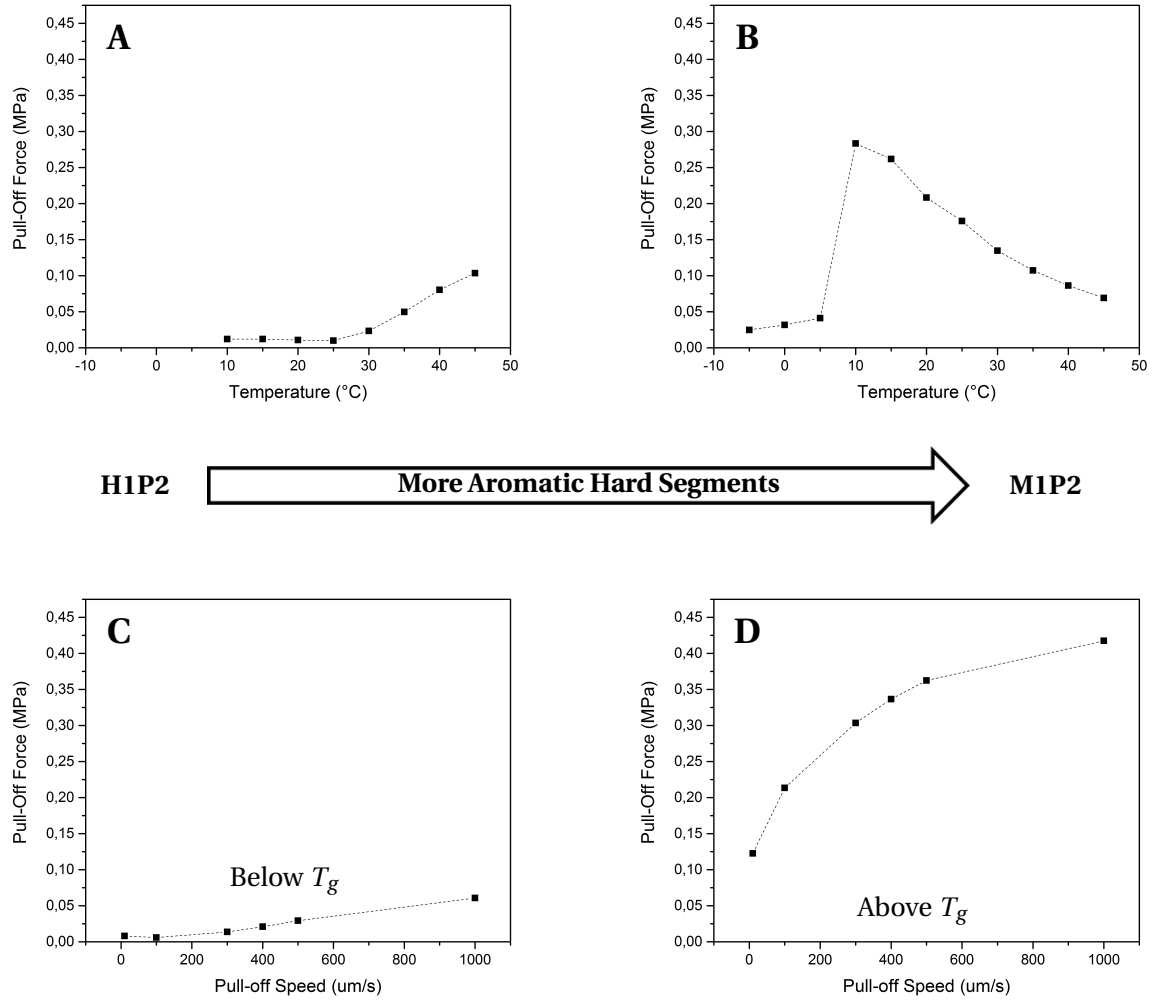

Figure 5.26: The effects of the hard block aromaticity on the adhesive performance. **A** shows the adhesion at $100 \mu m/s$ for completely aliphatic hard segments, with HDI being the only isocyanate for H1P2. **B** shows the same for purely aromatic hard segments, with MDI being the only isocyanate for M1P2. **C** shows the frequency response at $20°C$ for H1P2 and **D** shows the same for M1P2.

6 Conclusions and Recommendations

6.1 Conclusions

The adhesive performance of dry adhesives made with different tPUs was investigated. This shed light on the effects of both polymer architecture and polymer properties on dry adhesion and led to the following conclusions:

- It has been shown that viscous behaviour greatly improves adhesion due to stress relaxation during preloading and energy dissipation during pull-off.
- Increasing the hard block fraction lead to an increase in the temperature at which adhesion peaks, but a decrease in overall performance.
- Increasing the length of the soft segments decreased the adhesion both above and below T_g.
- Adding aromatic rings to the hard blocks greatly improved adhesion at all temperatures.
- Near and above T_g, the loss factor was shown to be a more reliable polymer property for adhesion prediction than bulk polymer stiffness, while the existing Kendall-Maugis model holds true well below T_g.
- A method for manufacturing dry adhesive from thermoplastic polymers with relatively high viscosity in the molten phase was devised.
- TPU micropillars have been shown to be capable of adhesive performance similar to state-of-the-art dry adhesives, despite being much larger, indicating that at a similar scale, they might greatly outperform existing dry adhesives.
- The highest adhesion was reached for M0,8P2 at a retraction strain rate of $1 Hz$ in a $20°C$ environment.
- Ageing and heat-treating the polymers was found to be an promising way to control the surface free energy.

To summarise, adhesion was best for polymers with a low hard block fraction and strong phase separation. This helped improve the viscoelasticity in the elastomeric regime, which was found to be highly beneficial to adhesion. The stress relaxation during preloading and the energy dissipation during pull-off greatly increased critical pull-off force. The combination of using a polymer with pronounced viscous behaviour, testing it at near its glass transition and/or at the quickest possible pull-off force yielded the best results. This was shown by M0,8P2 reaching similar pull-off stresses to state-of-the-art dry adhesives, despite a sub-optimal geometry.

Next to that, a new manufacturing method was engineered in order to create dry adhesives from molten thermoplasts with high viscosity. This greatly increases the range of polymers from which dry adhesives can be made, hopefully paving the way for future research into the material choice and optimisation in dry adhesives.

6.2 Recommendations

Further improvements and extensions to this research project could be done as follows:

- Incorporate the results presented in this report into an updated version of the Kendall-Maugis model, such that the model can be applied to viscoelastic polymers above T_g.
- Use polymer ageing to investigate the effects of surface free energy. While this also affects viscoelasticity, it greatly increases the surface free energy, allowing for easier isolation of the effects of this parameter.
- Adapt the measurement setup to allow for preloading based on deflection instead of compressive force.
- Update the manufacturing method such that dry adhesive pillars/pads with similar pillar radii to state-of-the-art dry adhesives can be made.
- Investigate how the polymer architecture can be used to control soft block crystallinity and how it affects adhesion.
- Discover whether the findings presented in this report for individual pillars are also applicable to full dry adhesive pads.
- Similar experiments with different pillar geometries are recommended, as it is important to determine whether the effects of polymer architecture on adhesion depend on geometric parameters.
- Perform adhesion experiments with damaged and self-healed pillars, to investigate if and how efficiently adhesive performance can be recovered.

Appendix A Sensitivity to Preloading Force

Preloading was done at a $30mN$ for all polymers, due to time and setup limitations. Since the stiffness of the polymers varied greatly, the pillar deflection at $20°C$ for this force varied from only 0,1% of the pillar length to almost 4%. During the preloading phase, it is crucial that the pillar tip is deflected enough to properly adapt to the target surface and adhere well. Therefore, the most objective comparison between the polymers requires preloading at a fixed deflection instead of a fixed force.

Since this was not possible, a fixed preload had to be chosen. The value of this preloading force was a trade of between ensuring good contact (requiring a high force) and ensuring that the pillars did not get damaged (requiring a low force). As testing all pillars at all temperatures was too time-consuming, only two of the softest pillars were tested at the $45°C$, where they were most susceptible to damage. Due to both accuracy and time-related reasons, the discretisation was done in steps of $0,01N$. Both the M1P2 and H1P2 pillars could withstand preloading forces of up to $0,03N$ before deforming plastically. This meant $0,03N$ was the highest possible preload that could be used for all pillars at all temperatures, which made it the most suitable value.

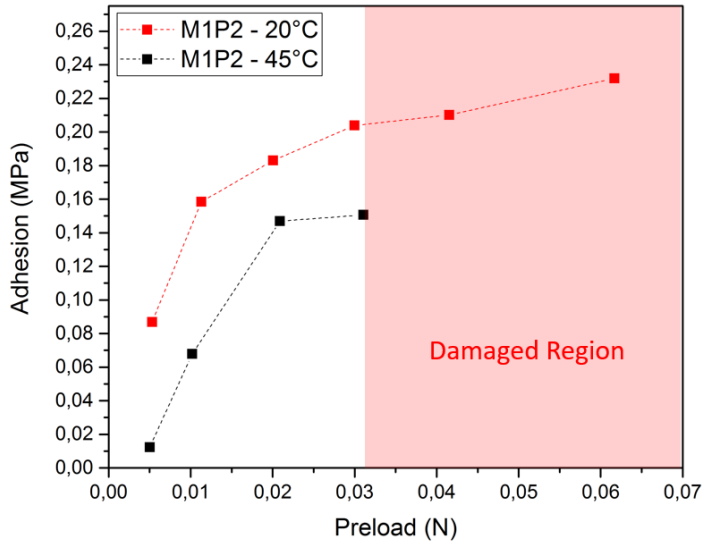

Figure A.1: The effect of preloading on the adhesive strength of a M1P2 pillar at 100 $\mu m/s$ for 20 and $45°C$.

As fig. A.1 shows, a preload $0,03N$ did not result in the highest possible adhesion. However, $0,03N$ is the lowest preloading that fell after the curve started to flatten out for the softer polymers. Therefore, while a higher preloading would lead to higher adhesion, the difference was small enough to be acceptable. However, one has to keep in mind that due to this fixed preloading force, the preloading strain will increase with temperature, causing unintended differences in the interfacial strength.

Appendix B Rheology for all Polymers

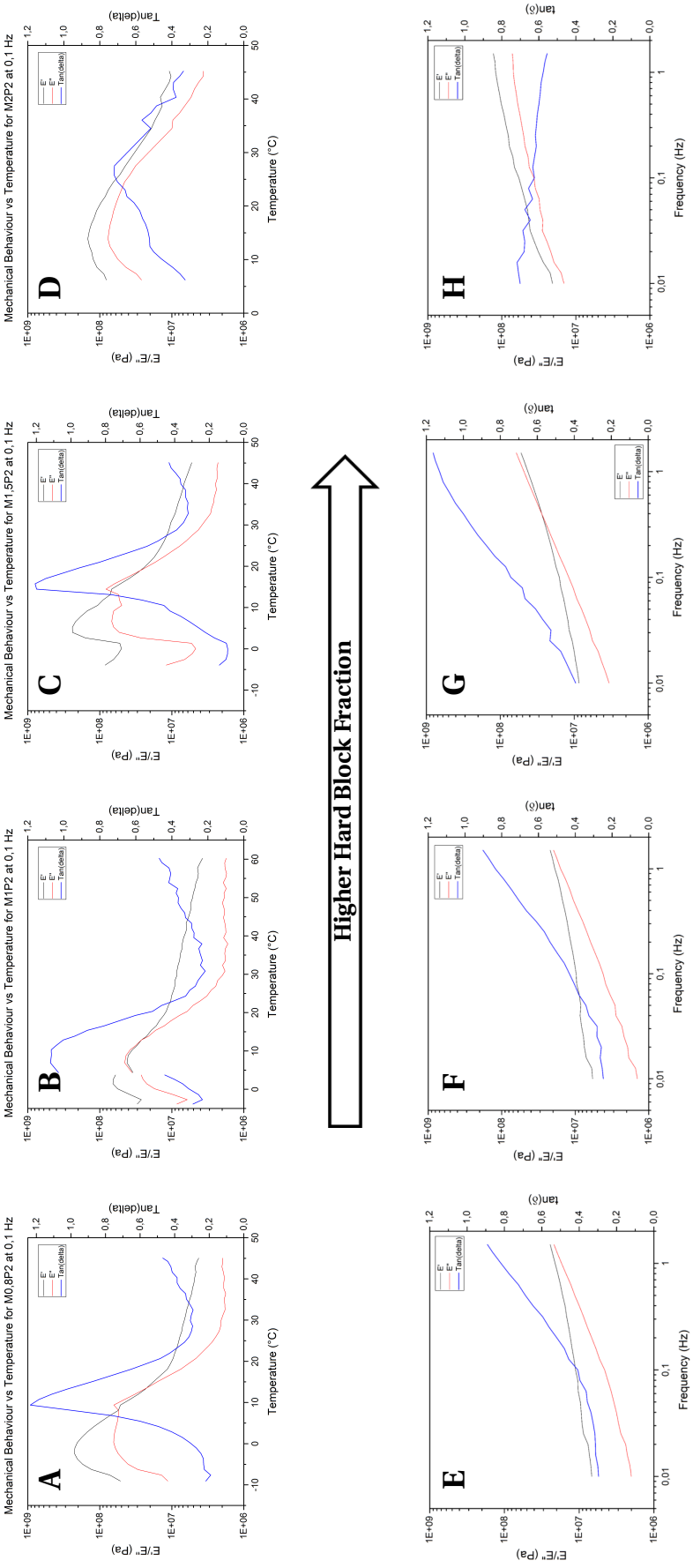

Figure B.1: The effects of hard block fraction on the mechanical properties of the bulk polymer. **A** shows the rheology at $0,1 Hz$ for the lowest hard block fraction, with the isocyanate being 16,9% of the total mass, for M0,8P2. **B** shows the same for M1P2. **C** shows the rheology for M1,5P2 and finally **D** shows the highest hard block fraction for M2P2 with a 20,3% of MDI. **E** shows the frequency response at $20°C$ for M0,8P2. **F** shows the same for M1P2 while **G** shows M1,5P2. Finally **H** shows the frequency response for M2P2.

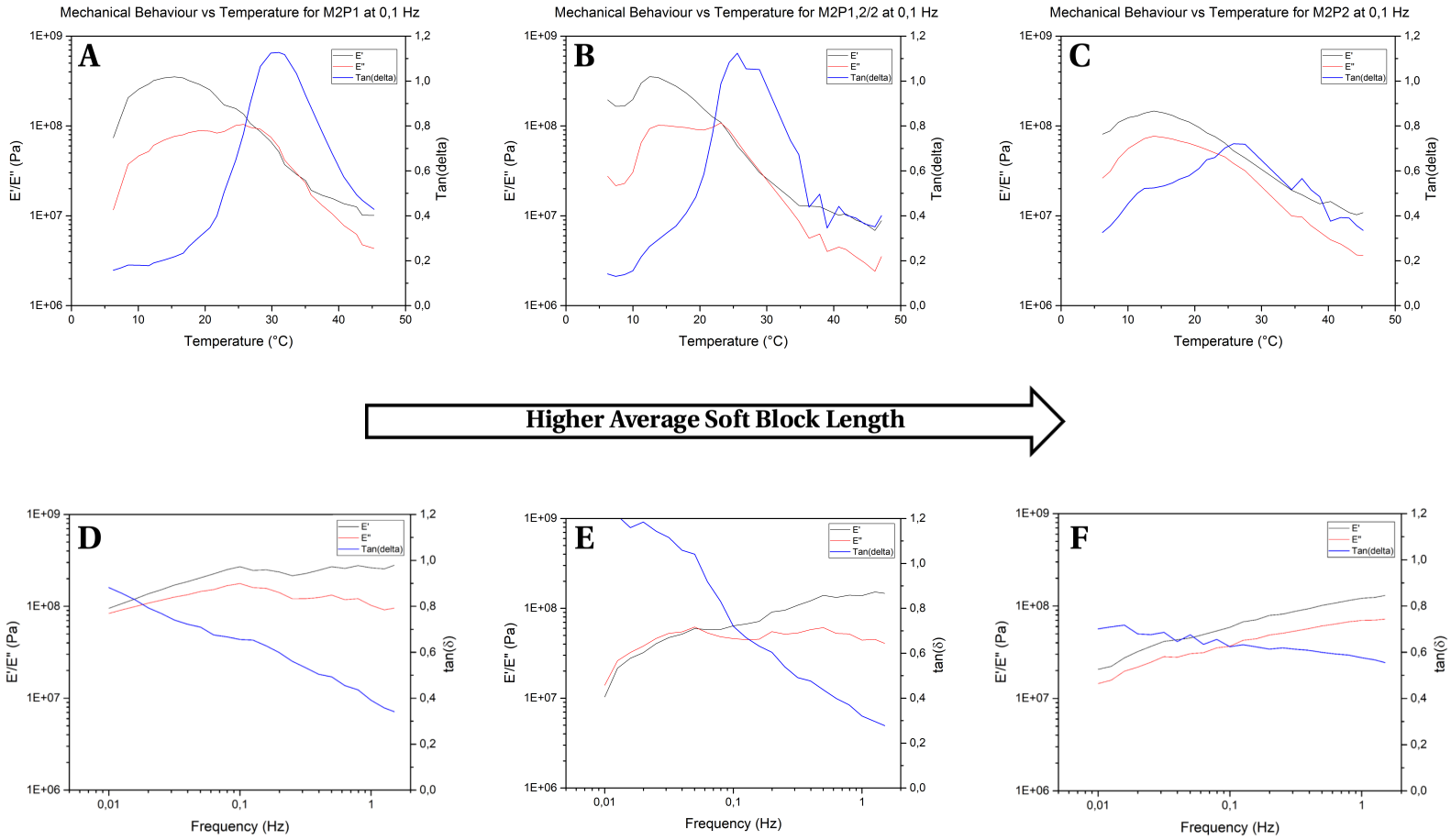

Figure B.2: The effects of soft segment length on the mechanical properties of the bulk polymer. **A** shows the rheology at $0,1\,Hz$ for the shortest soft segments, with the average polyol molecular weight being $1,2kDa$ for M2P1,2. **B** shows the same for an intermediate average length, $1,6kDa$ for M2P1,2/2. **C** shows the longest soft segments, with the polyol having an M_w of $2kDa$ for M2P2. **D** shows the frequency response at $20°C$ for M2P1,2, **E** for M2P1,2/2 and **D** shows the same for M2P2.

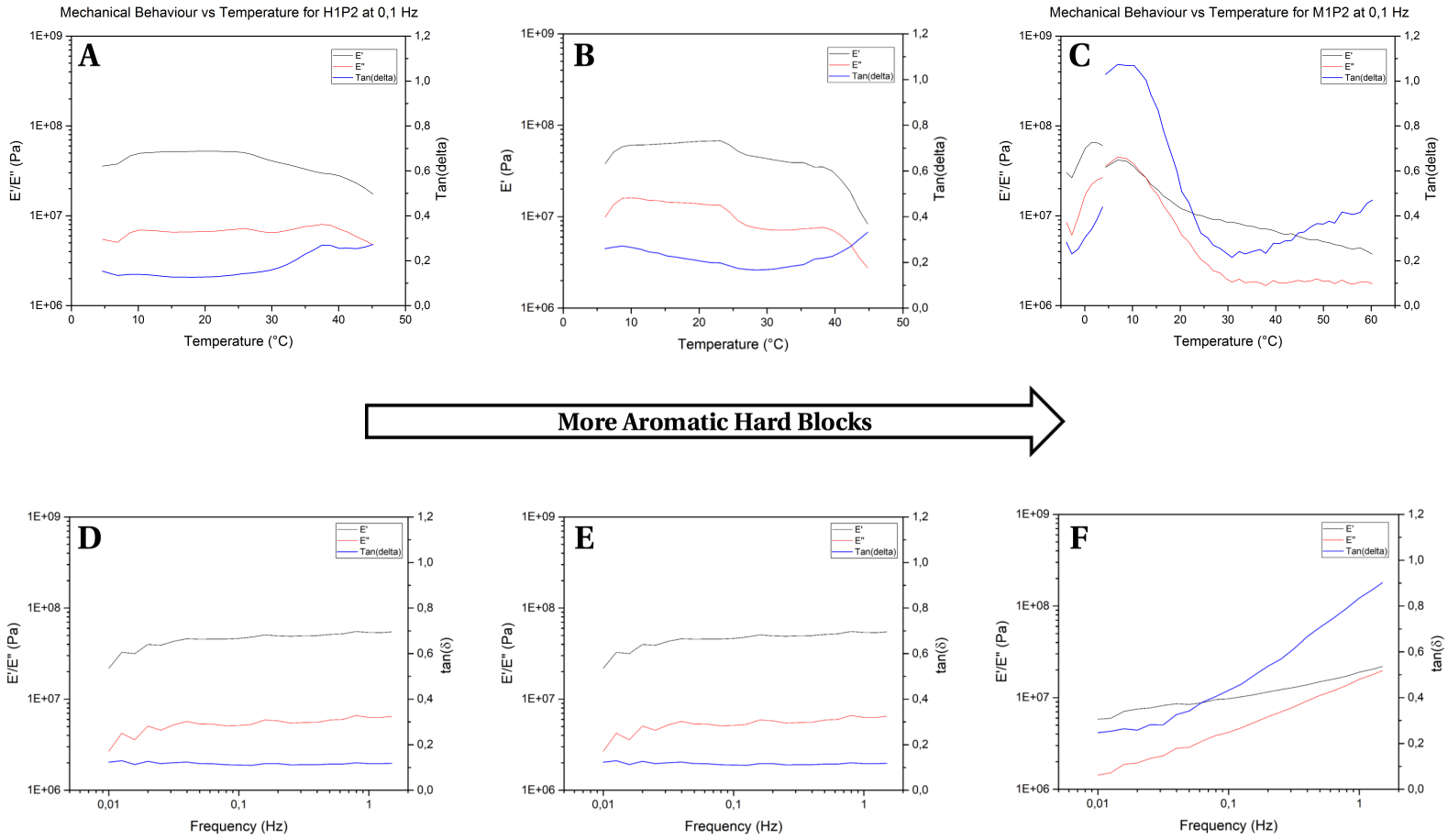

Figure B.3: The effects of the hard block aromaticity on the mechanical properties of the bulk polymer. **A** shows the rheology at $0,1Hz$ for completely aliphatic hard segments, with HDI being the only isocyanate for H1P2. **B** shows the same for a 50/50 molar mixture of HDI and MDI for H/M1P2. In **C** the same is shown for a purely aromatic hard segments, with MDI being the only isocyanate for M1P2. **D** shows the frequency response at $20°C$ for H1P2, **E** shows the same for H/M1P2 and **F** shows the same for M1P2.

Appendix C Adhesion for all Pillars

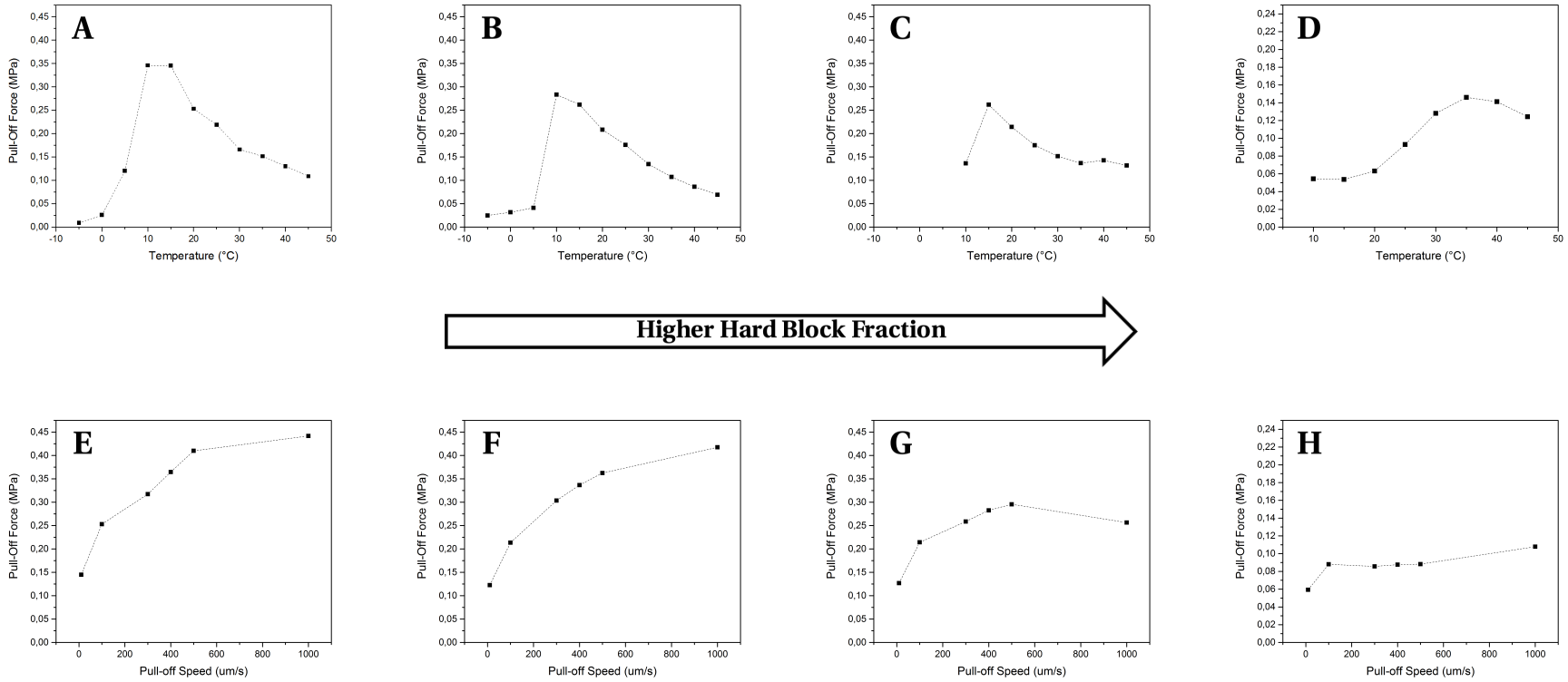

Figure C.1: The effects of hard block fraction on the adhesive performance. **A** shows the adhesion at $100 \mu m/s$ for the lowest hard block fraction, with the isocyanate being 16,9% of the total mass, for M0,8P2. **B** shows the same for M1P2 with XX% isocyanate. **C** shows the rheology for M1,5P2, which has XX% of isocyanate, and finally **D** shows the highest hard block fraction for M2P2 with a XX% of MDI. **E** shows the frequency response at $20°C$ for M0,8P2. **F** shows the same for M1P2 while **G** shows M1,5P2. Finally **H** shows the frequency response for M2P2.

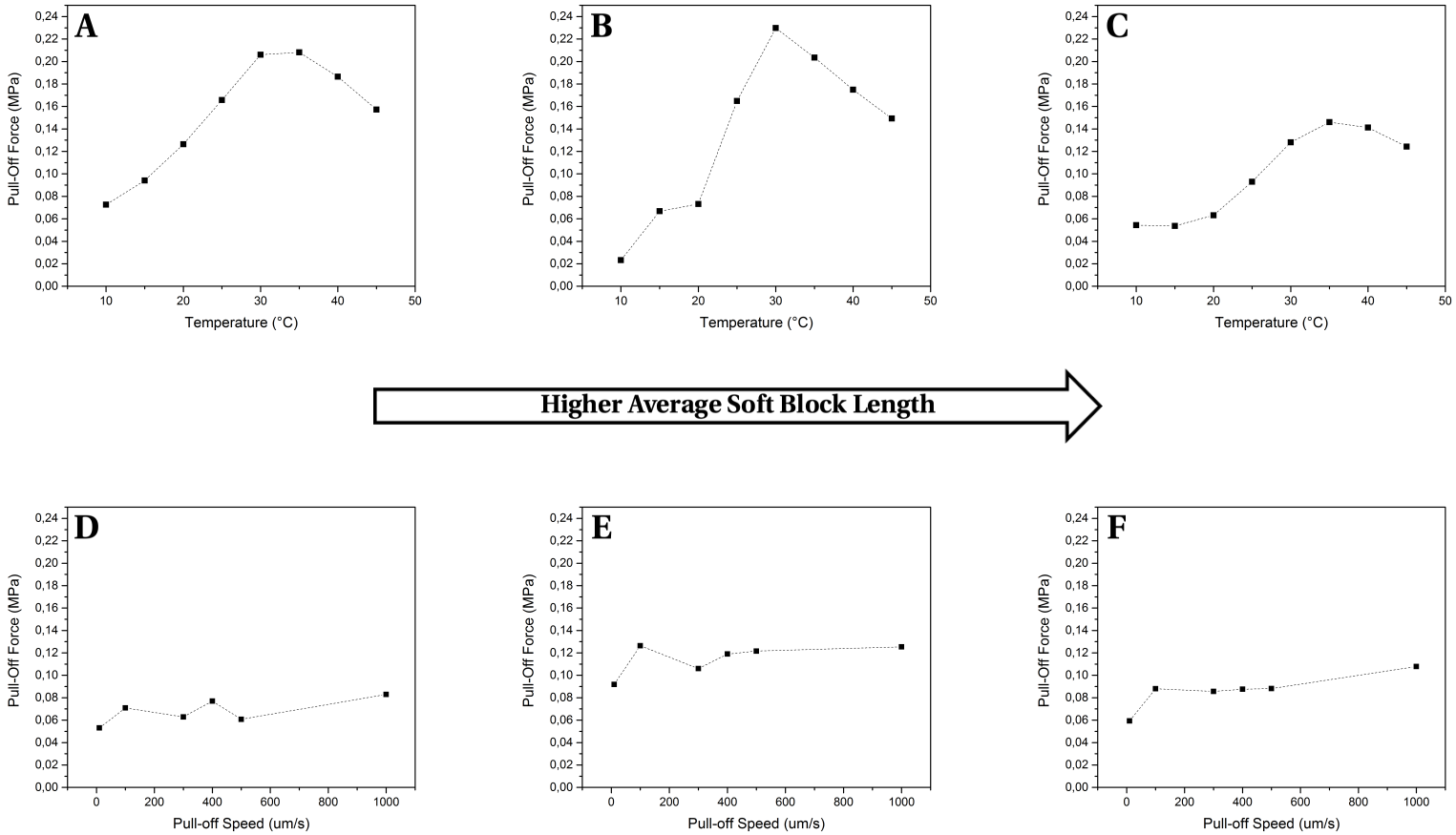

Figure C.2: The effects of soft segment length on the adhesive performance. **A** shows the adhesion at $100 \mu m/s$ for the shortest soft segments, with the average polyol molecular weight being $1,2 kDa$ for M2P1,2. **B** shows the same for an intermediate average length, $1,6 kDa$ for M2P1,2/2. **C** shows the longest soft segments, with the polyol having an M_w of $2 kDa$ for M2P2. **D** shows the frequency response at $20°C$ for M2P1,2, **E** for M2P1,2/2 and **D** shows the same for M2P2.

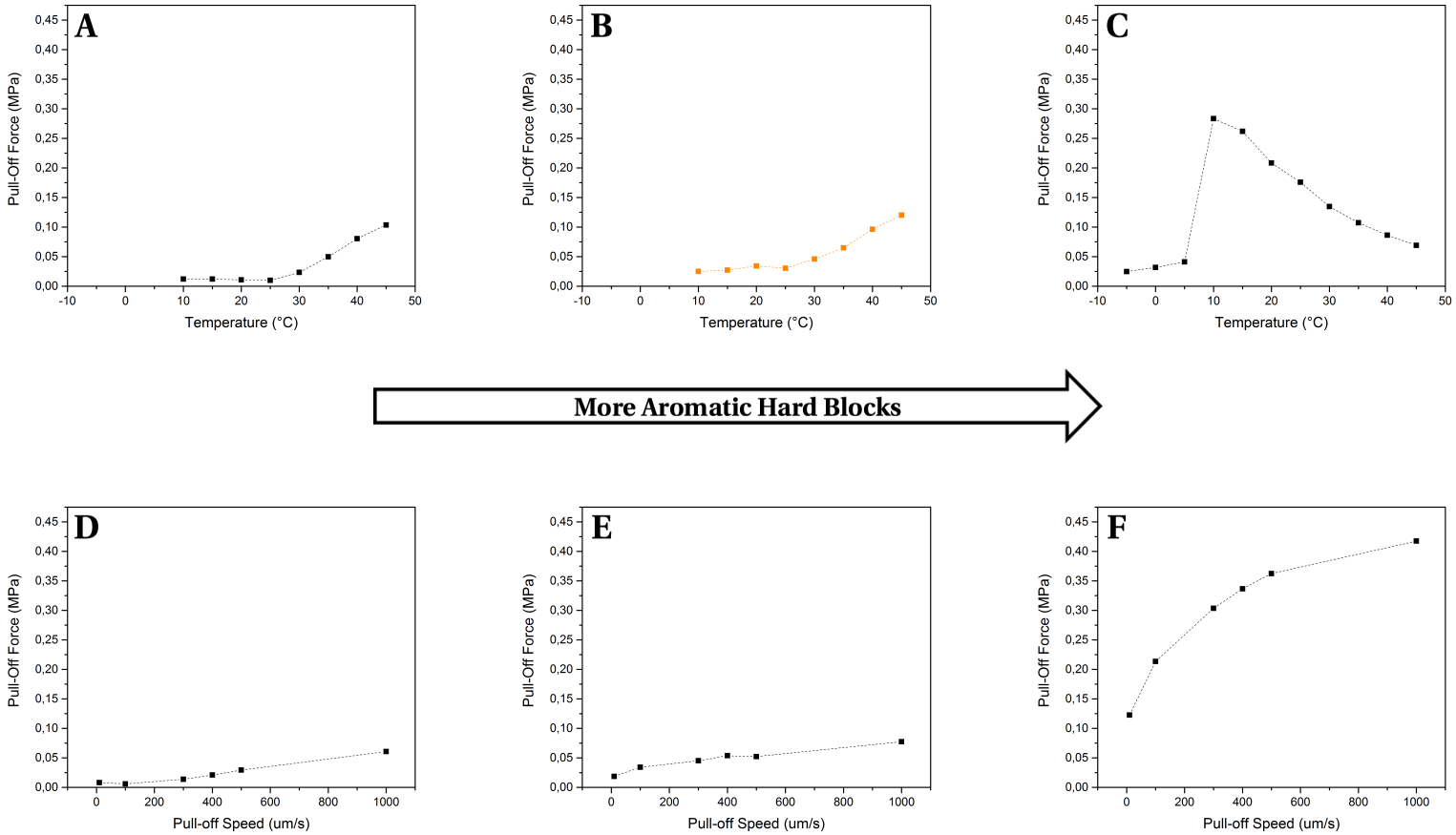

Figure C.3: The effects of the hard block aromaticity on adhesive performance. **A** shows the adhesion at $0,1\,Hz$ for completely aliphatic hard segments, with HDI being the only isocyanate for H1P2. **B** shows the same for a 50/50 molar mixture of HDI and MDI for H/M1P2. In **C** the same is shown for a purely aromatic hard segments, with MDI being the only isocyanate for M1P2. **D** shows the frequency response at $20°C$ for H1P2, **E** shows the same for H/M1P2 and **F** shows the same for M1P2.

Bibliography

[1] U. Abusomwan and M. Sitti. Effect of retraction speed on adhesion of elastomer fibrillar structures. *Applied Physics Letters*, 2012.

[2] L. Ahmed, B. Zhang, Spencer Hawkins, M. S. Mannan, and Z. Cheng. Study of thermal and mechanical behaviors of flame retardant polystyrene-based nanocomposites prepared via in-situ polymerization method. *Journal of Loss Prevention in the Process Industries*, 49:228–239, 07 2017. doi: 10.1016/j.jlp.2017.07.003.

[3] B. Aksak, K. Sahin, and M. Sitti. The optimal shape of elastomer mushroom-like fibers for high and robust adhesion. *Beilstein Journal of Nanotechnology*, 2014.

[4] K. Autumn, Y. A. Liang, S. T. Hsieh, W. Zesch, W. P. Chan, T. W. Kenny, R. Fearing, and R. J. Full. Adhesive force of a single gecko foot-hair. *Nature*, 45, 06 2000. doi: 10.1038/35015073.

[5] K. Autumn, M. Sitti, Y.A. Liang, A.M. Peattie, W.R. Hansen, S. Sponberg, T.W. Kenny, R. Fearing, J.N. Israelachvili, and R.J. Full. Evidence for van der waals adhesion in gecko setae. *PNAS*, 99, 09 2002. doi: 10.1073/pnas.192252799.

[6] V. Barreau, D. Yu, R. Hensel, and E. Arzt. Elevated temperature adhesion of bioinspired polymeric micropatterns to glass. *Journal of the Mechanical Behavior of Biomedical Materials*, 2017.

[7] R.H.C. Bonser. Hydration sensitivity of ostrich claw keratin. *Journal of Materials Science Letters*, 2002.

[8] R.H.C. Bonser, A.M. Taylor, and J.W. Farrent. The influence of hydration on the tensile and compressive properties of avian keratinous tissues. *Journal of material science*, 2004.

[9] A. Del Campo, C. Greiner, and E. Arzt. Contact shape controls adhesion of bioinspired fibrillar surfaces. *Langmuir*, 2007.

[10] G. Castellanos, E. Arzt, and M. Kamperman. Effect of viscoelasticity on adhesion of bio inspired micropatterned epoxy surfaces. *Langmuir*, 2011.

[11] J. Chen, J. Wang, S. Fan, and J. Chang. Reversible hydrophobic/hydrophilic adhesive of ps-b-pnipaam copolymer brush nanopillar arrays for mimicking the climbing aptitude of geckos. *J. Phys. Chem. C*, 12:6980–6992, 03 2012. doi: 10.1021/jp301068k.

[12] D. Drotlef, P. blumler, and A. del Campo. Magnetically actuated patterns for bioinspired reversible adhesion (dry and wet). *Adv. Mater.*, 26:775–779, 11 2014. doi: 10.1002/adma.201303087.

[13] S. Gorb, M. Varenberg, A. Peressadko, and J. Tuma. Biomemetic mushroom-shaped fibrillar adhesive microstructure. *Journal of the Royal Society*, 2007.

[14] G. Huber, H. Mantz, R. Spolenak, K. Mecke, K. Jacobs, S. Gorb, and E. Arzt. Evidence for capillarity contributions to gecko adhesion from single spatula nanomechanical measurements. *PNAS*, 2008.

[15] A. Jagota and S. Bennison. Mechanics of adhesion through a fibrillar microstructure. *Integrative & Comparative Biology*, 42:1140–1145, 12 2002. doi: 10.1093/icb/42.6.1140.

[16] K Johnson, K. Kendall, and A. Roberts. Surface energy and the contact of elastic solids. *Proc. R. Soc. Lond.*, 1971.

[17] M. Kamperman, E. Kroner, A. del Campo, R. M. McMeeking, and E. Arzt. Functional adhesive surfaces with gecko effect: The concept of contact splitting. *Adv. Eng. Mater.*, 12:335–348, 04 2010. doi: 10.1002/adem.201000104.

[18] K. Kendall. Soft and hard adhesion. *The adhesion and surface energy of elastic solids*, 1971.

[19] S. Kim and M. Sitti. Biologically inspired polymer microfibers with spatulate tips as repeatable fibrillar adhesives. *Appl. Phys. Lett*, 2006.

[20] E. Kizilkan and S. Gorb. Bioinspired further enhanced dry adhesive by the combined effect of the microstructure and surface free-energy increase. *ACS Applied Materials & Interfaces*, 2018.

[21] N. Lakhera, A. Graucob, A. S. Schneider, E. Kroner, E. Arzt, C. M. Yakacki, and C. P. Frick. Effect of viscoelasticity on the spherical and flat adhesion characteristics of photopolymerizable acrylate polymer networks. *International journal of Adhesion & Adhesives*, 44:184–194, 02 2013. doi: 10.1016/j.ijadhadh.2013.02.016.

[22] K. Liu, J. Du, J. Wu, and L. Jiang. Superhydrophobic gecko feet with high adhesive forces towards water and their bio-inspired materials. *Nanoscale*, 4:768–772, 02 2012. doi: 10.1039/C1NR11369K.

[23] Daniel Maugis. Contact, adhesion and rupture of elastic solids. *Contact, Adhesion and Rupture of Elastic Solids*, 130, 01 2000. doi: 10.1007/978-3-662-04125-3_3.

[24] M. Micciche, E. Arzt, and E. Kroner. Single macroscopic pillars as model system for bioinspired adhesives: Influence of tip dimension, aspect ratio, and tilt angle. *American Chemical Society Applied Material Interfaces*, 6:7076–7083, 4 2014. doi: 10.1021/am405873j.

[25] V. Montano, M.B. Wempe, Sam M.H. Does, J.C. Bijleveld, S. van der Zwaag, and S.J. Garcia. Controlling healing and toughness in polyurethanes by branch-mediated tube dilation. *Macromolecules*, 21: 8067–8078, 10 2019. doi: 10.1021/acs.macromol.9b01554.

[26] A. Infante Petidier. Effect of diisocyanate mixtures on the healing of thermoplastic polyurethanes [unpublished msc thesis], 06 2020.

[27] J. Puthoff, M. Prowse, M. Wilkinson, and K. Autumn. Energy storage, release and dissipation in the gecko adhesion system. *Materials research society symposium proceedings*, 2011.

[28] K. E. Riley and P. Hobza. On the importance and origin of aromatic interactions in chemistry and biodisciplines. *Acc. Chem. Res.*, 4:927–936, 08 2012. doi: 10.1021/ar300083h.

[29] A. Simaite and M. Spenko. Evaluation of silicone elastomers as structural materials for microstructured adhesives. *Bioinspiration & biomimetics*, 2019.

[30] M. Sitti and R. Fearing. Nanomolding based fabrication of synthetic gecko foot-hairs. In *Nanotechnology, 2002. IEEE-NANO 2002. Proceedings of the 2002 2nd IEEE Conference on*, pages 137–140, 2002.

[31] Sneddon and Ian N. Boussinesq's problem for a flat-ended cylinder. *Mathematical Proceedings of the Cambridge Philosophical Society*, 42(1):29–39, 1946. doi: 10.1017/S0305004100022702.

[32] R. Spolenak, S. Gorb, and E. Arzt. Adhesion design maps for bio-inspired attachment systems. *Acta biomaterialia*, 2005.

[33] John Tamelier, Sathya Chary, and Kimberly Foster. Importance of loading and unloading procedures for gecko-inspired controllable adhesives. *Langmuir : the ACS journal of surfaces and colloids*, 29, 07 2013. doi: 10.1021/la400835n.

[34] D. Yu, R. Hensel, D. Beckelmann, M. Opsolder, B. Schafer, K. Moh, P. de Oliveira, and E. Arzt. Tailored polyurethane acrylate blend for large-scale and high-performance micropatterned dry adhesives. *J. Mater. Sci*, 54:12925–12937, 06 2019. doi: 10.1007/s10853-019-03735-x.

[35] Y.Yoo, T. Kim, D. Choi, S. Hyun, H. Lee, K. Lee, S. Kim, B. Kim, Y. Seo, H. Lee, and J. Lee. Injection molding of a nanostructured plate and measurement of its surface properties. *Current Applied Physics*, 2008.